NASA CONTRACTOR REPORT

NASA CR-1061

NASA CR-1061

AN AN[illegible] CHEM[illegible] LAYER AND [illegible]

Part II

Finite D[illegible]esponse of Char[illegible] Chemica[illegible]

by Carl [illegible]

Prepared by
ITEK CO[illegible]
Palo Alto, [illegible]
for Manned [illegible]

NATIONAL [illegible]

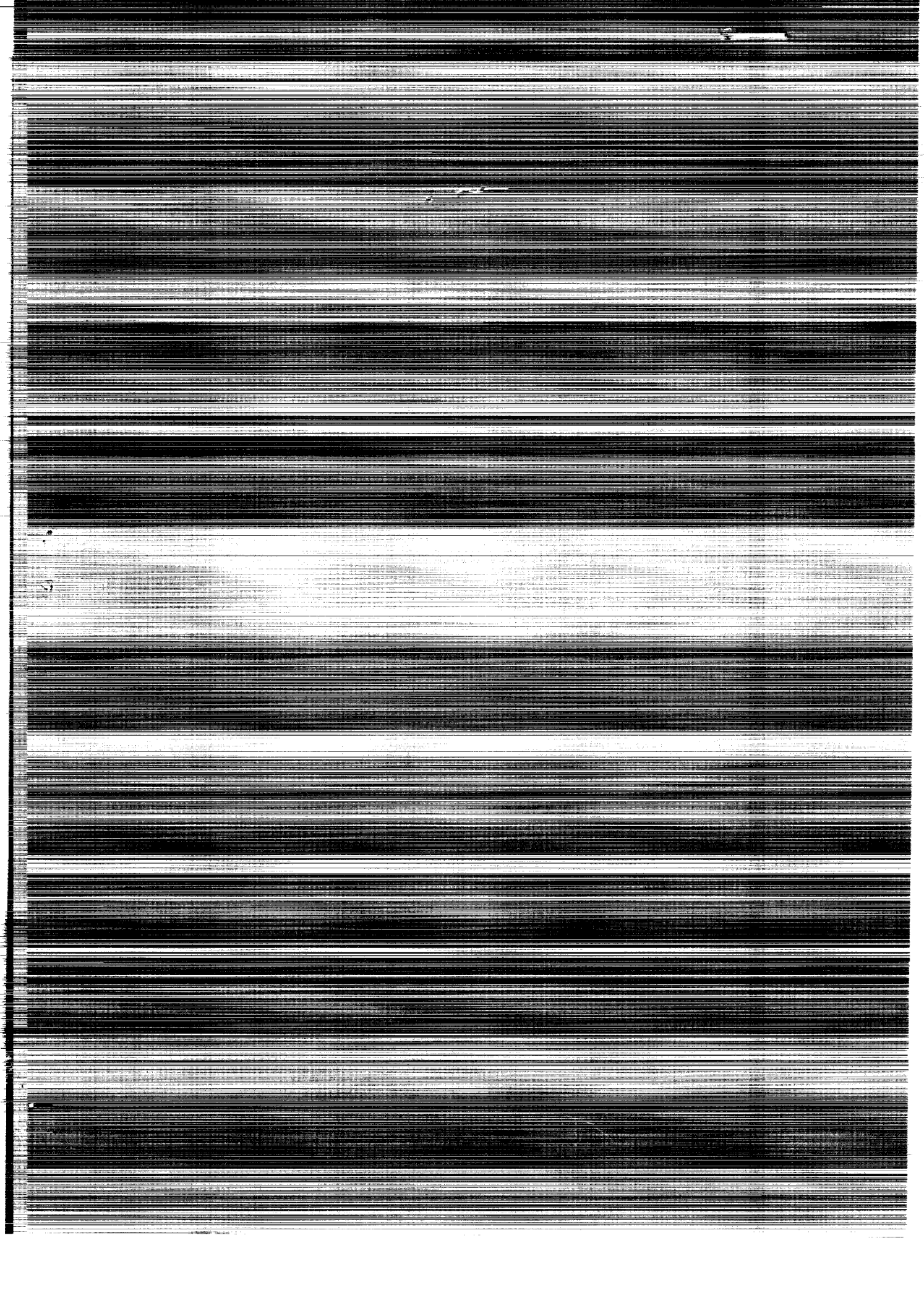

NASA CR-1061

AN ANALYSIS OF THE COUPLED CHEMICALLY REACTING BOUNDARY LAYER AND CHARRING ABLATOR

Part II

Finite Difference Solution for the In-Depth Response of Charring Materials Considering Surface Chemical and Energy Balances

By Carl B. Moyer and Roald A. Rindal

Issued by Originator as Aerotherm Report No. 66-7, Part II

Prepared under Contract No. NAS 9-4599 by
ITEK CORPORATION, VIDYA DIVISION
Palo Alto, Calif.

for Manned Spacecraft Center

NATIONAL AERONAUTICS AND SPACE ADMINISTRATION

For sale by the Clearinghouse for Federal Scientific and Technical Information
Springfield, Virginia 22151 – CFSTI price $3.00

ABSTRACT

This report presents an analysis of the in-depth response of materials exposed to a high temperature environment, and describes a computer program based upon the analysis.

The differential equations for the in-depth response are formulated and then cast into a finite difference form implicit in temperature. Three pyrolyzing constituents are allowed, with an accurate model of observed pyrolysis kinetics. Heat flow in-depth is one-dimensional, but cross-section area may vary with depth.

The program for in-depth response computation may be coupled to a variety of boundary conditions. One of the possible boundary conditions is a complete boundary layer solution described in other reports of this series. Another version of the program may be coupled to a general film coefficient model of the boundary layer; this boundary condition is described in some detail in the present report.

The report concludes with sample solutions generated by the computer program.

FOREWORD

The present report is one of a series of six reports, published simultaneously, which describe analyses and computational procedures for: 1) prediction of the in-depth response of charring ablation materials, based on one-dimensional thermal streamtubes of arbitrary cross-section and considering general surface chemical and energy balances, and 2) nonsimilar solution of chemically reacting laminar boundary layers, with an approximate formulation for unequal diffusion and thermal diffusion coefficients for all species and with a general approach to the thermochemical solution of mixed equilibrium-nonequilibrium, homogeneous or heterogeneous systems. Part I serves as a summary report and describes a procedure for coupling the charring ablator and boundary layer routines. The charring ablator procedure is described in Part II, whereas the fluid-mechanical aspects of the boundary layer and the boundary-layer solution procedure are treated in Part III. The approximations for multicomponent transport properties and the chemical state models are described in Parts IV and V, respectively. Finally, in Part VI an analysis is presented for the in-depth response of charring materials taking into account char-density buildup near the surface due to coking reactions in depth.

The titles in the series are:

Part I Summary Report: An Analysis of the Coupled Chemically Reacting Boundary Layer and Charring Ablator, by R. M. Kendall, E. P. Bartlett, R. A. Rindal, and C. B. Moyer.

Part II Finite Difference Solution for the In-depth Response of Charring Materials Considering Surface Chemical and Energy Balances, by C. B. Moyer and R. A. Rindal.

Part III Nonsimilar Solution of the Multicomponent Laminar Boundary Layer by an Integral Matrix Method, by E. P. Bartlett and R. M. Kendall.

Part IV A Unified Approximation for Mixture Transport Properties for Multicomponent Boundary-Layer Applications, by E. P. Bartlett, R. M. Kendall, and R. A. Rindal.

Part V A General Approach to the Thermochemical Solution of Mixed Equilibrium-Nonequilibrium, Homogeneous or Heterogeneous Systems, by R. M. Kendall.

Part VI An Approach for Characterizing Charring Ablator Response with In-depth Coking Reactions, by R. A. Rindal.

This effort was conducted for the Structures and Mechanics Division of the Manned Spacecraft Center, National Aeronautics and Space Administration under Contract No. NAS9-4599 to Vidya Division of Itek Corporation with Mr. Donald M. Curry and Mr. George Strouhal as the NASA Technical Monitors. The work was initiated by the present authors while at Vidya and was completed by Aerotherm Corporation under subcontract to Vidya (P.O. 8471 V9002) after Aerotherm purchased the physical assets of the Vidya Thermodynamics Department. Dr. Robert M. Kendall of Aerotherm was the Program Manager and Principal Investigator.

TABLE OF CONTENTS

TABLE OF CONTENTS (Continued)

TABLE OF CONTENTS (Concluded)

LIST OF FIGURES

LIST OF SYMBOLS

A	cross section area for a node	(ft^2)
A_{BW}	area of back wall of last node	(ft^2)
A_n	coefficient in Eq. (58). See also Appendix A.	($Btu/ft^3\ ^oF$)
A_n^*	value of A_n after first pass of Gauss reduction, See Eq. (62)	($Btu/ft^2\ ^oF$)
B	pre-exponential factor, Eq. (3)	(sec^{-1})
B_n	coefficient in Eq. (58). See also Appendix A	($Btu/ft^3\ ^oF$)
B_n^*	value of B_n after first pass of Gauss reduction, See Eq. (62)	($Btu/ft^3\ ^oF$)
B'	defined as $B'_c + B'_g$	(---)
B'_c	defined as $\dot{m}_c/\rho_e u_e C_M$	(---)
B'_g	defined as $\dot{m}_g/\rho_e u_e C_M$	(---)
C_H	Stanton number for heat transfer (corrected for "blowing", if necessary)	(---)
C_{H_0}	Stanton number for heat transfer not corrected for blowing	(---)
C_M	Stanton number for mass transfer	(---)
C_n	coefficient in Eq. (58). See also Appendix A	($Btu/ft^3 sec$)
C_p	specific heat	($Btu/lb\ ^oF$)
D_n	coefficient in Eq. (58). See also Appendix A	(Btu/ft^3)
D_n^*	value of D_n after first pass of Gauss reduction, See Eq. (62)	(Btu/ft^3)
$\overline{D}$	constant defined by Eq. (69)	(ft^2/sec)
$\mathscr{D}_{ij}$	binary diffusion coefficient	(ft^2/sec)
$E/R, E_i/R$	activation energy for decomposition	(^oR)
F	radiation view factor	(---)
F_i, F_j	empirical factors appearing in Eq. (69)	(---)
F_3, F_4, F_5	general denotations for functional relationship, Eqs. (58), (59)	(---)

LIST OF SYMBOLS (Continued)

f	general denotation for functional relationship	(---)
H	recovery enthalpy	(Btu/lb)
h	enthalpy	(Btu/lb)
$h_s^{T_b}$	sensible enthalpy measured <u>above</u> temperature T_b	(Btu/lb)
$h_i^{T_b}$	enthalpy of species i <u>at</u> temperature T_b	(Btu/lb)
h_w	enthalpy of gases adjacent to the wall	(Btu/lb)
$\bar{h}$	enthalpy term defined at Eq. (38)	(---)
I	total number of identifiable species	(---)
J	number of nodelets per node	(---)
j	nodelet index	(---)
$\tilde{J}_{k_w}$	diffusion flux of element k away from wall	(lb/ft^2 sec)
K	total number of elements in system	(---)
K_i	mass fraction of species i	(---)
$\tilde{K}_k$	mass fraction of element k (regardless of molecular configuration	(---)
KE	kinetic energy contribution to recovery enthalpy	(Btu/lb)
k	thermal conductivity, also element index	(Btu/ft sec$^\circ$F) or (---)
k_i	pre-exponential factor for constituent i, analogous to B	(sec^{-1})
L	total number of nodes	(---)
Le	Lewis number $\rho\mathcal{D}_{ij}C_p/k$	(---)
$\mathcal{M}$	system molecular weight $\sum x_i \mathcal{M}_i$	(lb/lb mole)
$\mathcal{M}_g$	system molecular weight, pyrolysis gas	(lb/lb mole)
$\mathcal{M}_i$	molecular weight of species i	(lb/lb mole)
m_i	reaction order for constituent i, see Eq. (10)	(---)
$\dot{m}$	mass flow rate per unit area from the surface	(lb/ft^2 sec)

$\dot{m}_c$	mass flow rate of char per unit surface area	(lb/ft^2 sec)
$\dot{m}_g$	mass flow rate of pyrolysis gas through a node	(lb/sec)
$\dot{m}_{g_s}$	mass flow rate of gas out a unit area of surface	(lb/ft^2 sec)
N	total number of nodes	(---)
NBM	denotes first node of back-up material	(---)
NL	denotes last node of ablation material	(---)
q	heat absorption term for decomposition	(Btu/lb)
q_{cond}	rate of energy conduction into solid material at surface	(Btu/ft^2 sec)
q_{diff}	rate of energy input to solid surface by diffusional processes in the boundary layer	(Btu/ft^2 sec)
$q_{rad\ in}$	rate of energy input to the surface by radiation from the boundary layer or from outside the boundary layer	(Btu/ft^2 sec)
$q_{rad\ out}$	rate of energy radiated away from surface	(Btu/ft^2 sec)
q^*	rate of energy removal from surface with condensed phases	(Btu/ft^2 sec)
r.f.	boundary layer recovery factor	(---)
R	universal gas constant	$\left(\frac{\text{ft\#}}{\text{lb-mole}^\circ\text{R}}\right)$
S	distance from original location of receding surface to current surface location	(ft)
$\dot{S}$	rate of change of S (surface recession rate)	(ft/sec)
T,t	temperature	($^\circ$R)
T_w, T_l	wall (surface) temperature	($^\circ$R)
T_μ	reference temperature for viscosity Eq. (82)	($^\circ$R)
u_e	velocity of gases at edge of boundary layer	(ft/sec)
v	gas velocity (see ρv)	(ft/sec)
x	coordinate normal to ablating surface, fixed to receding surface	
x	virgin mass fraction, $x = \frac{\rho_p}{\rho_p - \rho_c}\left(1 - \frac{\rho_c}{\rho}\right)$	
x_i	mole fraction of species i	(---)
y	coordinate normal to ablating surface, origin fixed in space relative to back wall	(ft)

Z_i	diffusion driving force $= \frac{K_i}{F_i \sum_j \frac{K_j}{F_j}}$, see Eq. (67)	(---)
Z_i^*	modified Z_i defined by Eq. (66)	(---)
$\tilde{Z}_k^*$	Z* for elements k independent of molecular configuration, defined by Eq. (65)	(---)

Greek

α	coefficient in Eq. (81)	(ft^{-2})
α_{ki}	mass fraction of element k in species i	(---)
α_w	absorptivity of the wall	(---)
β	coefficient in Eq. (81)	(ft^{-1})
γ	constant equal to 2/3 on empirical basis	(---)
Γ	volume fraction of resin in plastic, see Eq. (4)	$\frac{ft^3 resin}{ft^3 material}$
Δ	denotes change	(---)
$\Delta\theta$	time step in finite difference solution	(---)
δ	nodal thickness	(ft)
ϵ	error in an equation supposed to equal zero, departure from zero	(various)
ϵ_p	volume fraction of imagined undecomposed material in a sample of partially degraded material	$\frac{ft^3 virgin}{ft^3 material}$
ϵ_w	emissivity of the wall	(---)
θ	time	
μ	viscosity of pyrolysis gas	(lb/ft-sec)
μ_2	dimensionless factor defined by Eq. (68)	(---)
ρ	density	(lb/ft^3)
ρC_p	mean volume capacity defined by Eq. (28)	$(Btu/ft^3\ ^\circ R)$
$(\rho v)_w$	$\dot{m}_c + \dot{m}_{g_s}$	$(lb/ft^2 sec)$

ρ_c	char density	(lb/ft^3)
$\rho_e u_e$	mass flow at boundary layer edge	($lb/ft^2 sec$)
$\rho_e u_e C_H$	heat transfer convective film coefficient	($lb/ft^2 sec$)
$\rho_e u_e C_M$	mass transfer convective film coefficient	($lb/ft^2 sec$)
ρ_o	original density of a pyrolyzing component	(lb/ft^3 resin or lb/ft^3 reinforcement)
ρ_g	density of pyrolysis gas	(lb/ft^3)
ρ_p	density of virgin plastic	(lb/ft^3)
ρ_r	final density of a pyrolyzing component	(lb/ft^3 resin or lb/ft^3 reinforcement)
σ	Stefan-Boltzmann constant	($Btu/ft^2 sec^\circ R^4$)

Subscripts

A	denotes one pyrolyzing component of resin
B	denotes second pyrolyzing component of resin
BW	denotes back wall
b	denotes back face of ablating material
C	denotes reinforcement
c	denotes char
d	denotes decomposition
e	denotes boundary layer outer edge
g	denotes pyrolysis gas
H	see C_H
i,j	denotes any identifiable species: atom, ion, molecule
i	denotes pyrolyzing component; otherwise, general index
j	denotes nodelet
k	denotes element
L	denotes last node

M	see C_M
NL	denotes last ablating node
n	node index
o	denotes datum state for enthalpy; see also ρ_o
p	denotes virgin plastic
r	see ρ_r
res	denotes "reservoir" temperature with which back wall communicates
s	denotes "sensible" or "thermal" component of enthalpy
w	denotes wall, i.e., heated surface
0	see C_{H_0}
1,2	steps in iteration in Eq. (61), see also μ_2

Superscripts

T	on sensible enthalpy, denotes base temperature above which sensible enthalpy is measured; on total enthalpy, denotes temperature at which enthalpy is measured
o	denotes datum temperature for enthalpy
*	see A_n^*, B_n^*, D_n^*, q^*, Z_i^*, $\tilde{Z}_k^*$
~	refers to all appearances of element k regardless of molecular configuration
—	denotes average over time interval except on $\bar{h}$ (q.v.)
'(prime)	denotes "new", at $\theta + \Delta\theta$, except for B', B_c', B_g' (q.v.)

Special Symbols

$\triangleq$	defined as, equal to by definition
#	pounds force

FINITE DIFFERENCE SOLUTION FOR THE IN-DEPTH RESPONSE OF CHARRING MATERIALS CONSIDERING SURFACE CHEMICAL AND ENERGY BALANCES

SECTION 1
GENERAL INTRODUCTION

The present report describes a particular analysis and an associated computer program for predicting the transient thermal response of a charring or decomposing material exposed to a high temperature environment. For generality, the in-depth computation program may be coupled to associated programs which provide a heated surface boundary condition in the form of heat transfer rates and chemical erosion rates.

Section 2 below describes the general problem and offers a historical survey of solution attempts. Sections 3 and 4 present the details of the in-depth solution, and Section 5 describes one alternative treatment of the heated surface boundary condition. Section 6 describes a model for pressure drop in the char, and Section 7 gives a short description of the actual computer program and provides some examples of its use.

The general purpose of this report is to collect in one place certain descriptive background material and a number of mathematical derivations pertinent to the computer programs developed during this study. The chief program pertinent to this report is Version 2 of the Aerotherm Charring Material Ablation Program (the CMA program). Related programs are the Equilibrium Surface Thermochemistry Program (EST) and the Aerotherm Chemical Equilibrium Program (ACE). Instructions for operating these programs are not included in this report; the relevant User's Manuals are cited in Section 6 below.

SECTION 2
PROBLEM DESCRIPTION AND HISTORICAL ORIENTATION

2.1 GENERAL REMARKS

The basic problem is to predict the temperature and density histories of a thermally decomposing material exposed to some defined environment which supplies heat and which may chemically erode the material surface. The chief practical example of such a problem is the calculation of the performance of thermal insulation in hyperthermal environments, including the design of re-entry vehicle sacrificial heat shields and expendable rocket nozzle materials. Other practical problems include the combustion or charring of wood, the baking or various plastics, the combustion of solid rocket fuel, and in-depth pyrolysis reactions of all kinds.

The general prediction problem may conveniently be divided into two parts: the construction of a scheme for computing the in-depth behavior, and the specification of the heated surface boundary condition. The present paper is mainly concerned with the first problem, although the second topic is also given extensive discussion. It may be noted in passing that for quasi-steady ablation problems (constant wall temperature, steady recession rate, invariant temperature profile with respect to the moving surface), the details of the in-depth solution are not necessary for determining the surface temperature and the recession rate. The transient problem, on the other hand, does require a complete in-depth solution, and hence is a much more elaborate problem.

2.2 PROBLEM DESCRIPTION

The physical problem may be illustrated as follows:

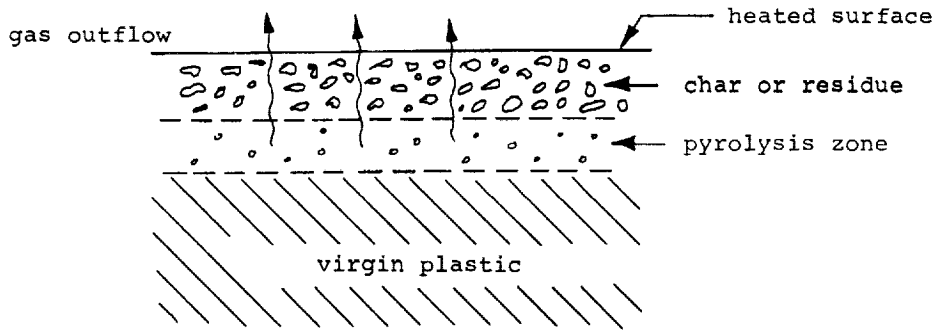

As the material is heated, the original virgin material (or rather one or more components of the original composite virgin material) pyrolyzes and yields a pyrolysis gas, which percolates away from the pyrolysis zone, and a porous residue, which for most materials of interest is a carbonaceous char, possibly reinforced with refractory fibers or cloth.

Superimposed on this basic problem may be a number of even more complex events. The pyrolysis gases percolating through the char may undergo further chemical reactions among themselves, and may react with the char, either eroding it or depositing additional residue upon it ("coking"). The char itself may collapse or fragment from mechanical or thermal stresses, and the refractory reinforcements may melt or suffer mechanical damage. Finally, various constituents of the residue structure may react chemically with each other, changing the nature of the char, and various mechanical forces may remove material from the surface.

Despite these complexities, it is found that the "simple physics" described by

$$\text{virgin plastic} \rightarrow \text{char} + \text{gas}$$

underlies a wide range of problems of technical interest, and for a great many materials, such as carbon phenolic, graphite phenolic, and wood, constitute all the events of interest. Such events as coking, mechanical erosion, melting, and subsurface reactions (other than pyrolysis) are less common and generally characterize specific problems.

Therefore in any effort to compute the in-depth response of pyrolyzing materials the first order of business is to characterize the heat conduction and the primary pyrolysis reaction, which have useful generality. Particular details of special char chemical systems can then be superimposed upon this general computational scheme as required. The present effort has been mostly devoted to the general conduction-pyrolysis problem. The numerical details are described in Section 3.

2.3 PROBLEM HISTORY

In general terms, the in-depth calculation requires the solution of a differential energy transport equation of the form (for one space dimension, and neglecting gas flows for the moment)

$$\frac{\partial}{\partial x}\left(k \frac{\partial t}{\partial x}\right) - \rho c_p \frac{\partial t}{\partial \theta} + q \frac{\partial \rho}{\partial \theta} = 0$$

plus an associated decomposition or charring kinetic relation

$$\frac{\partial \rho}{\partial \theta} = f(\rho, t)$$

This coupled pair of differential equations in general defies analytical treatment and requires, instead, some approximate technique of solution. Perhaps the first general attack on this problem was published by Bamford, Crank, and Malan in 1946 (Reference 1). This paper presented a temperature-implicit finite difference method, later elaborated in Reference 2, which became known as the Crank-Nicolson method. The second paper also presented two methods suitable for differential analyzer or analog computations.

Applications of ablating or sacrificial insulations for rocket nozzles and for re-entry vehicle heat shields in the 1950's naturally stimulated a great deal of development work on charring material predictive techniques.

References 3 - 30 provide a representative sampling of that part of the literature which is aimed primarily at the analysis of the in-depth response of charring materials. (A more complete bibliography may be found in Reference 31.)

Many of these analyses, particularly References 9, 15, 18, 22, 23, 24, 27, and 28, were associated with the development of computer programs for in-depth response computation. All of these programs treat the in-depth problem in very much the same way, with only relatively unimportant variations in the numerical formulation and the treatment of the pyrolysis kinetics.

The present computation scheme does not differ to any very great extent from the best versions of earlier programs. It does feature a very great fidelity to the observed physics of charring materials, a difference scheme which rigorously conserves mass and energy, an economical implicit finite difference formulation, and the capability of handling general two-dimensional geometries with the limitation of one-dimensional energy flow.

SECTION 3

ANALYSIS AND COMPUTATIONAL PROCEDURE FOR CHARRING MATERIAL RESPONSE

3.1 PROBLEM FORMULATION

3.1.1 Introduction

Analysis of a complete transient charring material ablation problem necessarily involves a computation of the internal thermal response of the charring material. As discussed in Section 2 above, this computation constitutes only a transient heat conduction calculation including the effects of internal thermal decomposition with pyrolysis gas generation, coupled to an appropriate set of boundary conditions. The sections below present the fundamental assumptions and equations invovled in the in-depth solution.

3.1.2 Basic Differential Equations

For the basic in-depth solution, it is assumed that thermal conduction is one-dimensional; however, the cross-section area (perpendicular to the conduction flux) is allowed to vary with depth in an arbitrary manner. This corresponds to a thermal stream tube. Furthermore, it is assumed that any pyrolysis gases formed are in thermal equilibrium with the char. For the present discussion, it is assumed that the pyrolysis gases do not react chemically with the char in any way. Thus coking or further chemical erosion are

excluded. These effects will be discussed in Section 3.1.4 below. Finally, any pyrolysis gas formed is assumed to pass immediately out through the char, that is, it has zero residence time in the char. Cracking or other chemical reactions involving only the pyrolysis gases may be simulated with an appropriate gas specific heat.

The one-dimensional energy differential equation for this problem is readily formulated as

$$\frac{\partial}{\partial \theta} (\rho h A)_y = \frac{\partial}{\partial y} \left(kA \frac{\partial T}{\partial y} \right)_\theta + \frac{\partial}{\partial y} (\dot{m}_g h_g)_\theta \tag{1}$$

where ρ is the density, k is the thermal conductivity, A is area, h is enthalpy, and $\dot{m}_g$ the local gas flow rate.

The conservation of mass equation is

$$\left(\frac{\partial \dot{m}_g}{\partial y} \right)_\theta = A \left(\frac{\partial \rho}{\partial \theta} \right)_y \tag{2}$$

Evaluation of this expression requires a specification of the decomposition rate $\partial\rho/\partial\theta)_y$. A great amount of laboratory pyrolysis data, such as that presented in Ref. 32, suggest that the decomposition rate may be taken as an Arrhenius type of expression

$$\left(\frac{\partial \rho}{\partial \theta} \right)_y = -B\, e^{-E/RT}\, \rho_o \left(\frac{\rho - \rho_r}{\rho_o} \right)^m \tag{3}$$

and for even greater generality it has been found useful and sufficient to consider up to three differently decomposing constituents (Ref. 32)

$$\rho = \Gamma(\rho_A + \rho_B) + (1 - \Gamma)\rho_C \tag{4}$$

where for example $(\rho_A + \rho_B)$ might be the density of resin (or analogous binder) in the ablating material, ρ_C would be the density of the reinforcement and Γ the volume fraction of resin in the virgin plastic composite. Each density ρ_A, ρ_B, and ρ_C, may follow an independent decomposition equation of the type of Eq. (3).

It is possible to handle the decomposition in other ways than by Eq. (3). A popular simplification is to treat density as a function of temperature only. An even more drastic simplification converts the virgin material to complete char at one particular "charring temperature." Other techniques specify some char thickness as a function of time, or of heating rate. All of these simplifications are, of course, open to objection. Equation (3) is not only the most realistic physically, but is usually easy to handle in computation.

3.1.3 Boundary Conditions

Suitable boundary and initial conditions for the set of equations (1) through (4) may be readily formulated. The boundary conditions at the front and back faces of the ablating material are usually surface energy balances. Of these, the front or "active" surface boundary condition is the most complex. It is handled in slightly different ways depending on which boundary layer treatment is being coupled to the in-depth reaponse program.

Basically, the surface energy balance may be pictured as

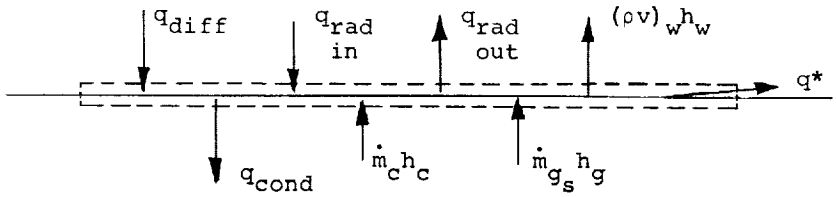

where the indicated control volume is fixed to the receding surface. Energy fluxes leaving the control volume include conduction into the material, radiation away from the surface, energy in any flow of condensed phase material such as liquid runoff, and gross blowing at the surface. Energy inputs to the control volume include radiation in from the boundary layer and enthalpy fluxes due to char and pyrolysis gas mass flow rates. The final input in the sketch is denoted q_{diff}. It includes all diffusive energy fluxes from the gas boundary layer. If the in-depth response computation is being coupled to an exact boundary layer solution, the term q_{diff} will be available directly as

a single term (which is, of course, a complex function of many boundary layer properties). If, on the other hand, the in-depth response is being coupled to a simplified boundary layer scheme, such as a convective film coefficient model, then the term q_{diff} has a rather complicated appearance. Section 5 below contains a further discussion of this aspect of the total computation.

For the present, it suffices to note that computation of the surface energy balance requires the following information from the in-depth solution:

a. the instantaneous pyrolysis gas rate delivered from in-depth to the surface, $\dot{m}_g$

b. a relation between the surface tmmperature and the rate of energy conduction into the material, q_{cond}

With these two pieces of information the surface energy balance then determines the char consumption rate $\dot{m}_c$ and the surface temperature T_w. It will be useful to keep in mind that, from this point of view, the purpose of the in-depth solution at any instant is to provide information about $\dot{m}_g$ and $q_{cond}\ (T_w)$. In some circumstances, of course, it is of interest merely to specify the heated surface temperature and recession rate. In this case no surface energy balance is required.

It is usually of interest to have only one ablating surface. The back-wall or non-ablating wall boundary condition may be modelled with a film coefficient heat transfer equation.

3.2 FINITE DIFFERENCE DEVELOPMENT

3.2.1 Introduction

Section 3.1.2 above sets forth the governing differential equations whose solution is required to define the interal response of the charring material. As in many other problems, however, the differential equations cannot be solved in general, and it is necessary instead to solve finite difference equations* which model the differential equations, and the analyst hopes, retain the same mathematical properties as the original differential equations. A number of plausible difference equations can be proposed, and without the benefit of actual experience it is generally impossible to select any particular differencing scheme as superior to any other. In the past few years a

*It is possible, of course, to use simpler schemes than finite difference equations. Reference 33 is a sample of the several integral analysis approaches which have been tried. Such techniques are usually of insufficient accuracy to be generally useful, however.

few general differencing principles have been made reasonably clear, however, so that the analyst is not completely in the dark. The following section offers some background on this topic.

3.2.2 Differencing Philosophy

This section sets down the general principles upon which the finite differencing of the governing equations is based. These principles have proved sound and useful, particularly for complex problems.

In common with all difference procedures, the area of interest (here, the charring material) is divided into a number of small zones, each considered to be homogeneous. All derivatives in the governing differential equations are then replaced by some difference expression from zone to zone. These zones, called nodes, thus provide the basic conceptual structure upon which the differencing procedure is based.

The following principles of differencing and nodal sizing have been followed in the programming work:

(1) The nodes have a fixed size. This avoids the slight additional computation complexity of shrinking nodes, and more importantly, makes principle (2) easier to satisy, in addition to preserving a useful nodal spacing throughout the history of a given problem.

(2) Since the nodes are fixed in size, not all of them can be retained if the surface of the material is receding due to chemical or mechanical erosion. From time to time a node must be dropped, and experience shows that it is much more preferable to drop nodes from the back (non-ablating) face of the material rather than from the front face. See, for example, Ref. 34 for a discussion of this problem. This means that the nodal network is "tied to the receding surface," and that material appears to be flowing through the nodes. This involves a transformation of differential equations (1) and (2) to a moving coordinate system and somewhat complicates the algebra of the difference equations modelled on these differential equations. Disposing of nodes from the front surface, however, often leads to undesirable oscillations.

(3) The difference forms of derivatives are kept simple and are formed so as to provide a direct physical analog of the differential event leading to the derivative. This approach may be contrasted to those approaches which seek elaborate difference approximations to derivative expressions. Experience shows that the scheme advocated here, while sometimes at a minor disadvantage in accuracy, greatly simplifies the attainment of a major objective: a difference scheme which conserves energy and mass. Many of the more

elaborate difference schemes fail to meet these "simple" but crucial conservation criteria, and hence frequently converge to erroneous or spurious solutions.

(4) The difference equation for energy is formulated in such a way that it reduces to the difference equation for mass conservation when temperatures and enthalpies are uniform. Any lack of consistency between the energy and mass equations complicates, and may entirely defeat, convergence to a meaningful result.

(5) The difference energy equations are written to be "implicit" in temperature. That is, all temperatures appearing are taken to be "new" unknown temperatures applicable at the end of the current time step. It is well established that implicit procedures are generally more economical than explicit procedures, at least for the majority of ablation problems of interest in the current work.

(6) In constrast to point (5), the decomposition relations are written as "explicit" in temperature. To implicitize temperature in these highly nonlinear equations necessarily involves either a time-consuming iteration procedure or an elaborate linearization, which is not necessary for most materials.

(7) Since experience has shown that material decomposition rates are strongly dependent on temperature, it is highly desirable to perform the mass balance operations in a different, tighter network than that used for the energy balance equations. For greatest generality and utility, the number of these mass balance "nodelets" per energy balance "node" should be freely selectable.

3.2.3 Transformation of Differential Equations

3.2.3.1 General Remarks

Solution of the in-depth response will be by difference equations. The most convenient finite difference equations governing particular physical phenomena may often be derived directly from considering a control volume of finite (not infinitesimal) extent. Such is the case, for example, when characterizing the thermochemical response of charring materials having constant cross-sectional area (the flat plate case). For the present problem, however, where the cross-sectional area may be an arbitrary function of distance below the surface, substantial simplifications may be realized if the equations are first considered in differential form. Specifically, differences in cross-sectional area with respect to space and time appear in the

difference equations derived from the finite control volume approach. The neglect of these terms is difficult to rationalize from the difference equations; however, if the differential equation is employed, these terms may be demonstrated to vanish identically. The resulting differential equations may then be expanded into finite difference form yielding a set of finite difference equations substantially simpler than those derived directly from analyzing a finite control volume. The differential equations are considered first, and subsequently expanded to finite difference form.

As discussed in Section 3.2.2 above, it is deemed convenient to base the difference formulation on a nodal network fixed to the heated surface. Since this surface will be receding, material will appear to flow into and out of the nodes. The differential equations presented as Eqs. (1) and (2) require transformation to a moving coordinate system to include this aspect of the problem and to provide the proper model for differencing. The mass equation is treated first, in Section 3.2.3.3. Discussion of the energy equation follows. First, however, some observations about the geometry are required.

3.2.3.2 Geometrical Considerations

The generalized geometry being considered and the coordinate system to be employed for the subsequent differential and finite difference equations are shown in Figure 1.

Geometrical considerations are introduced to the subsequent equations in the form of specification of the cross-sectional area as a function of distance below the initial surface, $A = A(y)$. In the event consideration of certain special geometries is desired, for example, cylindrically symmetric ($A \propto r^{0}$), these functional relationships may be simply obtained to yield the cross-sectional area as a function of distance below the initial surface.

It is important to observe that the origin of the y coordinate is fixed in space (relative, say, to the back wall). Thus a control volume at "constant y" contains a fixed, identified piece of material. The origin of the x-coordinate, on the other hand, is tied to the receding heated surface.

3.2.3.3 Conservation of Mass In Moving Coordinate System

Decomposition of the ablation material in-depth is characterized by an irreversible reaction of the following form:

$$\text{plastic} \rightarrow \text{char} + \text{gas}$$

Initially the ablation material is considered to be all plastic, and after decomposition it is all char. Intermediate states need not be considered until later. The mass conservation equation is written neglecting the mass of the gas at any point as being small compared to the mass of solid material and assuming that the transit time of the gas from the point of decomposition to the heated surface is small. Within these constraints the mass conservation equation may be written

$$\left.\frac{\partial \dot{m}_g}{\partial y}\right)_\theta = \frac{\partial}{\partial \theta}(\rho A)_y = A\left.\frac{\partial \rho}{\partial \theta}\right)_y + \rho\left.\frac{\partial A}{\partial \theta}\right)_y \tag{5}$$

where the subscripts indicate variables held constant when performing partial differentiation, but $A = A(y)$ alone, so the term

$$\rho\left.\frac{\partial A}{\partial \theta}\right)_y = 0 \tag{6}$$

and the mass conservation equation becomes

$$\left.\frac{\partial \dot{m}_g}{\partial y}\right)_\theta = A\left.\frac{\partial \rho}{\partial \theta}\right)_y \tag{7}$$

given earlier as Eq. (2). In the above equation, $\dot{m}_g$, represents the mass flow rate of gas past a point, and its derivative with respect to distance is seen to equal the gas generation rate. The total gas flow rate passing a point is obtained by integration of Eq. (7)

$$\dot{m}_g = -\int_y^{y_b} A\left.\frac{\partial \rho}{\partial \theta}\right)_y dy \tag{8}$$

The material density, ρ, and density change rate resulting from decomposition $(\partial\rho/\partial\theta)_y$, is obtained from considering the material formulation. The virgin plastic may consist of up to three decomposible constituents, and the density of the composite is given by Eq. (4)

$$\rho = \Gamma(\rho_A + \rho_B) + (1 - \Gamma)\,\rho_C \tag{4}$$

where $(\rho_A + \rho_B)$ is the density of the resin, ρ_c is the density of the reinforcement, and Γ is the volume fraction of resin in the virgin plastic composite. The division of resin into A and B components is a consequence of the experimentally observed two-stage decomposition process of phenolic resin. The rate of change of density resulting from decomposition is given by differentiating equation (4) with respect to time at constant y.

$$\left.\frac{\partial \rho}{\partial \theta}\right)_y = \Gamma\left(\frac{\partial \rho_A}{\partial \theta} + \frac{\partial \rho_B}{\partial \theta}\right)_y + (1-\Gamma)\left(\frac{\partial \rho_C}{\partial \theta}\right)_y \tag{9}$$

where decomposition of each constituent is given by a rate equation of the Arrhenius form.

$$\left.\frac{\partial \rho_i}{\partial \theta}\right)_y = -k_i e^{-E_i/RT} \rho_{o_i}\left(\frac{\rho_i - \rho_{r_i}}{\rho_{o_i}}\right)^{m_i} \quad \text{for} \quad i = A,B,C \tag{10}$$

It is now necessary to relate these density changes at constant y to the density changes at constant x since we plan to work with the x coordinate system. At any instant in time the density may be expressed purely as a function of spatial position and time, $\rho = \rho(y,\theta)$. Then

$$d\rho = \left.\frac{\partial \rho}{\partial y}\right)_\theta dy + \left.\frac{\partial \rho}{\partial \theta}\right)_y d\theta \tag{11}$$

Differentiating with respect to time at constant x yields

$$\left.\frac{\partial \rho}{\partial \theta}\right)_x = \left.\frac{\partial \rho}{\partial y}\right)_\theta \left.\frac{\partial y}{\partial \theta}\right)_x + \left.\frac{\partial \rho}{\partial \theta}\right)_y \tag{12}$$

From Figure 1 the x and y coordinates are related to the amount of surface recession

$$y = S + x \tag{13}$$

from which

$$\left.\frac{\partial y}{\partial \theta}\right)_x = \frac{dS}{d\theta} \equiv \dot{S} \tag{14}$$

where the surface recession rate, $\dot{S}$, is written as an absolute derivative since $S = S(\theta)$ alone. Substituting this expression into the above equation yields

$$\left.\frac{\partial \rho}{\partial \theta}\right)_x = \left.\frac{\partial \rho}{\partial \theta}\right)_y + \left.\frac{\partial \rho}{\partial x}\right)_\theta \dot{S} \tag{15}$$

which, with Equations (9) and (10), represents the desired form of the mass conservation equation.

3.2.3.4 Conservation of Energy in Moving Coordinate System

The energy equation is written first with respect to a spatially fixed coordinate system. For this purpose, the following functional relationships are presumed:

$$h = h(T,\rho)$$

$$T = T(y,\theta)$$

$$\rho = \rho(y,\theta)$$

$$A = A(y)$$

$$S = S(\theta)$$

therefore

$$h = h(y,\theta)$$

The differential equation governing the conservation of energy within the charring material is obtained by considering the control volume in Figure 1 and equating the net energy transfer rate to the rate of energy change. The resulting equation was cited as Equation (1)

$$\overbrace{\frac{\partial}{\partial \theta}(\rho h A)_y}^{\text{storage}} = \overbrace{\frac{\partial}{\partial y}\left(kA\frac{\partial T}{\partial y}\right)_\theta}^{\text{conduction}} + \overbrace{\frac{\partial}{\partial y}\left(\dot{m}_g h_g\right)_\theta}^{\text{convection}} \tag{1}$$

For the numerical solution it is convenient to consider a coordinate system fixed to the receding surface, as discussed above. To transform the above differential equation, which is written for a point, y = constant, to an equation written for the moving coordinate system, x = constant, the storage term in Eq. (1) may be related to its counterpart in the moving coordinate system by expanding the energy change employing the chain rule:

$$\rho hA = \rho hA(y,\theta)$$

$$d(\rho hA) = \frac{\partial}{\partial y}(\rho hA)_\theta \, dy + \frac{\partial}{\partial \theta}(\rho hA)_y \, d\theta$$

Differentiating partially with respect to time at constant x yields:

$$\frac{\partial}{\partial \theta}(\rho hA)_x = \frac{\partial}{\partial y}(\rho hA)_\theta \left(\frac{\partial y}{\partial \theta}\right)_x + \frac{\partial}{\partial \theta}(\rho hA)_y \tag{16}$$

Introducing Equation (14) and rearranging obtains

$$\frac{\partial}{\partial \theta}(\rho hA)_y = \frac{\partial}{\partial \theta}(\rho hA)_x - \dot{s}\frac{\partial}{\partial y}(\rho hA)_\theta \tag{17}$$

Substition of Equation (19) into Equation (1) with the observation that partial differentiation with respect to x or y at constant time is equivalent, results in the transformed energy equation

$$\overbrace{\frac{\partial}{\partial \theta}(\rho hA)_x}^{\text{I}} = \overbrace{\frac{\partial}{\partial x}\left(kA\frac{\partial T}{\partial x}\right)_\theta}^{\text{II}} + \overbrace{\dot{s}\frac{\partial}{\partial x}(\rho hA)_\theta}^{\text{III}} + \overbrace{\frac{\partial}{\partial x}(\dot{m}_g h_g)}^{\text{IV}} \tag{18}$$

The above terms will be considered separately below.

Term I

$$\frac{\partial}{\partial \theta}(\rho hA)_x = \rho h\left(\frac{\partial A}{\partial \theta}\right)_x + A\frac{\partial}{\partial \theta}(\rho h)_x \tag{19}$$

It is convenient to express the enthalpy change rate in terms of temperature and density change rates. For that purpose it is necessary to set down some specific model for computing enthalpy. It is deemed convenient and fairly reasonable to imagine that partially pyrolyzed material may be regarded, for the purpose of computing material properties, as a mixture of pure char and pure plastic. A convenient quantity for algebraic manipulation is then ϵ_p, the volume fraction of imagined undecomposed material in the control volume. For undecomposed material ϵ_p is 1; for pure char $\epsilon_p = 0$, and for intermediate states of decomposition it may be anywhere in between. Then the density may be written

$$\rho = \epsilon_p \rho_p + (1 - \epsilon_p)\rho_c \tag{20}$$

The total enthalpy per unit volume may be written as the mass weighted average of the enthalpy of the parts

$$\rho h = \epsilon_p \rho_p h_p + (1 - \epsilon_p)\rho_c h_c \tag{21}$$

where

$$h_p = h_p^o + \int_o^T C_{p_p}\, dT \tag{22}$$

and

$$h_c = h_c^o + \int_o^T C_{p_c}\, dT \tag{23}$$

Differentiating Equation (21) obtains

$$\frac{\partial}{\partial\theta}(\rho h) = \rho_p h_p \frac{\partial \epsilon_p}{\partial\theta} + \rho_p \epsilon_p \frac{\partial h_p}{\partial\theta} + \rho_c \frac{\partial h_c}{\partial\theta} - \rho_c h_c \frac{\partial \epsilon_p}{\partial\theta} - \epsilon_p \rho_c \frac{\partial h_c}{\partial\theta} \tag{24}$$

Differentiating Equations (22) and (23), and noting that the char and plastic heats of formation are constant, we have

$$\frac{\partial h_p}{\partial\theta} = C_{p_p} \frac{\partial T}{\partial\theta} \quad \text{and} \quad \frac{\partial h_c}{\partial\theta} = C_{p_c} \frac{\partial T}{\partial\theta} \tag{25}$$

Differentiation of Equation (20) results in

$$\frac{\partial \epsilon_p}{\partial\theta} = \frac{1}{\rho_p - \rho_c} \frac{\partial \rho}{\partial\theta} \tag{26}$$

Substitution of Equations (25) and (26) into (24) yields the desired relation between enthalpy change rate, temperature change rate, and decomposition rate

$$\frac{\partial}{\partial\theta}(\rho h)_x = \left(\frac{\rho_p h_p - \rho_c h_c}{\rho_p - \rho_c}\right)\left(\frac{\partial \rho}{\partial\theta}\right)_x + \rho C_p \left(\frac{\partial T}{\partial\theta}\right)_x \tag{27}$$

where

$$\rho C_p \triangleq \rho_p \epsilon_p C_{p_p} + (1 - \epsilon_p)\rho_c C_{p_c} \tag{28}$$

The specific heat, C_p, is the mass weighted average specific heat of the char and virgin plastic parts, and, as such, it represents the specific heat of the material evaluated in the absence of chemical reactions.

Utilizing the above, and Equation (12), Term I in the differential Equation (11) may be written as follows:

$$\frac{\partial}{\partial\theta}(\rho hA)_x = \rho h\left(\frac{\partial A}{\partial\theta}\right)_x + A\left[\frac{\rho_p h_p - \rho_c h_c}{\rho_p - \rho_c}\left(\frac{\partial\rho}{\partial\theta}\right)_x + \rho C_p\left(\frac{\partial T}{\partial\theta}\right)_x\right] \tag{29}$$

Term II

Term II in Equation (18) will not require any modification.

Term III

For Term III we have

$$\dot{S}\frac{\partial}{\partial x}(\rho hA)_\theta = \dot{S}\rho h\left(\frac{\partial A}{\partial x}\right)_\theta + \dot{S}A\frac{\partial}{\partial x}(\rho h)_\theta \tag{30}$$

Now $A = A(y)$ alone, but $y = x + S$, and $S = S(\theta)$ alone, so we may write $A = A(x,\theta)$

$$dA = \left(\frac{\partial A}{\partial x}\right)_\theta dx + \left(\frac{\partial A}{\partial\theta}\right)_x d\theta \tag{31}$$

Differentiating partially with respect to time at constant y obtains

$$\left(\frac{\partial A}{\partial\theta}\right)_y = \left(\frac{\partial A}{\partial x}\right)_\theta\left(\frac{\partial x}{\partial\theta}\right)_y + \left(\frac{\partial A}{\partial\theta}\right)_x \tag{32}$$

But, since $A = A(y)$ alone, $\partial A/\partial\theta)_y = 0$. Also, since $y = x + S$

$$\left(\frac{\partial x}{\partial\theta}\right)_y = -\frac{dS}{d\theta} = -\dot{S} \tag{33}$$

Combining the above results in

$$\dot{S}\left(\frac{\partial A}{\partial x}\right)_\theta = \left(\frac{\partial A}{\partial\theta}\right)_x \tag{34}$$

Substituting Equation (34) into (30) yields a new expression for Term III.

$$\dot{S}\frac{\partial}{\partial x}(\rho hA)_\theta = \rho h\left(\frac{\partial A}{\partial\theta}\right)_x + \dot{S}A\frac{\partial}{\partial x}(\rho h)_\theta \tag{35}$$

Term IV

Term IV may be written

$$\frac{\partial}{\partial x}\left(\dot{m}_g h_g\right)_\theta = \dot{m}_g \left.\frac{\partial h_g}{\partial x}\right)_\theta + h_g \left.\frac{\partial \dot{m}_g}{\partial x}\right)_\theta \tag{36}$$

Since differentiation with respect to x and y at constant time are equivalent, substitution of the mass conservation Equation (7) into the above gives

$$\frac{\partial}{\partial x}\left(\dot{m}_g h_g\right) = \dot{m}_g \left.\frac{\partial h_g}{\partial x}\right)_\theta + h_g A \left.\frac{\partial \rho}{\partial \theta}\right)_y \tag{37}$$

Substitution of Equations (25), (35), and (37) into the energy differential Equation (18) yields

$$\rho C_p \left.\frac{\partial T}{\partial \theta}\right)_x = \frac{1}{A}\frac{\partial}{\partial x}\left(kA \left.\frac{\partial T}{\partial x}\right)_\theta - \bar{h} \left.\frac{\partial \rho}{\partial \theta}\right)_x + \frac{\partial}{\partial x}(\rho h)_\theta \dot{s} + \frac{\dot{m}_g}{A} \left.\frac{\partial h_g}{\partial x}\right)_\theta + h_g \left.\frac{\partial \rho}{\partial \theta}\right)_y \tag{38}$$

where

$$\bar{h} \triangleq \frac{\rho_p h_p - \rho_c h_c}{\rho_p - \rho_c}$$

The terms in Equation (38) represent, from left to right, the sensible energy accumulation, the net conduction, the chemical energy accumulation, net energy convected as a consequence of coordinate motion, net energy convected by the pyrolysis gases passing through, and the energy convected away by pyrolysis gases generated at the point. All terms are evaluated per unit volume. Note that the pyrolysis gas flow rate past a point, $\dot{m}_g$, is the total flow rate (see Equation (8)) and must be divided by area to be on the same basis as the other terms in the equation.

The finite difference formulation of the above derived differential equations for mass conservation (Equations (9), (10) and (15)) and energy conseration (Equation (38)) are presented in the two succeeding sections.

Before those types are considered, however, it is of passing interest to note that Equation (38) which turns out to be a convenient form for machine treatment, can be cast into more appealing form. Some tedious but straightforward algebra, the details of which are given in Appendix D, yields

$$\rho C_p \left.\frac{\partial T}{\partial \theta}\right|_x = \frac{1}{A}\frac{\partial}{\partial x}\left(kA \left.\frac{\partial T}{\partial x}\right|_\theta\right) + (h_g - \bar{h}) \left.\frac{\partial \rho}{\partial \theta}\right|_y + \dot{s}\rho C_p \left.\frac{\partial T}{\partial x}\right|_\theta + \left.\frac{\dot{m}_g}{A}\frac{\partial h_g}{\partial x}\right|_\theta \quad (39)$$

With the energy equation in this form, each term has a more readily perceivable physical significance.

As a final note, it may be observed that equations (9), (10), and (15) for mass conservation and Equation (38) for energy conservation cannot be used as models for the last ablating node, which is a shrinking as opposed to a drifting node. It will prove not necessary to have differential equations for this node; the difference equations may be obtained directly.

3.2.4 Difference Forms

3.2.4.1 Mass Equation

3.2.4.1.1 Nodes other than the first or last

Experience with the finite difference solution of the preceding differential equations has shown that, generally, a much finer definition of the space derivative is required for an accurate solution of the mass conservation equation than for the energy conservation equation. This is the case because, for most material-boundary condition combinations of interest, the density profile through the material is much steeper than the corresponding temperature profile. As a result, the finite difference spatial grid size selected to represent the mass conservation solution is much smaller than that selected to represent the energy equation solution. Space derivatives for the energy equation solution are obtained by considering an array of nodes, while space derivatives for the mass conservation equations are based upon consideration of a number of nodelets in each node. A schematic representation of the spatial grid is shown in Figure 2 where it is seen that each node (n) remains a fixed distance below the surface (x_n) and has a constant thickness, δ_n. The last node in the ablation material (n = NL) is the one exception to this in that it will continually shrink as surface recession proceeds until it vanishes at which point the next to last node becomes the new last node. Special treatment afforded the last ablating node to include consideration of the shrinking process is described subsequently, in Section 3.2.4.1.3. Referring to Figure 2 it is noted that each node is subdivided into J nodelets, each designated n_j where j ranges from 1 to J for each node. The mass balance equation is satisfied for each nodelet in the following development.

The finite difference representation of Equation (15) results from considering the density change rate of a nodelet. Since the nodes and nodelets remain a fixed distance below the surface ($x_{n,j}$ = const), the density change rate of a nodelet corresponds to the time derivative of density at constant x

$$\frac{\rho'_{n,j} - \rho_{n,j}}{\Delta\theta} = \frac{(\rho_{n,j+1} - \rho_{n,j})\dot{s}}{\delta_{n,j}} + \left(\frac{\partial\rho_{n,j}}{\partial\theta}\right)_d \tag{40}$$

where primed quantities are evaluated at the time $\theta' = \theta + \Delta\theta$, and the subscript d refers to decomposition which is the density change rate at constant y. The nodelet temperature, $T_{n,j}$ required for evaluating the decomposition term (Equation (10)) is obtained by linear interpolation between adjacent nodal centers. As a consequence of the subsequent convenience of obtaining the total nodal density by simple averaging of nodelet densities, the nodelets within a node are selected to be of equal volume. The following sketch illustrates the scheme for obtaining nodelet temperatures for the special case of four nodelets per node (J = 4).

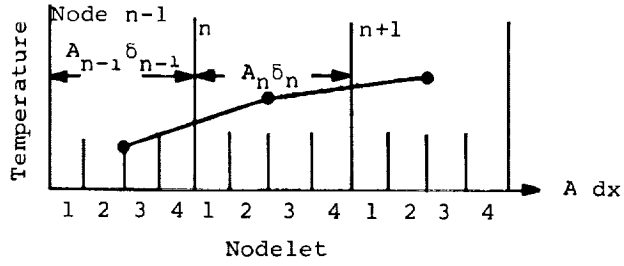

From this sketch it is noted, for example, that

$$T_{n,2} = T_{n-1} + \frac{T_n - T_{n-1}}{(A_n\delta_n + A_{n-1}\delta_{n-1})/2}\left[\frac{A_{n-1}\delta_{n-1}}{2} + \frac{3}{8}\delta_n A_n\right] \tag{41}$$

or, more generally,

$$T_{n,j} = T_{n-1} + \frac{T_n - T_{n-1}}{(A_n\delta_n + A_{n-1}\delta_{n-1})/2}\left[\frac{A_{n-1}\delta_{n-1}}{2} + (j - 0.5)\frac{A_n\delta_n}{J}\right] \tag{42}$$

for

$$j \leq \frac{J}{2}$$

and

$$T_{n,j} = T_n + \frac{T_{n+1} - T_n}{(A_{n+1}\delta_{n+1} + A_n\delta_n)/2} \left[\frac{(j - 0.5)}{J} - 0.5\right] A_n\delta_n \qquad (43)$$

for

$$j > \frac{J}{2}$$

The nodelet density change rate of constituent i resulting from decomposition is obtained from Equation (10) utilizing the above nodelet temperatures.

$$\left.\frac{\partial\rho_{i,n,j}}{\partial\theta}\right)_D = -k_i e^{-E_i/RT_{n,j}} \rho_{o_i}\left(\frac{\rho_{i,n,j} - \rho_{r_i}}{\rho_{o_i}}\right)^{m_i} \qquad (44)$$

It is noted that the decomposition rate depends upon two quantities, $\rho_{i,n,j}$ and $T_{n,j}$, which may vary during a time interval ($\Delta\theta$). If temperature and density variations during a time interval are large enough to significantly effect the decomposition rate, either the time step size must be reduced or a temperature and density more representative of the average over the time interval should be employed in order to obtain a stable solution. Most generally, for problems of practical interest, a nodelet undergoing decomposition is experiencing a density decrease and a temperature increase. Equation (44) suggests that using the density, $\rho_{i,n,j}$, at the beginning of the time interval will result in too large a decomposition rate while using the temperature, $T_{n,j}$, at the beginning of the time interval will result in too small a decomposition rate, for most cases of interest. Since instabilities are usually associated with too large rather than too small a change rate, it is appropriate to consider an implicit treatment of the density while treating the temperature in an explicit manner, at least as a first try. Such an explicit treatment of the temperature is possible because the decomposition energy of organic constituents is small and, as such, the coupling between energy and mass conservation equations is weak for nodes in the decomposition region.

An effective "implicit" treatment of the density in the decomposition equation may be readily obtained from direct integration of Equation (44) holding the temperature fixed over the time interval. The following results:

$$\left(\frac{\partial \rho_{i,n,j}}{\partial \theta}\right)_D = \left(\frac{\rho'_{i,n,j} - \rho_{i,n,j}}{\Delta\theta}\right)_y$$

$$= \frac{\rho_{ri} - \rho_{i,n,j} + \left[(\rho_{i,n,j} - \rho_{ri})^{1-m_i} - \frac{1 - m_i}{\rho_{oi}^{m_i - 1}} k_i e^{-E_i/RT_{n,j}} \Delta\theta\right]^{\frac{1}{1-m_i}}}{\Delta\theta} \tag{45}$$

for $m_i \neq 1$, and

$$\left(\frac{\partial \rho_{i,n,j}}{\partial \theta}\right)_D = \left(\frac{\rho_{i,n,j} - \rho_{ri}}{\Delta\theta}\right)\left[\exp\left(- k_i e^{-E_i/RT_{n,j}} \Delta\theta\right) - 1\right] \tag{46}$$

for $m_i = 1$

These implicit relations yield a much more stable solution than is obtained with Equation (44) treating the density explicitly.* The overall density change rate of a nodelet resulting from decomposition is obtained by summing the decomposition rates of each constituent via Equation (10). The total nodelet density change rate over a time interval due to decomposition and coordinate system motion is obtained from Equation (40).

Since the energy equation is solved on the basis of full nodes rather than nodelets it is necessary to evaluate the total nodal density change rate. For an even number of equally sized nodelets in each node, $\delta_{n,j} \cdot A_{n,j} =$ constant, that is, such that each nodelet has the same volume, the total nodal density change is the arithmetic average of the density changes of all of the nodelets:

$$\frac{\rho'_n - \rho_n}{\Delta\theta} = \frac{1}{J \cdot \Delta\theta} \sum_{j=1}^{J} \left(\rho'_{n,j} - \rho_{n,j}\right) = \dot{s}\left[\frac{\rho_{n,2} - \rho_{n,1}}{\delta_n} + \frac{\rho_{n,3} - \rho_{n,2}}{\delta_n}\right.$$

$$\left. + \cdots\cdots + \frac{\rho_{n+1,1} - \rho_{n,J}}{\delta_n}\right] + \frac{1}{J} \sum_{j=1}^{J} \left(\frac{\partial \rho_{n,j}}{\partial \theta}\right)_d$$

*Calculational results utilizing both integrated and explicit density dependence in the decomposition equation are presented subsequently in Appendix B. Use of the integrated form was suggested in Reference 1, but this device appears to have been largely overlooked in more recent work.

where it is noted that $\rho_{n,J+1}$ is equivalent to $\rho_{n+1,1}$. This equation can be simplified to

$$\frac{\rho'_n - \rho_n}{\Delta\theta} = \dot{s}\,\frac{\rho_{n+1,1} - \rho_{n,1}}{\delta_n} + \frac{1}{J}\sum_{j=1}\left(\frac{\partial\rho_{n,j}}{\partial\theta}\right)_d \qquad (47)$$

3.2.4.1.2 The surface node

In order to have the surface node be at the surface temperature, it is convenient to consider the first node as a half node, with half as many nodelets as the other nodes. With the exception of the surface nodelet, the density evaluation for nodelets of the first node can be performed according to Equation (43), just as for all the nodelets discussed so far.

For the surface nodelet it is necessary for consistency with whatever solution procedures are supplying the surface energy balance information that any material leaving the surface is pure char and hence has the pure char density. If this were not the case, then the surface boundary condition solutions, which are based upon the idea of pure char injection into the surface control volume depicted on page 6, could not be coupled in a consistent way with the in-depth response solution.*

3.2.4.1.3 The last ablating node

The last ablating node must be considered separately, since the rear boundary of this node is stationary with respect to a fixed coordinate system. Within this node, therefore, a variation occurs between the moving and fixed coordinate system. Hence Equation (14) must take the form

$$\left(\frac{\partial y}{\partial\theta}\right)_{x,j} = \dot{s}\cdot\frac{J-j}{J} \qquad (48)$$

for nodelet j $(1 < j < J)$ and where it is noted that the relative motion of the x and y coordinate systems varies from 0 at the rear face of the last node to nearly $\dot{s}$ at its forward face. This results in a slightly modified nodelet mass balance equation, namely,

*This implies that if pyrolysis kinetics are slow a dilemma can arise in the form of mass accumulation in the surface nodelet. This rarely happens. When it does, the wrong tool is being applied to the problem.

This restriction on leaving density is only necessary when a chemistry solution is being used to provide the surface boundary condition. For specified surface recession rate the actual surface nodelet density can be used and no consistency problems arise.

$$\frac{d\rho_{N,j}}{d\theta} = \left(\frac{\partial \rho_{N,j}}{\partial \theta}\right)_d + \frac{\dot{S}}{\delta_{N,j}} \frac{J - j}{J} (\rho_{N,j+1} - \rho_{N,j}) \tag{49}$$

The total density change of the last node will then be the sum of the density changes of each of the nodelets or

$$\frac{d\rho_N}{d\theta} = \frac{1}{J} \sum_{j=1}^{J} \left(\frac{\partial \rho_{N,j}}{\partial \theta}\right)_d + \frac{\dot{S}}{J\delta_N} \sum_{j=1}^{J} (J - j)(\rho_{N,j+1} - \rho_{N,j})$$

$$= \frac{1}{J} \sum_{j=1}^{J} \left(\frac{\partial \rho_{N,j}}{\partial \theta}\right)_d + \frac{\dot{S}}{\delta_N} (\rho_N - \rho_{N,1}) \tag{50}$$

3.2.4.2 Energy Equation

3.2.4.2.1 Nodes other than the first or last

A finite difference representation of Equation (38) can be formulated in a variety of ways. As with the mass equation, however, every effort will be made here to preserve a correspondence with a finite nodal energy balance. For example, the total enthalpy change rate given by Equation (27),

$$\frac{\partial}{\partial \theta} (\rho h)_x = \rho C_p \left(\frac{\partial T}{\partial \theta}\right)_x + \bar{h} \left(\frac{\partial \rho}{\partial \theta}\right)_x \tag{51}$$

represents the nodal enthalpy change resulting from a change in density and a change in temperature. Since enthalpy is a function of T and ρ only in the present analysis, the path followed in going from one temperature-density state to another is inconsequential. A constant temperature path followed by a constant density path, as illustrated,

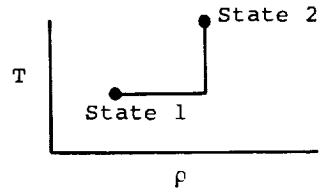

yields the following interpretation of the two terms on the right side of Equation (51)

$$\rho C_p \left.\frac{\partial T}{\partial \theta}\right)_x + \bar{h} \left.\frac{\partial \rho}{\partial \theta}\right)_x = \rho' \bar{C}_p \frac{\Delta T}{\Delta \theta} + \bar{h} \cdot \frac{\Delta \rho}{\Delta \theta} \tag{52}$$

where $\bar{h}$ is evaluated at the initial temperature, and $\rho' \bar{C}_p$ is evaluated at the final density and initial temperature. To be precise $\bar{C}_p$ should be evaluated at some mean temperature as well as at the terminal density, but otherwise the relation is exact since $\bar{h}$ is constant at constant temperature and ρ is constant along the second segment of the selected path.

Equation (38) can be written in finite difference form as

$$\begin{aligned}\left(\rho' \bar{C}_p\right)_n (T'_n - T_n) = \frac{\Delta\theta}{\delta_n A_n} \left(\frac{T_{n-1} - T_n}{\frac{\delta_{n-1}/2}{k_{n-1}A_{n-1}} + \frac{\delta_n/2}{k_n A_n}} - \frac{T_n - T_{n+1}}{\frac{\delta_n/2}{k_n A_n} + \frac{\delta_{n+1}/2}{k_{n+1}A_{n+1}}} \right) + \left\{ h_{g_n} \left(\frac{\partial \rho_n}{\partial \theta}\right)_d \right. \\ - \bar{h} \frac{\Delta \rho_n}{\Delta \theta} + \frac{\dot{m}_{g_n}}{A_n} \frac{h_{g_{n+1}} - h_{g_n}}{\delta_n} \\ \left. + \frac{\dot{S}}{\delta_n} \left[(\rho h)_{T_{n+1}, \rho_{n+1,1}} - (\rho h)_{T_n, \rho_{n,1}} \right] \right\} \Delta\theta \end{aligned} \tag{53}$$

where the use of the nodelet densities in the evaluation of ρh in the final term is motivated by the desire to maintain a consistency between this equation and the mass balances (see Eq. (40)).* In effect the node is considered to be at constant temperature but with nodelet to nodelet density variations.

Explicit temperature treatment of this equation is obvious. Implicit temperature treatments of all orders of complexity are also possible and the selection of the appropriate treatment must be based on a variety of factors - but primarily economy, accuracy, and stability. Because the mass equation is solved explicitly with respect to temperature, it is possible to first solve the mass equation to obtain decomposition rates over the time interval and then, employing these rates, solve the energy equation implicitly in temperature as follows:

*Furthermore, if nodelet densities in the ρh term are replaced by node densities, the overall sub-surface energy balance will not be independent of the choice of enthalpy datum temperature, as can be shown by a lengthy algebraic development.

$$\left(\rho'\bar{C}_p\right)_n (T'_n - T_n) = \frac{\Delta\theta}{\delta_n A'_n}\left(\frac{T'_{n-1} - T'_n}{\frac{\delta_{n-1}/2}{k_{n-1}A'_{n-1}} + \frac{\delta_n/2}{k_n A'_n}} - \frac{T'_n - T'_{n+1}}{\frac{\delta_n/2}{k_n A'_n} + \frac{\delta_{n+1}/2}{k_{n+1}A'_{n+1}}}\right)$$

$$+\left\{\left[h_{g_n} + \left(\frac{\partial h_g}{\partial T}\right)_n (T'_n - T_n)\right]\left(\frac{\partial \rho_n}{\partial \theta}\right)_d - \bar{h}_n \left(\frac{\Delta\rho}{\Delta\theta}\right)_n\right.$$

$$+\frac{\dot{m}_{g_n}}{A'_n}\frac{\left[h_{g_{n+1}} + \left(\frac{\partial h_g}{\partial T}\right)_{n+1}(T'_{n+1} - T_{n+1}) - h_{g_n} - \left(\frac{\partial h_g}{\partial T}\right)_n (T'_n - T_n)\right]}{\delta_n}$$

$$+\frac{\dot{s}}{\delta_n}\left[(\rho h)_{n+1,1} + \left(\rho C_p\right)_{n+1,1}(T'_{n+1} - T_{n+1}) - (\rho h)_{n,1}\right.$$

$$\left.\left.- \left(\rho C_p\right)_{n,1}(T'_n - T_n)\right]\right\}\Delta\theta \qquad (54)$$

where the primed quantities are evaluated at the time $\theta' = \theta + \Delta\theta$. The above equation, with the assumption of constant $\partial h_g/\partial T$, $\bar{C}_p$, and other coefficients over the time interval for a given node permits the direct solution of the energy equation using a simple tri-diagonal matrix solution, as will be described below. Note that the constant specific heat, $\bar{C}_{p_n}$, is evaluated at the final density, ρ'_n, and the initial temperature, T_n, for an implicit solution of the energy equation after an explicit solution of the mass equation.

Equation (54) applies for all ablating nodes except the first and last. Also, for the second node $\delta_{n-1}/2$ becomes δ_1 since the first node is located at the heated surface. The treatment of the two boundary nodes will be considered in the next sections.

3.2.4.2.2 The surface node

As noted in Section 3.2.4.1.2, the surface node is treated as a "half-node" with temperature equal to surface temperature. Two characteristics of this system are significant: the extremely important surface temperature is immediately available for the surface boundary condition specification, and errors in energy content of the "constant temperature" nodes tend to cancel at successive nodal centers as indicated schematically on the following page.

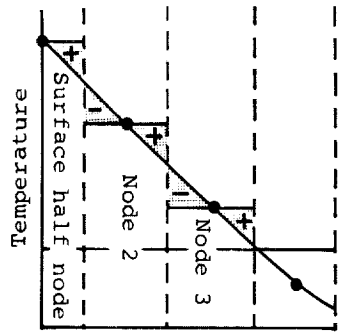

It will be recalled from the introductory Section 3.1.3 on boundary conditions that one of the key purposes of the in-depth response solution is to provide a function $q_{cond}\ (T_w)$. How this is finally accomplished will not become clear until Section 3.4 below, but it is clear enough that the quantity q_{cond}, which ultimately will be calculated as part of the surface energy balance, will play the central role in linking the in-depth solution to the surface energy balance.

Therefore the energy input to the first node will be left simply as q_{cond}, which will replace a term of the form

$$\frac{T_{n-1} - T_n}{\frac{\delta_n/2}{k_n A_n} + \frac{\delta_{n-1}/2}{k_{n-1} A_{n-1}}}$$

Thus we have the energy difference equation for the first node as

$$(\rho' \bar{C}_p)_1 (T_1' - T_1) = \frac{\Delta\theta}{\delta_1 A_1'} \left[q_{cond} - \frac{T_1' - T_2'}{\frac{\delta_1}{k_1 A_1'} + \frac{\delta_2/2}{k_2 A_2'}} \right]$$

$$+ \Delta\theta \left\{ \left[h_{g_1} + \left(\frac{\partial h_g}{\partial T} \right)_1 (T_1' - T_1) \right] \left(\frac{\partial \rho_1}{\partial \theta} \right)_d - \bar{h}_1 \left(\frac{\Delta\rho}{\Delta\theta} \right)_1 \right.$$

(equation continued on following page)

(equation continued from preceding page)

$$+ \frac{\dot{m}_{g_1}}{A'_1} \frac{\left[h_{g_2} + \left(\frac{\partial h_g}{\partial T}\right)_2 (T'_2 - T_2) - h_{g_1} - \left(\frac{\partial h_g}{\partial T}\right)_2 (T'_1 - T_1) \right]}{\delta_1}$$

$$+ \frac{\dot{s}}{\delta_1} \left[(\rho h)_{2,1} + (\rho C_p)_{2,1} (T'_2 - T_2) - (\rho h)_1 - (\rho C_p)_1 (T'_1 - T_1) \right] \Bigg\} \tag{55}$$

3.2.4.2.3 The last ablating node

The energy balance for this node must also be considered separately. Using the mass balance equation above (Eq. (50)) as a guide* the following representation of the energy equation for the last node of the ablating material is obtained:

$$\left(\rho' \bar{C}_p\right)_n (T'_n - T_n) = \frac{2\Delta\theta}{\delta_n A_n} \left(\frac{T_{n-1} - T_n}{\frac{\delta_{n-1}}{k_{n-1} A_{n-1}} + \frac{\delta_n}{k_n A_n}} - \frac{T_n - T_{n+1}}{\frac{\delta_n}{k_n A_n} + \frac{\delta_{n+1}}{k_{n+1} A_{n+1}}} \right)$$

$$- \bar{h} \Delta\rho_n + h_{g_n} \left(\frac{\partial \rho_n}{\partial \theta}\right)_d \Delta\theta + \frac{\dot{s}\Delta\theta}{\delta_n} \left[(\rho h)_{T_n, \rho_n} - (\rho h)_{T_n, \rho_{n,1}} \right] \tag{56}$$

where it is noted that the final term is roughly half of its counterpart in Equation (53) due to the reduced average coordinate motion of this node. This reduction is realized by utilizing the ρh difference across only half the node rather than the full node. The implicit representation of this finite difference equation is:

$$\left(\rho' \bar{C}_p\right)_n (T'_n - T_n) = \frac{2\Delta\theta}{\delta_n A'_n} \left(\frac{T'_{n-1} - T'_n}{\frac{\delta_{n-1}}{k_{n-1} A'_{n-1}} + \frac{\delta_n}{k_n A'_n}} - \frac{T'_n - T'_{n+1}}{\frac{\delta_n}{k_n A'_n} + \frac{\delta_{n+1}}{k_{n+1} A'_{n+1}}} \right)$$

$$+ \left\{ \left[h_{g_n} + \left(\frac{\partial h_g}{\partial T}\right)_n (T'_n - T_n) \right] \left(\frac{\partial \rho_n}{\partial \theta}\right)_d \right\} \Delta\theta - \bar{h}_n (\Delta\rho)_n$$

$$+ \frac{\dot{s}\Delta\theta}{\delta_n} \left[(\rho h)_n + \left(\rho C_p\right)_n (T'_n - T_n) - (\rho h)_{n,1} - \left(\rho C_p\right)_{n,1} (T'_n - T_n) \right] \tag{57}$$

*For an isothermal system with all components having the same enthalpy per unit mass, the energy equation should reduce to the mass equation if absolute consistency is achieved.

with the assumption of constant coefficients this equation will also fall within the framework of the tri-diagonal matrix solution to be discussed below.

The nodelet density in the "leaving" ρh term of Equations (56) and (57) parallels the nodelet density usage in the mass equation (50). The "entering" ρh term retains the nodal density. If this procedure is not followed, a lengthy algebraic development shows that the overall in-depth energy solution will not be independent of the choice of enthalpy datum state.

3.2.4.2.4 Back-up nodes

Energy equations for the back-up nodes are the same as Equation (54) and (57) without the decomposition and convection terms, since the nodal structure only moves in the ablating material. The back-up nodal structure remains fixed.

3.2.4.2.5 Last node

The last node of all, whether an ablating node or a node back-up material, does not of course conduct energy to an adjacent node. Hence the conduction term

$$\frac{T_n - T_{n+1}}{\frac{\delta_n/2}{k_n A_n} + \frac{\delta_{n+1}/2}{k_{n+1} A_{n+1}}}$$

is replaced by a term

$$\frac{T_n - T_{res}}{\frac{\delta_s/2}{k_n A_n} + \frac{1}{h_{res} A_{n+1}}}$$

where h_{res} is a back wall convective heat transfer coefficient (which can include the effects of radiation) and T_{res} is some reservoir sink temperature with which the last node communicates thermally.

3.3 SOLUTION STRUCTURE PREPARATORY TO COUPLING TO THE SURFACE BOUNDARY CONDITION

3.3.1 Tri-diagonal Formulation of the Finite Difference Energy Relations

For a given node n, except the first or last, the finite difference energy relation involves three unknown temperature, T'_{n-1}, T'_n, and T'_{n+1}. For the

last node N, there are only two unknown temperature, T'_{n-1} and T'_n, while the first node equation involves only T'_1 and T'_2, in addition to the heat flux q_{cond}.

If we arrange all the energy relations in order we obtain an array of the form

$$
\begin{aligned}
B_1 T'_1 + C_1 T'_2 &= F_3(q_{cond}) \\
A_2 T'_1 + B_2 T'_2 + C_2 T'_3 &= D_2 \\
A_3 T'_2 + B_3 T'_3 + C_3 T'_4 &= D_3 \\
A_4 T'_3 + B_4 T'_4 + C_4 T'_5 &= D_4 \\
&\ \ \vdots \\
A_N T'_{N-1} + B_N T'_N + 0 &= F_4(T_{res})
\end{aligned}
\tag{58}
$$

The expressions for the coefficients A_n, B_n, C_n and D_n are readily apparent for the finite difference energy equations (50) and (51). For reference, the detailed expressions for the coefficients are assembled in Appendix A.

3.3.2 Solution of Mass Relations and Evaluation of Tri-diagonal Matrix Elements

It is now possible to see clearly what needs to be done for each time step $\Delta\theta$ of the solution in order to prepare for coupling to the surface energy balance. First, using the current values of ρ_n and $\dot{S}$ and T_n, the mass relations (40), (44), (47), (49), and (56) can be solved, yielding "new" gas flow rates $\dot{m}_{g_n}$.

This information may then be used to compute the coefficients of the tri-diagonal energy equation matrix. Once this matrix is set up, the required surface energy relation $q_{cond} = q_{cond}(T_w)$ may be obtained directly, as described in the next section.

3.3.3 Reduction of Tri-diagonal Matrix to Surface Energy Relation

Referring to the array of in-depth energy equations set down symbolically as Set (58) in Section 3.3.1 above, it may be seen that, beginning with the last node, the highest-indexed unknown temperature may be eliminated from each equation of Set (58) in turn. (This is the standard first step in the routine reduction of a tri-diagonal matrix.) Of the resulting simpler set of equations (shown as Set (62) below and discussed at that time) only the top-most is of immediate interest. It may be arranged as

$$q_{cond} = F_5 (T'_1) \tag{59}$$

where F_5 is a simple linear relation. It will be noted that this reduction implies that the A, B, C, and D terms involve only known quantities evaluated at the beginning of the time step. In particular, the surface recession rate $\dot{S}$ is treated in this explicit manner. This causes little error since the energy terms in depth involving $\dot{S}$ are small compared to other energy terms.

Since $T_1 = T_w$, Equation (59) is the desired relation between q_{cond} and T_w implied by the in-depth solution.

It is now necessary to harmonize this in-depth relation with the surface energy balance. This will be discussed in the following section.

3.4 COUPLING IN-DEPTH RESPONSE TO SURFACE ENERGY BALANCE

3.4.1 General Form of Energy Relation

If the surface boundary condition involves an energy balance with convective energy input, the final in-depth relation Equation (55) must now be

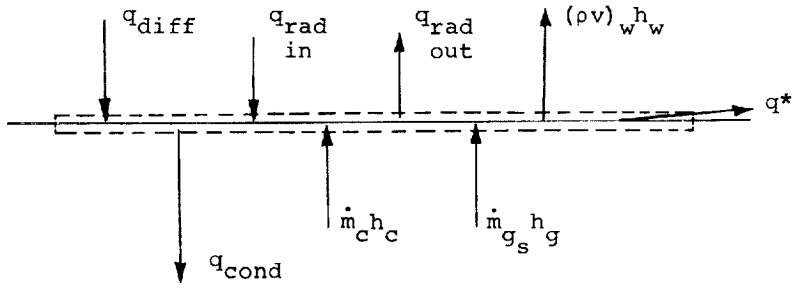

coupled to the surface energy balance illustrated in the sketch above. The surface energy balance may be written

$$q_{diff} + q_{\substack{rad \\ in}} + \dot{m}_c h_c + \dot{m}_g h_g - q_{\substack{rad \\ out}} - (\rho v)_w h_w - q^* - q_{cond} = 0 \qquad (60)$$

where

$$(\rho v)_w = \dot{m}_{g_s} + \dot{m}_c - \dot{m}^*$$

We note that $\dot{m}_g$ and $q_{cond} = F_s(T_w)$ are delivered by the in-depth solution. Other dependencies of interest are

$$h_g = h_g(T_w) ,$$

$$h_c = h_c(T_w) ,$$

$$q_{\substack{rad \\ out}} = q_{\substack{rad \\ out}}(T_w)$$

For the other terms, we have

$\dot{m}^*$, q_{diff}, $q_{\substack{rad \\ in}}$, h_w, q^* = functions of boundary layer edge enthalpy, pressure, boundary layer aerodynamic solution, conservation of chemical element laws, chemical equilibria and/or kinetic relations, upstream events, $\dot{m}_c, T_w$.

3.4.2 Tabular Formulation of Surface Quantities

From the standpoint of the surface energy balance solution the desired relationship may be summarized as

$$\dot{m}^*, q_{diff}, q_{\substack{rad \\ in}}, h_w, q^* = \text{functions of } (\dot{m}_c, T_w)$$

where all the other aspects of the solution are subsumed in some other computational procedure, the details of which are not of immediate interest. This other computational procedure might be based upon a simple film coefficient model of the boundary layer, as will be described below, or it might be based on a very detailed boundary layer solution.

In almost all cases, however, it proves expedient to do this solution outside the charring material solution routine and to make the results available to the surface energy balance operation in the form of tables of q_{diff}, $q_{rad\ in}$, h_w, q^*, and T_w as functions of $\dot{m}_c$, $\dot{m}_{g_S}$, and another variable which is essentially time θ and includes all time dependent aspects such as pressure.

3.4.3 Solution Procedure for the Surface Energy Balance

The energy balance solution procedure is then fairly obvious. An initial guess of the char consumption rate, $\dot{m}_c$, is obtained in some manner. With this $\dot{m}_c$, and with the $\dot{m}_g$ supplied by the in-depth solution, the quantities q_{diff}, $q_{rad\ in}$, h_w, q^*, and T_w are obtained by table look up in the tables provided by the outside surface solution routine. The quantities h_c, h_g and $q_{rad\ out}$ can then be formulated using the T_w so obtained.

Then the surface energy balance (60) can be computed. In general, however, the sum of the terms will not equal zero but some non-zero quantity ϵ called the error. Some appropriate iteration procedure must be devised to select successively better estimates of $\dot{m}_c$ which drive the error ϵ to zero. Experience shows that Newton's procedure, in which the derivative of the error with respect to $\dot{m}_c$ is used to compute the next guess for $\dot{m}_c$ as schematically illustrated below, gives good results.

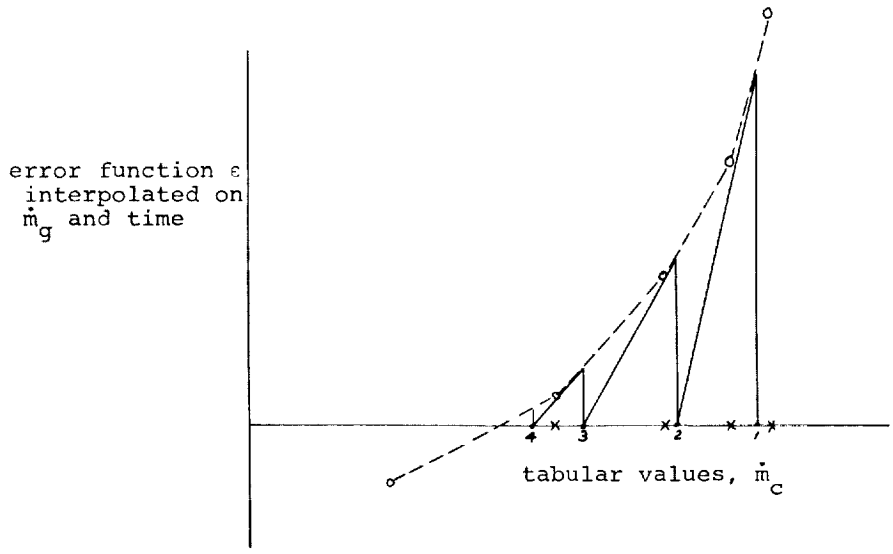

$$\dot{m}_{c_2} = \dot{m}'_{c_1} - \frac{\epsilon}{(d\epsilon/d\dot{m}_c)_1} \tag{61}$$

Since the actual ε function is almost linear between tabular points (radiation introduces slight curvature) this scheme converges rapidly to an answer. Possible traps due to kinks or elbows in the ε function are avoided by limiting corrections on $\dot{m}_c$ to one tabular interval at a time.

3.4.4 Completing the In-depth Solution

Once the surface energy balance has been satisfied to an acceptable level of accuracy, the new surface temperature, T_1', may be substituted in the reduced array of temperatures which began as Set (58). The highest-indexed unknown temperature has been eliminated from each equation in this set in the process of deriving Equation (59). The remaining array looks like

$$
\begin{aligned}
A_2 T_1' + B_2^* T_2' &= D_2^* \\
A_3 T_2' + B_3^* T_3' &= D_3^* \\
A_4 T_3' + B_4^* T_4' &= D_4^* \\
&\vdots \\
A_N T_{N-1} + B_N^* T_N' &= F_4 (T_{res}) \qquad (62)
\end{aligned}
$$

Since T_1' is now known, the first equation of Set (62) yields T_2' directly, then the second equation yields T_3', and so on until the new temperature set is complete.

As a final step, new values for temperature dependent properties can be selected for each node and the entire system is then ready for a new time step, beginning with the decomposition event.

Alternatively, the question arises whether it might be prudent to iterate the entire time step calculation to implicitize the quantity $\dot{S}$ (for which a new value may be computed from the new $\dot{m}_c$), as well as to implicitize the decomposition kinetics and all temperature dependent properties. Usually, however, the quantity $\dot{S}$ exerts only a weak influence on the in-depth solution (which tends to adjust itself to damp out the effects of oscillating $\dot{S}$ values). Furthermore, all important temperature dependent property effects have already been partly implicitized in the in-depth energy solution through linearization. Thus the $\dot{S}$ aspect and the properties aspect do not seem to provide much motivation for iteration.

The decomposition problem is another matter. It is clear that leaving the temperature dependence explicit in the decomposition kinetics is inviting trouble, since for most practical problems of interest the temperature rise is great and the decomposition rates are very sensitively dependent on temperature. Indeed, practical experience shows that for violent transients the problem solution procedure can be disrupted by instabilities due to this explicit temperature dependence.

It is possible that a linearization of this dependence may be sufficient to effect the solutions to most problems without the necessity for iteration. In that case the in-depth temperature matrix is triangular instead of tridiagonal, but the basic solution procedure is not much modified. This device has not yet been incorporated in the charring ablation computer program described in Section 6 below.

3.5 SOLUTION WITHOUT ENERGY BALANCE

The surface boundary condition need not, of course, be an energy balance. Surface temperature and recession rate might be specified. In that case T_1' is known, and the solution of Section 3.4.4 can be completed at once. The quantity q_{cond} is only of "cultural" interest now.

This option is especially useful for parametric studies matching internal thermocouple response predictions to the measured thermocouple responses, using measured surface temperature and recession data, in order to "back-out" thermal conductivity data, determining conductivity as a function of temperature and density. Frequently this procedure is required before a surface energy balance type of calculation can be done since the required thermal conductivity information is not generally available for many materials.

3.6 SOLUTION WITH RADIATION INPUT ONLY AND NO RECESSION

To simulate "cool-down" or "soak-out" problems, convective energy input can be ignored and surface recession supressed. The surface temperature can be determined with a simple version of Equation (60) in which the terms q_{diff}, $q_{rad\ in}$, $\dot{m}_c$, and q^* are zero and for which the terms $\dot{m}_g h_g$ and $(\rho v)_w h_w$ cancel. In this case the wall temperature is the independent variable.

SECTION 4
SOME NOTES ON PROPERTY VALUES

4.1 INTRODUCTION

Some remarks on the various physical property values required for the in-depth solution may help to clarify certain aspects of both the analysis of Section 3 above and the associated computer program. Features which are especially important or somewhat unusual (when compared to most other computation schemes) will be stressed.

4.2 DENSITIES

Section 3.2.3.3 above describes how the decomposition kinetic relations are written for three independently pyrolyzing components requiring ρ_{o_i}, the initial (virgin) density for each component i, and ρ_{r_i}, the final (char) density for each component. Thus the user must supply ρ_{o_i} and ρ_{r_i} for each component, and the resin volume fraction Γ. The program itself computes the overall virgin and char densities from this data.

The user frequently starts with measured values of virgin and char densities and partitions these densities up among the decomposing constituents according to the decomposition kinetic data he is trying to match. The next section gives some discussion of this point.

4.3 KINETIC DATA

Equation (4b) of Section 3.2.3.3 indicates that in addition to the ρ_{o_i} and ρ_{r_i} data, the kinetic constants k_i, m_i and ε_i/R are required for each constituent of the decomposing material. The required data, much of which may be located in the literature, are obtained from thermogravimetric (TGA) experiments. The observed decomposition kinetics may be modelled with one, two, or three kinetic regimes as required. Experience shows that more than three regimes are not required for materials of current interest. Indeed, the great majority of materials is well described by only a single kinetic relation.

As noted in Section 4.2 above, the selection of the decomposing constituents influences the partition of the densities among the component densities ρ_{o_i} and ρ_{r_i}.

It will be noted that the decomposing constituents are selected to match TGA data and have no explicit connection to the identification of actual molecule types. Of course, it frequently happens that constituents clearly

identifiable on TGA traces do represent particular molecules or groups of similar molecules, but this is a secondary matter of no significance to the in-depth solution.

4.4 SPECIFIC HEATS

The transient in-depth solution naturally requires data on the specific heats of the virgin material and the char. These are supplied to the program as tabular functions of temperature.

For partially degraded material with $\rho_c < \rho < \rho_p$, the analysis of Section 3.2.3.4 above has introduced the model that the specific heat is a particular kind of mass mean specific heat. In this model, partially degraded material is thought of as a mixture of pure char and pure virgin material. The specific heat (and hence the enthalpy) of partially pyrolyzed material is thus a mass weighted average of the virgin and char specific heats.

This model is convenient and plausible. Furthermore, the specific heats of virgin and char material usually differ only slightly, so that the choice of a mixture model is not very important.

4.5 HEAT OF FORMATION

Enthalpies for char and virgin material are computed as integrals of the specific heat function from the datum temperature to the temperature of interest, plus a heat of formation. Equations (22) and (23) above indicate this calculation. Hence, the user of the computer program must supply heat of formation data. For most materials such data may be found in various tabulations, or may be derived from heat of combustion or heat of pyrolysis data. In the case of materials for which no measured data are available, the required heats of formation may usually be obtained by theoretical methods or from rules of thumb regarding the amount of energy associated with each type of chemical bond. For most materials the heats of formation of char and virgin plastic have only a minor effect on any ablation results, and hence, great accuracy is not required.

The pyrolysis gas heat of formation is much more significant and will be discussed in Section 4.7.

4.6 HEAT OF PYROLYSIS

Inspection of the energy Equation (39) reveals that the "heat of pyrolysis" or energy effect associated with the degradation of virgin material to char is given by $(\overline{h} - h_g)$, Btu per pound of pyrolysis gas formed. The computer

program automatically calculates this temperature dependent quantity as needed, employing the input specific heat functions and heats of formation.

4.7 PYROLYSIS GAS ENTHALPY

The in-depth energy Equations (38) and (39) indicate that it is most convenient to have the pyrolysis gas thermal properties as a simple tabulation of enthalpy versus temperature. If it can be assumed that the pyrolysis gases are in chemical equilibrium as they pass through the char, it is a simple matter to run a series of equilibrium chemistry solutions with any convenient computation scheme to obtain the necessary enthalpy table, provided that the elemental make-up of the gas is known. The required elemental data can be obtained from virgin and char density and elemental analysis measurements.

Unfortunately, such equilibrium calculations often indicate that solid carbon particles should precipitate out of the pyrolysis gas. Allowing these particles to collect on the char structure complicates the analysis enormously (see the sixth report of the present series). Thus the analyst is tempted to either

(1) Allow the solid carbon to form, but require it to travel out of the char with the gases

(2) Suppress carbon formation in the enthalpy calculation, thus introducing a kinetic consideration.

Both of these techniques are often tried in practice.

To do an accurate calculation of the pyrolysis gas enthalpy accounting for all possible kinetically controlled reactions would be very difficult and would require information about the initial molecular configurations in the pyrolysis gas, information not usually available. It is important to recognize, however, that the in-depth solution only requires an enthalpy-temperature function, so that any physical model for which data are available can be accommodated without any changes. In this sense the treatment of the pyrolysis gas kinetics is quite general, excluding only carbon deposition ("coking") and char erosion. Changes of gas enthalpy with pressure are secondary and are ignored.

It is unfortunate that energy absorption by the pyrolysis gases as they pass through the char is very important for most materials of interest. Hence, it is important to choose a physical model which is accurate in obtaining the gas enthalpy curve.

4.8 THERMAL CONDUCTIVITY

Thermal conductivity, as a function of temperature, is required for the virgin material and the char. Conceptually, this presents no difficulties although in practice good data are very hard to obtain. (Many of the applications of the computer program are for backing-out conductivity data from measured thermocouple responses taken from instrumented test samples.)

The treatment of conductivity for partially degraded material is a controversial, interesting, obscure, and very important topic. In the past it it was deemed sufficient to follow the model used for specific heat and to use a linear interpolation on virgin material mass fraction:

$$k = xk_p + (1 - x)k_c$$

where the partially degraded material is regarded as a mixture of virgin material and pure char. The quantity x is the pounds of virgin per pound of partially degraded substance. It equals unity for virgin plastic and zero for pure char, and at intermediate densities can be shown to be

$$x = \frac{\rho_p}{\rho_p - \rho_c}\left(1 - \frac{\rho_c}{\rho}\right)$$

Recent experiments have shown, however, that while this model may be a good one for specific heat it can sometimes be a very poor one for thermal conductivity. Many materials display, shortly after decomposition begins, a conductivity appreciably lower than either the virgin conductivity or the char conductivity, a circumstance which cannot be predicted by the model described above. Therefore, a recent modification to the computer program* has introduced a more general expression

$$k = f_1(x)k_p + f_2(x)k_c$$

where f_1 and f_2 can be input as general tabular functions of x. With this device, formerly inexplicable in-depth thermocouple response could be "predicted" quite accurately. It appears that the surface temperature history is

*This work is reported in Rindal, R. A., Clark, K. J., and Moyer, C. B.: Experimental and Theoretical Analysis of Ablative Material Response in a Liquid Propellant Rocket Engine, Fourth Quarterly Progress Report, NASA Lewis Research Center, Cleveland, Ohio, Contract No. NAS3-7945, 1966.

little affected by the new model for mixture conductivity, but the temperature profile through the narrow pyrolysis zone is drastically altered for those materials in which the conductivity depression is marked, in particular the rapid decomposers such as nylon phenolic.

4.9 SURFACE EMISSIVITY ε

The role and importance of this temperature dependent quantity need no elaboration. The chief difficulty is to obtain good data. If partially degraded material is at the surface, the emissivity of virgin material and char may be averaged in the same manner as the specific heat.

4.10 HEAT OF ABLATION, HEAT OF COMBUSTION

The reader will note that no such quantity as heat of ablation or heat of combustion is required as input information for the surface energy balance options of the analysis. It will be recalled that in these options the in-depth solution is coupled to a general chemistry solution. Heats of ablation and heats of combustion are empirical devices designed to circumvent the chemistry solution. These approaches have their advantages, but they are difficult to generalize. The only reliable general procedure involves a complete surface chemistry solution. With such a solution in hand it is possible to calculate the heat of ablation or heat of combustion as a matter of interest and for correlating purposes.

4.11 SURFACE SPECIES

The identity of the chemical species existing at the ablating surface is usually not evident a priori for complex materials. This information is not required as input, however. It is a consequence of the chemistry solution.

4.12 CONCLUSION

The analysis has been formulated to require the input of fundamental physical information in such a way as to preclude any inconsistencies in energy terms (such as enthalpies) and in mass terms. Within these restrictions, only input of directly measureable data is required. The three items which are probably most important in their influence on computed results, the gas enthalpy, the thermal conductivity, and the surface emissivity, are unfortunately the items most difficult to obtain good data for, but this, of course, is an inherent feature of the problem, not a peculiarity of the analysis presented.

SECTION 5

NOTES ON FILM COEFFICIENT MODEL OF THE BOUNDARY LAYER WITH HEAT TRANSFER, MASS TRANSFER, AND CHEMICAL REACTION

5.1 INTRODUCTION

Section 3.4 above described in general terms how the in-depth energy solution can be coupled to the heated surface energy balance boundary condition. This coupling is made, through the energy balance, to some computational scheme which accounts for the basic transport physics (momentum, energy, chemical species) and the basic conservation laws for the boundary layer.

The boundary layer integral matrix procedure developed under the present contract and presented in coded form as the BLIMP program consitutes a very accurate and complete procedure for generating boundary layer transport solutions suitable for this coupling. As might be expected, however, this complex routine consumes much valuable computer time for each solution. Hence, economic considerations encourage the use of some simpler boundary layer procedure whenever possible.

For this purpose the basic in-depth charring material solution procedure has been coupled to a film coefficient boundary layer model which offers speedy and economical approximate solutions which still retain all of the essential chemical features of ablation events. Thus the in-depth program exists in coupled form in two distinct versions, one coupled to the BLIMP program, and one coupled to a film coefficient model. Section 3.4 above describes the coupling in general terms applicable to both coupled versions. For details on the BLIMP program and the associated integral analysis the reader may refer to the summary report of the present series (in preparation - see Foreword) and to Reference 35. Unfortunately, a corresponding detailed presentation of the fundamentals of the film coefficient model used for the other coupled version has not previously been presented. Therefore the present section offers a few remarks on the film coefficient model as supplementary information. Since the chief purpose of the present report is to describe the in-depth solution procedure, the following remarks on the film coefficient surface model will be in outline form, with arguments and developments omitted.

5.2 GENERAL POSITION, IMPORTANCE, AND HISTORY OF FILM COEFFICIENT MODELS APPLIED TO MASS TRANSFER WITH CHEMICAL REACTIONS

5.2.1 General Remarks

Probably the great majority of boundary layer heat and mass transfer solutions with chemical reactions have been built on either

(1) An empirical approach for any given problem, or

(2) A complete, accurate solution applied to specific, restricted chemical systems.

Each of these alternatives can be well defended for particular problems. In the development of large and costly computer programs, however, it is important to build in as much generality as possible. It has been known for a long time that film coefficient boundary layer models, originally developed for heat transfer calculations, can provide much generality by an extension to include mass transfer effects. The film coefficient approach provides the necessary transport information, and some appropriate chemical solution routine can provide the necessary chemistry solution.

The fundamental analysis involved in using such a film coefficient scheme involves two key parts:

(1) Derive the film coefficient mass transport relations, and

(2) Derive the film coefficient energy transport relation

The actual use of the formulation requires another step, that of calculating the film coefficients $\rho_e u_e C_H$ and $\rho_e u_e C_M$. This final aspect is not simple, especially for high rates of mass transfer (blowing) from the surface, and indeed for strongly non-similar boundary layers probably cannot be carried out in a useful way. Nevertheless this task can be carried out for a great many problems of importance.

The first two tasks cannot be carried out without specific consideration of the calculation of the film coefficients unless rather loose, heuristic arguments are accepted. The number of cases in which Steps (1) and (2) can be carried out with precision is rather small.

In one particular case, however, Steps (1) and (2) can be carried out: if $Le = 1$ and all mass diffusion coefficients are equal, then for a great many problems it is possible to calculate $\rho_e u_e C_H$, demonstrate that $C_M = C_H$, and carry out Steps (1) and (2) without difficulty, regardless of the complexity of the chemical events involved. References 36 and 37 provide many examples of combined heat and mass transfer for this case, covering a very wide range of application areas. This simple model is included as part of the coupled computational procedures, but since it appears as a special case of a more general formulation to be described below, any further discussion will be postponed.

Although the $Le = 1$ and $C_M/C_H = 1$ case provides very powerful simplicities in analysis, it is quite frequently not an accurate representation

of the physical situation in rocket nozzle and reentry problems. The very wide range of molecular weights of the chemical species involved makes the equal diffusion coefficient assumption inaccurate.

Therefore, there is a strong incentive to extend the film coefficient formulation to cases in which, as a first improvement, $C_M \neq C_H$, and as a further improvement, the mass diffusion coefficients are not equal. In the sections below we shall consider these improvements in turn.

5.2.2 History of Film Coefficient Model for $C_M \neq C_H$

It can be shown, for the case in which $Le \neq 1$ but all the mass diffusion coefficients are equal, that it is generally possible and useful to write the diffusive flux of a chemical element away from the wall to the boundary layer as

$$\tilde{j}_{k_w} = \rho_e u_e C_M (\tilde{K}_{k_w} - \tilde{K}_{k_e}) \tag{63}$$

Extended discussions of this relation may be found in References 24, 26, 37, and 38.

The corresponding energy transfer relation is not so easily established, unfortunately. Exact arguments can be carried through only for the case $C_M = C_H$; for the present case some limiting or perturbation type arguments can be carried through for special problems. For example, the case of no net mass transfer and a frozen boundary layer is considered in a heuristic way in References 37 and 39. Spalding gives a summary of the state-of-the-art for this special problem in Reference 40, along with an extensive bibliography. Lees discusses this case in Reference 41, along with a number of other cases to be mentioned later, as do Fay and Riddell for the specific case of air in Reference 42. For "almost frozen" boundary layers (still with no net mass addition) Spalding gives brief discussions of the recommended film coefficient energy equation in References 37 and 40. For very reactive boundary layers with no net mass addition, discussions are given by Lees in Reference 41, quoting only Fay and Riddell's results for air in Reference 42.

For the more important case of net mass addition to the boundary layer with chemical reactions, the discussions presented in the literature for the case $C_M \neq C_H$ appear to be limited to Lees in Reference 41 for the frozen boundary layer and to References (26) and (38). The Lees analysis considers the governing boundary layer differential equations and derives, for the frozen boundary layer case, an expression for the rate of energy transfer to the wall

in which heat and mass transfer coefficients have been identified. The development of References (26) and (38), most completely presented in Reference (38), features a looser argument based on the similar appearance of the momentum, mass, and energy differential equations of the boundary layer. The analysis of Lees and the argument of Reference (38) lead to essentially the same surface energy equation, which will be discussed in Section 5.3 below.

5.2.3 History of Extension to Unequal Mass Diffusion Coefficients

Reference 26 proposes a film coefficient model extended to account for the effects of unequal diffusion coefficients. This extension, which appears to be unique, is discussed in Section 5.3 below.

5.3 DISCUSSION OF FILM COEFFICIENT EXPRESSIONS

5.3.1 Mass Transfer

For equal mass diffusion coefficients, the diffusive mass transport rate of an element k away from the surface is given by Equation (63). This equation can be "derived" for many cases of interest by a solution of the governing boundary layer differential equation. In such a derivation, C_M takes on the meaning of a convenient collection of physical quantities which is essentially independent of the "driving forces" $\tilde{K}_{k_w}$ and $\tilde{K}_{k_e}$. Of course, Equation (63) can define or correlate C_M in all problems, but it is generally preferable to adhere to the first interpretation.

For unequal mass diffusion coefficients, Reference (26) shows that if the mass diffusion coefficients are related to each other in a particular way (which, in fact, appears to represent reality very closely) then it can be hypothesized from a study of the relevant differential equations that the diffusion rate of a chemical element at the wall should be represented by

$$\tilde{J}_{k_w} = \rho_e u_e C_M (\tilde{Z}^*_{k_w} - \tilde{Z}^*_{k_e}) \tag{64}$$

where

$$\tilde{Z}^*_k \triangleq \sum_{i=1}^{I} \alpha_{ki} Z^*_i \tag{65}$$

$$Z_i^* \triangleq \frac{Z_i^{\gamma} K_j^{1-\gamma}}{\sum_j Z_j^{\gamma} K_j^{\gamma-1}} \tag{66}$$

$$Z_i \triangleq \frac{\mathcal{M}_i x_i}{F_i \mu_e} = \frac{\mathcal{M} K_i}{F_i \mu_e} \quad \text{since} \quad \mathcal{M}_i x_i = \mathcal{M} K_i \tag{67}$$

and

$$\mu_e \triangleq \sum_i \frac{\mathcal{M}_i x_i}{F_i} = \mathcal{M} \sum \frac{K_i}{F_i} \tag{68}$$

The factors F_i in these equations derive from the particular relation between the binary diffusion coefficients which must hold if the governing differential equations are to reduce to the forms from which Relation (64) can be inferred. This relation is

$$\mathcal{D}_{ij} = \frac{\overline{D}}{F_i F_j} \tag{69}$$

and can be regarded as an accurate correlation of experimental data for the binary diffusion coefficient $\mathcal{D}_{ij}$. The quantity $\overline{D}$ is a constant for a given pressure. The constants F_i depend weakly on temperature.

Thus the rate of diffusion of a chemical element away from the wall is given by either Equation (63) if the diffusion coefficients are equal, or by Equation (64) for unequal diffusion coefficients. Note that for equal diffusion coefficients $\tilde{Z}_k = \tilde{K}_k$ so that Equation (64) reduces to Equation (63), as it must.

Equations (63) and (64) thus provide the specification of the diffusive fluxes necessary to the surface mass balance operations. The overall surface mass balance for an element k thus becomes for an ablating, pyrolyzing material (in the absence of condensed phase removal)

$$\dot{m}_c \tilde{K}_{k_c} + \dot{m}_{g_s} \tilde{K}_{k_g} = \rho_e u_e C_M (\tilde{Z}^*_{k_w} - \tilde{Z}^*_{k_e}) + (\rho v)_w \tilde{K}_{k_w} \tag{70}$$

Use of this equation will be discussed in Section 5.4 below.

5.3.2 Energy Equations

The expression for the diffusive energy flux from the boundary layer to the wall obtained by Reference 26 for equal diffusion coefficient (which is

very similar to the less general expressions derived by Lees) is

$$q_{diff} = \rho_e u_e C_H \left(H_{sr}^{T_b} - h_{sw}^{T_b} \right) + \rho_e u_e C_M \sum_i (K_{i_e} - K_{i_w}) h_i^{T_b}, \quad T_b = T_w \tag{71}$$

In this equation it will be noted that the enthalpies of the edge gas and the surface gas have been divided into "sensible" and "chemical" parts. This division has been necessary in order to assemble the boundary layer differential equation terms into groups which resemble groups in the mass and momentum differential equations. This resemblance leads to Equation (71) as an energy model of Equation (63). However, in order to establish the resemblance it turned out to be necessary to say that the split between "chemical" and "sensible" enthalpy occurs at T_w. All enthalpy at this temperature is to be called "chemical" enthalpy and all additional enthalpy at temperatures above this "split temperature" or "base temperature" is the "sensible enthalpy" contribution. The base temperature is not to be confused with the "datum temperature," at which the total enthalpy of certain basis chemicals (usually the elements in certain defined states of aggregation) is zero.

This enthalpy splitting artifice employed to obtain Equation (71) need not be retained any longer however. The term H_{sr}, measured above the base temperature $T_b = T_w$, may be written

$$H_{sr}^{T_w} = \underbrace{\sum_i K_{i_e} \left[\int_{T_w}^{T_r} C_{P_i} dT + \int_{T_o}^{T_w} C_{P_i} dT + h_i^{T_o} \right]}_{H_{er}^{T_o}} + (rf) KE_e$$

$$- \underbrace{\sum_i K_{i_e} \left[\int_{T_o}^{T_w} C_{P_i} dT + h_i^{T_o} \right]}_{h_{ew}^{T_o}} \tag{72}$$

where the total (sensible + chemical) enthalpy of the edge gases at the wall temperature, h_{ew}, has been added and subtracted in order to form the difference:

$$H_{sr}^{T_w} = (H_r - h_w)_{\text{edge gas}} \tag{73}$$

Recalling that $h_{sw}^{T_w} = 0$, we may write

$$\left(H_{sr}^{T_w} - h_{sw}^{T_w} \right) = \left(H_r - h_w \right)_{\text{edge gas}} \tag{74}$$

where the total enthalpies in the above relation may be evaluated above any datum temperature. Note that the enthalpy of the edge gas at wall temperature is for the chemical composition <u>frozen</u> at the boundary layer edge conditions, <u>not</u> the equilibrium enthalpy of edge gas at the wall temperature. Hence the diffusive flux q_{diff} becomes

$$q_{diff} = \rho_e u_e C_H (H_r - h_w)_{\substack{\text{edge} \\ \text{gas}}} + \rho_e u_e C_M \sum_i (K_{i_e} - K_{i_w}) h_i^{T_w} \tag{75}$$

The T_w in the final term is now the last remnant of the splitting operation, but $h_i^{T_w}$ merely means the enthalpy of molecular species i at the wall temperature. The quantity $(H_r - h_w)_{\text{edge gas}}$ does not depend on the choice of the base state since each enthalpy is for the same physical material, namely frozen edge gas.

Now the overall surface energy balance may be written as

$$\rho_e u_e C_H (H_r - h_w)_{\substack{\text{edge} \\ \text{gas}}} + \rho_e u_e C_M \left[\sum_i (K_{i_e} - K_{i_w}) h_i^{T_w} + B_c' h_c + B_g' h_g - B' h_w \right]$$

$$+ \alpha_w q_{rad} - F\sigma\epsilon T_w^4 - q_{cond} = 0 \tag{76}$$

Only one final detail deserves attention. Equations (75) and (76) have been derived in Reference 38 with rather loose arguments. Any checks on the correctness and applicability of these equations are of importance. One key check requires the results computed from Equation (76) to be independent of the enthalpy datum state. A lengthy argument can be constructed to show that this is the case. (Equation (75) alone does depend on the datum state, of course, through the $h_i^{T_w}$ term.)

As a final point it may be observed that the derivation of Equations (75) and (76) given in Reference 26 does not include any restrictions about the

location of the chemical reactions. It cannot be firmly concluded, however, that Equation (75) holds for a strongly reacting boundary layer (except, of course, in cases where Equation (75) is used to define C_M or C_H). Indeed, the separation between the frozen term for heat transfer and the enthalpy term for mass transfer suggests that Equation (75) applies only to a frozen boundary layer, reactive wall case. Furthermore, frozen boundary layer analyses lead to equations equivalent to Equation (75) in References 40 and 41. Lastly, physical arguments can be constructed to suggest that for highly reactive boundary layers it should be impossible to write general equations of the form of Equation (75). The discussion of pages 263-275 of Reference 37 is of interest in this regard.

It may be expected that Equations (75) and (76) may apply with good accuracy to frozen and nearly frozen boundary layer problems, but are probably less accurate for reactive boundary layers. An indication of the accuracy of equations such as (75) for highly reactive boundary layers may be obtained by referring to the numerical boundary layer solutions of Fay and Riddell (Reference 42). Fay and Riddell's results differed only slightly whether the boundary layer was treated as frozen with a catalytic wall or if equilibrium was assumed throughout the boundary layer. Even though their solutions are limited to air stagnation flow it is believed reasonable to generalize their conclusion* to include gases other than air and for body locations other than the stagnation point. If this generalization is accepted, Equation (75) may be employed for equilibrium, as well as frozen boundary layers, with little loss in accuracy.

Reference 26 extends Equations (75) and (76) to the case of unequal mass diffusion coefficients by analogy arguments. The resulting equations resemble Equation (64). The diffusional energy flux to the wall becomes

$$q_{diff} = \rho_e u_e C_H (H_r - h_w)_{\substack{edge \\ gas}} + \rho_e u_e C_M \sum_i (Z^*_{i_e} - Z^*_{i_w}) h_i^{T_w} \qquad (77)$$

and the overall energy balance becomes

*"... the heat transfer is almost unaffected by a nonequilibrium state of the boundary layer provided the wall is catalytic and the Lewis Number near unity."

$$\rho_e u_e C_H (H_r - h_w)_{\substack{edge \\ gas}} + \rho_e u_e C_M \left[\sum_i (Z^*_{i_e} - Z^*_{i_w}) h_i^{T_w} + B'_c h_c + B'_g h_g - B' h_w \right]$$

$$+ \alpha_w q_{rad} - F\sigma\varepsilon T_w^4 - q_{cond} = 0 \qquad (78)$$

Equations (77) and (78) are somewhat less well founded than the corresponding Equations (75) and (76), but the equations do have plausibility. Furthermore, the equations reduce to Equations (75) and (76) for equal diffusion coefficients, as they should, and Equation (78) can be shown to be independent of the enthalpy datum state and thus fulfills a basic physical requirement.

5.4 USE OF FILM COEFFICIENT EQUATIONS TO CALCULATE SURFACE ENERGY BALANCE

5.4.1 Basic Aspects

The film coefficient model has provided simple expressions for the diffusive transport rates of mass and energy through the boundary layer to the wall. It is now necessary to indicate how these relations may be expeditiously used in computing the surface energy balance. Section 3.4.2 above describes how it is useful before doing the surface energy balance, to have the diffusive flux terms and h_w, q^*, and T_w as functions of $\dot{m}_c$ and $\dot{m}_{g_s}$ before forming the energy balance. For this purpose, the film coefficient mass transport relations may be coupled to some convenient chemistry routine which solves the coupled mass balance + chemistry problem. Equations (75) and (78) suggest that $\dot{m}_c$ and $\dot{m}_{g_s}$ can be normalized on $\rho_e u_e C_M$ to increase the generality of this procedure. B'_c and B'_g can then be regarded as independent variables in the construction of a table of values of T_w, $\sum Z^*_{i_e} h_i^{T_w}$, and $\sum Z^*_{i_w} h_i^{T_w}$ for given pressure, edge composition, char composition, and gas composition. (The term q^* may be lumped with this last term if desired.)

The resulting table meets all the requirements outlined in Section 3.4.2 and can be used for an iterative determination of that B'_c which satisfies the surface energy balance, given B'_g from the in-depth solution.

The Aerotherm Equilibrium Surface Thermochemistry Program (EST) is a coupled mass balance - equilibrium chemistry routine which generates such tables for chemical equilibrium conditions. Reference 43 describes this program. A somewhat newer version with improved computational techniques is denoted the Aerotherm Chemical Equilibrium Program (ACE) and is described

in Reference 44. This program allows certain reactions to be kinetically controlled and hence has more generality.

5.4.2 Input and Correction of Heat Transfer Coefficient

To employ the film coefficient formulation just described, the program user must provide the program with values of the heat transfer coefficient $\rho_e u_e C_M$ as functions of time. Two practical problems must be settled in this respect:

(1) How is C_M related to C_H?

(2) Can both C_M and C_H be specified as functions of edge conditions (i.e., of time) independent of the subsequent problem solution (i.e., mass transfer rates and body shape)?

In answer to the first question it may be stated that within the present formulation it is adequate to take the ratio C_M/C_H as a constant. The value of this constant is a measure of the ratio of the mean mass transfer aspects of the boundary layer to the mean heat transfer aspects. For equal mass diffusion coefficients, a vast amount of experimental data (as summarized, for example, in Reference (37)) suggest the correlation $C_M/C_H = Le^{\gamma}$. It may be hypothesized that for unequal mass diffusion coefficients the same procedure may be employed with the Lewis Number, Le, defined by the procedure set forth in Reference 26 involving $\bar{D}$. Thus, the input to the program consists of a time table of values for $\rho_e u_e C_M$ and the constant factor C_M/C_H.

The answer to question (2), changes of C_H with body shape are occasionally of interest and may easily be accounted for. A more important problem concerns the dependence of C_H on the actual rate of mass transfer. This problem has been ignored up to now, the implication being that C_H is determined by the boundary layer edge aerodynamics alone. This is known to be incorrect. The value of C_H depends fairly strongly on $\dot{m}$. If we denote the C_H with $\dot{m} = 0$ as C_{H_0}, this dependence is shown by both data and analysis to be accurately represented by

$$\frac{C_H}{C_{H_0}} = \frac{\varphi}{e^{\varphi}-1} \tag{79}$$

where

$$\varphi \triangleq \frac{2\lambda \dot{m}}{\rho_e u_e C_{H_0}} \tag{80}$$

Equation (79) accurately correlates a large amount of laminar data if λ is chosen as 0.5. For turbulent flow a λ of 0.4 appears to be slightly better. The computer program provides for λ as an input parameter and then automatically computes the "blowing reduction."

5.5 CONCLUSIONS

A film coefficient model for boundary layer heat and mass transfer with chemical reactions can be developed for the governing differential equations of the boundary layer. Of the resulting film coefficient expressions, those for mass transport can be coupled to any convenient chemistry routine to provide boundary conditions for an in-depth response calculation. The boundary information and the in-depth calculation are coupled through the film coefficient surface energy balance, providing a complete link between the boundary layer and the sub-surface material.

The film coefficient model of the boundary layer provides a powerful, economical, and quite general alternative to empirical procedures and to elaborate "exact" procedures. The model can be proved to be accurate for a wide range of problems, and appears to apply with good accuracy for an even wider range of problems for which good accuracy proofs cannot be constructed.

SECTION 6
PRESSURE DROP

The pressure drop across the char layer resulting from pyrolysis gas flow is of interest because it may give rise to excessive char stress levels. Knowledge of the pressure distribution through the char is necessary for evaluating char layer stress levels. An empirical relation for evaluating the pressure distribution through the char layer is rationalized and presented first, in Section 6.1 and is followed, in Section 6.2 by the finite difference formulation.

6.1 PRESSURE DROP CORRELATION EQUATION

In order to obtain an expression relating local pressure in the char layer to other pertinent variables it is useful to examine experimental data taken for a range of variation of the pertinent parameters of interest, and to deduce the most significant effects by generalizing this data. The data presented by Green in Reference 45 is employed for this purpose. Green presents a compilation of data for flow of various gases through a wide variety of porous media for a large range of flow conditions. In order to relate

pressure gradients to viscous and inertial forces he employs the correlation equation first proposed by Reynolds:

$$\frac{dP}{dy} = \alpha\mu v + \beta\rho v^2 \tag{81}$$

where the first term represents viscous forces and the second, momentum forces. The quantities α and β are empirical coefficients, μ is the gas viscosity, and ρ is the gas density. The velocity (v) in Equation (81) is a "superficial velocity" defined on the basis of the gas flow rate per unit projected area in a plane normal to the velocity vector.

$$v \triangleq \frac{\dot{m}_g}{\rho A} \tag{82}$$

Referring to the above equations, the ratio of inertial to viscous forces may be written as:

$$\frac{\text{Inertial Force}}{\text{Viscous Force}} = \frac{\beta\dot{m}_g}{\alpha\mu A}$$

The compilation of data presented by Green includes tabulations of the empirical coefficients α and β for a wide variety of porous media including packed beds of irregular and spherical particles ranging in nominal size from 0.08 inch to 0.1875 inch and for close packed wire screens ranging from 60 to 5 mesh. The nominal range of porosities included varies from 0.3 to 0.8. The experimentally derived coefficients α and β are shown in Figure 3 along with a straight line fit to the data.

$$\alpha = 0.794 \times 10^4 \beta$$

where α has units of ft^{-2} and β has units of ft^{-1}. The correlation is not excellent, but appears appropriate for order-of-magnitude considerations. Substituting this relation into the equation obtains

$$\frac{\text{Inertial Force}}{\text{Viscous Force}} = 1.26 \times 10^{-4} \frac{\dot{m}_g}{\mu A}$$

For the temperature range of interest ($2000^\circ R$ - $5000^\circ R$) the gas viscosity will range from about 0.3×10^{-4} to 0.5×10^{-4} lb/ft-sec. Considering a gas viscosity of 0.4×10^{-4} lb/ft-sec, the ratio of inertial to viscous forces may be written:

$$\frac{\text{Inertial Force}}{\text{Viscous Force}} = 3.15 \frac{\dot{m}_g}{A}$$

where $\dot{m}_g/A$ has the units of lb/ft^2-sec. It may therefore be concluded that for pyrolysis gas flow rates of 0.01 lb/ft^2-sec and less, the inertial terms may be ignored in which case Equation (81) reduces to Darcy's Law.

$$\frac{dP}{dy} = \alpha \mu v$$

where α^{-1} is the permeability. It is believed appropriate, however, that the more complete correlation Equation (81) be employed for pressure drop calculations in the char layer of ablating materials since it is valid for a wider range of conditions of practical interest.

6.2 FINITE DIFFERENCE FORMULATION

It is desired to cast the pressure drop correlation Equation (81) into a form including only variables which are readily available from the computation scheme for solving the mass and energy conservation equations (Section 3.2.4).

The velocity of the gas passing through the porous char is related to the gas flow rate per unit area by Equation (82). Introducing the gas state equation ($P = \rho_g RT/\mathcal{M}_g$) into Equation (82) yields:

$$v = \frac{\dot{m}_g}{P\mathcal{M}_g A} RT \tag{83}$$

It is convenient to define a viscosity law for the pyrolysis gas

$$\mu = \mu_o \left(\frac{T}{T_o} \right)^n \tag{84}$$

Substituting Equations (83) and (84) in (81) yields the following relation for a linear pressure drop across a node (n, see Figure 2).

$$\left(\frac{dP}{dy} \right)_n = \left[\alpha \mu_o \left(\frac{T}{T_o} \right)^n + \beta \frac{\dot{m}_g}{A} \right]_n \left(\frac{\dot{m}_g RT}{P\mathcal{M}_g A} \right)_n \tag{85}$$

where the coefficients α, β, and the gas molecular weight, $\mathcal{M}_g$ are input as functions of temperature and $\dot{m}_{g_n}$ represents the pyrolysis gas flow rate entering the node n. Equation (85) is solved for $n = 1,2,3 \ldots$, down to the first node in the virgin material where $\dot{m}_{g_n} = 0$. The pressure at the

top of node 1 is taken equal to the prescribed boundary layer edge pressure ($P_1 = P_e$). The pressure at the top of any other node is related to the pressure drop across and pressure at the top of the node above it.

$$P_n = P_{n-1} + \left.\frac{dP}{dy}\right|_{n-1} \delta_{n-1} \tag{86}$$

or

$$P_n = P_e + \sum_{i=1}^{n-1} \left.\frac{dP}{dy}\right|_i \delta_i \tag{87}$$

The computation is performed in an explicit manner, that is, after obtaining solution of the energy and mass conservation equations, a single pass through the nodal network from heated surface (n = 1) to the virgin material yields the pressure distribution entirely in terms of conditions existing at the end of the previous time step.

SECTION 7

SOME OPERATIONAL DETAILS OF THE AEROTHERM CHARRING MATERIAL ABLATION PROGRAM, VERSION 2

7.1 INTRODUCTION

While it is not the purpose of the present document to offer a detailed description of the charring material computer program which is based upon the analysis presented in Section 3 above, it does seem useful to include a few words of program description at this time. Complete descriptions, user's manual, and flow charts are given in References 46, 47, and 48.

7.2 PROGRAM DESCRIPTION

7.2.1 General Remarks

The Charring Material Ablation (CMA) program is a coded procedure for calculating the in-depth thermal response of a charring, ablating material. The solution is obtained through difference equations discussed in Section 3 above. This section presents a brief over-view of the program operation and output.

7.2.2 Program Objectives

The program produces in-depth temperature and density histories, plus surface recession rate as a function of time. In addition to this basic output, the program outputs a number of integrated energy terms and various material property data of interest. Section 7.2.5 below gives a more detailed description of the program output.

7.2.3 Program Capabilities

The Charring Material Ablation Program is an implicit, finite-difference computational procedure for computing the one-dimensional transient transport of thermal energy in a three-dimensional isotropic material which can ablate from a front surface and which can decompose in depth. Decomposition reactions are based on a three-component model. The program permits up to eight different backup materials of arbitrary thickness. The back wall of the composite material may transfer energy by convection and radiation.

In one program configuration, the ablating surface boundary condition may take one of three forms:

Option 1 - Film coefficient model convection-radiation heating with coupled mass transfer, including the effects of unequal heat and mass transfer coefficients (non-unity Lewis number) and unequal mass diffusion coefficients. Surface thermochemistry computations presume chemical equilibrium at the surface.

Option 2 - Specified surface temperature and surface recession rate

Option 3 - Specified radiation view factor and incident radiation flux, as functions of time, for a stationary surface.

Any combination of the first three options may be used for a single computation. Option 3 is appropriate to cooldown after termination of convective heat input and is often useful in conjunction with Option 1 and 2.

In another configuration, the program may be coupled to the Boundary Layer Integral Matrix Procedure. In this arrangement, the total assembly is designated the CABLE program and is described in other reports of this series (see Foreword).

The program permits the specification of a number of geometries:

(1) Plane

(2) Cylindrical or annular, with heated surface either inner or outer

(3) Spherical or spherical shell, with heated surface either inner or outer

(4) General "thermal stream tube" geometry, area varying as depth to any power

(5) General "thermal stream tube" geometry, area varying arbitrarily with depth.

The rear surface of the last node may be specified as insulated, or may experience convective and radiative heat transfer to a "reservoir" at a specified reservoir temperature if a rear surface convection coefficient and an emissivity are input.

Material properties such as thermal conductivity, specific heat, and emissivity are input as functions of temperature for virgin plastic and char. For partially decomposed material, the program performs an appropriate averaging to determine effective material properties.

7.2.4 Solution Procedure

The basic solution procedure is by a finite difference approach. For each time step, the decomposition relations are solved and then the in-depth energy fluxes constructed in general terms. These are then harmonized with a surface energy balance (if a surface energy balance option is being used) and the in-depth temperatures determined. New material property values are set up and the solution is ready for the next time increment.

7.2.5 Output Information

The CMA program outputs instantaneous mass ablation rates and blowing parameters for char and pyrolysis gas, total integrated mass ablation of char and pyrolysis gas, total recession and recession rates of surface, of the char line, and of the pyrolysis line. It also outputs the surface energy flux terms, namely, the energy convected in, energy radiated in, energy reradiated out, chemical generation, and conduction away (q_{cond}). Further, it describes how the input energy of q_{cond} is "accommodated" or "partitioned" in the solid material. Part of the energy is consumed in decomposing the plastic, part is consumed in sensible enthalpy changes of the solid, and part is "picked-up" by the pyrolysis gases as they pass through the char.

Finally, nodal temperature, density and enthalpy are given for every desired output time, as well as a description of the current material state for each node.

Thermocouple and isotherm output can also be called for. Figure 4 shows a representative page of output from a problem solution.

7.2.6 Operational Details

7.2.6.1 Storage Requirements

The storage requirements for the CMA program depend strongly upon the coupling mode in use. Coupling to a film coefficient model for the surface energy balance involves so much table storage that the program will barely fit a 32,000 word machine with full table sizes. In certain cases a reduction in table sizes will allow the program to fit on a smaller machine. Coupled to the CABLE program, which eliminates the need for storing extensive boundary condition tables, the CMA program requires less than 8000 words of storage.

7.2.6.2 Running Time

Computation time depends, of course, on the problem being computed, but experience to date indicates that CMA computations run in roughly 1/3 of real time for "typical" charring material problems, for machines of the IBM 7094 speed class.

7.3 SAMPLE PROBLEM SOLUTIONS

7.3.1 Some Typical Problems

As an illustration of the general performance of the charring material computer program, Figure 5 presents a graphic representation of the in-depth density history for a nylon-phenolic heat shield material exposed to a typical air reentry environment. The peak cold wave heat flux was about 800 $Btu/ft^2 sec$. Figure 6 shows some in-depth thermocouple temperature response predictions compared to test data. Figure 7, from a different problem, shows a machine made plot generated by a plot routine coupled to the CMA program.

7.3.2 Additional Examples

Additional examples of the program performance may be found in Appendices B and C. Appendix B, which is an early technical note written during the development of the program, reports the results of heat conduction solution tests. Appendix C describes some computational experiments exploring interesting aspects of solution smoothness for various charring material problems.

SECTION 8
SUMMARY AND CONCLUSION

8.1 GENERAL REMARKS

The preceding sections have described the analysis and an associated computer program for the calculation of the in-depth response of a charring or pyrolyzing material. The general objective of the development effort has been to produce a computation scheme which accounts for those physical events common to a wide range of technically important applications, so that the resulting program has as much generality and flexibility as possible. To this end, the analysis accounts for the basic in-depth pyrolysis problem, which is observed to be common to a wide range of problems, and excludes coking (char densification), subsurface char erosion by pyrolysis gases, thermal expansion, condensed phase char reactions, and mechanical damage mechanisms. All of these are particular to particular materials, or material types. For such materials, the basic program can be modified to include these special effects.

The basic program generates a one-dimensional in-depth solution, but the cross sectional area of the material analyzed may vary with depth (thermal stream tube). Pyrolysis may occur through three distinct Arrhenius-type kinetic reactions.

An important feature of the program is the range of physically realistic boundary conditions available for the heated surface. These include

(1) Specified temperature and recession rate

(2) Radiation energy balance with zero recession and no convection (cool down or soak out)

(3) Coupling through a film coefficient model to surface thermochemistry solution including general heterogeneous equilibrium, or heterogeneous equilibrium modified by certain rate controlled reactions, both models including the effects of the melting and total removal of surface species formed at temperature above their melt or fail temperatures

(4) Coupling to a general, non-similar, reacting boundary layer solution including homogeneous and hetergeneous kinetic effects, with surface melting or failing.

This range of possibilities offers opportunities for economy during routine in-depth studies or during computations for which film coefficient models are adequate, while preserving the capability of doing very accurate coupled, simultaneous boundary layer and in-depth solutions.

8.2 EXPERIENCE WITH THE IN-DEPTH SOLUTION ROUTINE (CMA)

The in-depth solution routine has been applied to a fairly wide variety of materials and some brief account of these applications may provide some useful orientation. By suppressing pyrolysis effects, the program can be used for simple transient heat conduction problems; applications here have included such refractories as alumina, boron nitride, tungsten, and graphite. The program has been used very extensively for graphite and carbon phenolic rocket nozzle studies. These computations include numerous series of specified temperature and recession rate runs to back out thermal conductivity data for these materials, as well as a very large number of coupled solutions.

The program has been run on many parametric studies of nylon phenolic with generally excellent results. The very rapid decomposition rate of this material occasionally has caused oscillations in the pyrolysis gas flow rate, with attendant minor oscillations in surface temperature and surface recession rate. Fortunately, overall aspects of the solution, such as total recession, mean temperatures, and isotherm penetration seem unaffected by these oscillations. Appendix C gives an extensive discussion of the oscillation problem. In one pathological case for nylon phenolic, a step application of a very high heat flux caused a total disintegration of the solution process. This disintegration appeared to be due to the explicit decomposition treatment combined with the implicit energy treatment and could be circumvented by a slight softening of the step transient. No other solution breakdowns have been observed with the program.

The program has also been applied to asbestos phenolic with good results.

The program has been extensively used for silica-containing insulators such as silica phenolic. The results here have been excellent so long as the main assumptions of the analysis are not violated. Materials with much silica occasionally display physical events such as thick liquid layer runoff and subsurface char reactions, for example condensed phase silica-carbon reactions. Since the program was not designed to account for these events it is not always applicable to these materials.

The program was once used to predict the freezing of water, for which case the freezing reaction was input as one of the Arrhenius reactions available in the program structure. The results were quite accurate.

8.3 CONCLUSION

The analysis presented here and programmed as the CMA program has been applied to a wide range of materials of technical interest. The results have been excellent and the program appears to be thoroughly checked out and operational.

REFERENCES

1. Bamford, C. H., Crank, J., and Malan, D. H.: The Combustion of Wood. Part I. Proceedings of the Cambridge Philosophical Society, Vol. 42, 1946, pp. 166-182.

2. Crank, J., and Nicolson, P.: A Practical Method for Numerical Evaluation of Solutions of Partial Differential Equations of the Heat-Conduction Type. Proceedings of the Cambridge Philosophical Society, Vol. 43, 1940, pp. 50-67.

3. Barriault, R. J.: One-Dimensional Theory for a Model of Ablation for Plastics that Form a Charred Surface Layer. AVCO-RAD TM-58-130, November 1958.

4. Grosh, R. J.: Transient Temperature in a Semi-Infinite Porous Solid with Phase Change and Transpiration Effects. WADD TR 60-105, January 1960.

5. Barriault, R. J., and Yos, J.: Analysis of the Ablation of Plastic Heat Shields that Form a Charred Surface Layer. ARS Journal, Vol. 30, No. 9, September 1960, pp. 823-829.

6. Schwartz, H. S., ed.: Conference on Behavior of Plastics in Advanced Flight Vehicle Environments. Wright Air Development Division, United States Air Force, Wright Patterson Air Force Base, Ohio, WADD-TR-60-101 (AD-247 100), September 1960.

7. Barry, W. T., and Sutton, W. H.: The Importance of Char Structure in the Ablation Performance of Organic Polymers. General Electric Co., Missile and Space Division, Report No. R60SD329, March 1960.

8. Beecher, N., and Rosensweig, R. E.: Ablation Mechanisms in Plastics with Inorganic Reinforcement. ARS Journal, Vol. 31, No. 4, April 1961, pp. 530-539.

9. Munson, T. R., and Spindler, R. J.: Transient Thermal Behavior of Decomposing Materials. Part I, General Theory and Application to Convective Heating. AVCO Corp., Wilmington, Mass., AVCO RAD-TR-61-10, May 1961 (also Institute of Aerospace Sciences, 30th Annual Meeting, New York, New York, January 22-24, 1962, Paper No. 62-30).

10. Lapple, C. W., Brady, A. P., and Chamberlain, D. C., Jr.: Mechanism of Ablation of Char-Forming Ablative Plastics. Stanford Research Institute, Menlo Park, California, ASD-TR-61-204, September 1961.

11. Lafazan, S., and Siegel, B.: Ablative Thrust Chambers for Space Application. Paper No. 5, 46th National Meeting of the American Institute of Chemical Engineers, Los Angeles, California, February 5, 1962.

12. Hurwicz, H.: Aerothermochemistry Studies in Ablation. Combustion and Propulsion, Fifth AGARD Colloquium, Braunschweig, Germany, April 9-13, 1962, MacMillan Company, New York, 1963, pp. 403-455.

13. McFarland, B., Joerg, P., and Taft, M.: Criteria for Plastic Ablation Materials as Functions of Environmental Parameters. Aerojet-General Corp., Azusa, California, ASD-TR-61-439, May 1962.

14. Scala, S. M. and Gilbert, L. M., "The Thermal Degradation of a Char Forming Plastic During Hypersonic Flight. ARS Journal, Vol. 32, No. 6, June 1962, pp. 917-924.

15. Swann, R. T., and Pittman, C. M.: Numerical Analysis of the Transient Response of Advanced Thermal Protection Systems for Atmospheric Entry. NASA TN D-1370, July 1962.

16. Lafazan, S., and Welsh, W. E., Jr.: The Charring Ablator Concept: Application to Lifting Orbital and Superorbital Entry. Symposium on Dynamics of Manned Lifting Planetary Entry, Philadelphia, Pa., October 1962.

17. Mathieu, R. D.: Response of Charring Ablators to Hyperthermal Environments. General Electric Co., Missile and Space Division, Philadelphia, Pa., Report R63SD20, February 1963.

18. Kratsch, K. M., Hearne, L. F., and McChesney, H. R.: Thermal Performance of Heat Shield Composites During Planetary Entry. Unnumbered paper presented at the American Institute of Aeronautics and Astronautics - National Aeronautics and Space Administration National Meeting, Palo Alto, Calif., September 30-October 1, 1963 (also Lockheed Missiles and Space Company, Sunnyvale, Calif., Report LMSC-803099 (October 1963), reprinted in Engineering Problems of Manned Interplanetary Exploration, American Institute of Aeronautics and Astronautics, New York, 1963)

19. Quinville, J. A., and Solomon, J.: Ablating Body Heat Transfer. Aerospace Corp., El Segundo, Calif., SSD-TDR-63-159 (AD-429 198), January 15, 1964.

20. Reinikka, E. A., and Wells, P. B.: Charring Ablators on Lifting Re-entry Vehicles. Journal of Spacecraft and Rockets, Vol. 1, No. 1, January-February 1964, pp. 73-77.

21. Steg, L. and Lew, H.: Hypersonic Ablation. The High Temperature Aspects of Hypersonic Flow, W. C. Nelson, ed., Proceedings of the AGARD-NATO Specialists Meeting, Rhode-Saint-Genèse, Belgium, 3-6 April, 1962, MacMillan Co., New York, 1964, pp. 629-680 (also General Electric Co., Missile and Space Vehicle Department, Philadelphia, Pa., R62SD55, May 1962).

22. Wells, P. B.: A Method for Predicting the Thermal Response of Charring Ablation Materials. Boeing Co., Seattle, Wash., Report D2-23256 (AD-443 144), July 1964.

23. Rivers, W. J., Van Wyk, R., Seader, J. D., Friedman, H. A., and Chu, H. N.: Final Report, Effect of Rocket Engine Combustion on Chamber Materials, Part I: One Dimensional Computer Program. Rocketdyne, Division of North American Aviation, Inc., Canoga Park, Calif., AFRPL-TR-65-13 (AD-455 560), January 1965.

24. McCuen, P. A., Schaefer, J. W., Lundberg, R. E., and Kendall, R. M.: A Study of Solid-Propellant Rocket Motor Exposed Materials Behavior. Vidya Division, Itek Corp., Palo Alto, Calif., AFRPL-TR-65-33 (AD-462 331), February 26, 1965.

25. Schultz, F. E., and Cline, P. B.: Final Report, Analytical Comparisons of Ablative Nozzle Materials. General Electric Co., Reentry Systems Department, Philadelphia, Pa., NASA CR 54257, July 1, 1965.

26. Kendall, R. M., Rindal, R. A., and Bartlett, E. P.: Thermochemical Ablation. American Institute of Aeronautics and Astronautics, Thermophysics Specialist Conference, Monterey, Calif., September 13-15, 1965, AIAA Paper No. 65-642 (to be published in AIAA Journal).

27. Friedman, H. A., Persselin, S. F., McFarland, B. L., and Seader, J. D.: Final Report, Effect of Rocket Engine Combustion on Chamber Materials, Part II: Two-Dimensional Computer Program. Rocketdyne, Division of North American Aviation, Inc., Canoga Park, Calif., AFRPL-TR-65-176 (AD-473 111), September 1965.

28. Curry, Donald M.: An Analysis of a Charring Ablation Thermal Protection System. National Aeronautics and Space Administration, Manned Spacecraft Center, Houston, Texas, NASA TN D-3150, November 1, 1965.

29. Swann, R. T., Dow, M. B., and Tompkins, S. S.: Analysis of the Effects of Environmental Conditions on the Performance of Charring Ablators. Journal of Spacecraft and Rockets, Vol. 3, No. 1, January 1966, pp. 61-67.

30. Friedman, H. A., and McFarland, B. L.: "Two-Dimensional Transient Ablation and Heat Conduction Analysis for Multimaterial Thrust Chamber Walls. American Institute of Aeronautics and Astronautics Second Propulsion Joint Specialist Conference, Colorado Springs, Colorado, June 13-17, 1966, AIAA Paper No. 66-542.

31. Israel, M. H., and Nardo, S. V.: An Annotated Bibliography on Ablation and Related Topics. Polytechnic Institute of Brooklyn, New York, New York, PIBAL Report No. 686 (AD-603 139), May 1964.

32. Goldstein, H. E.: Kinetics of Nylon and Phenolic Pyrolysis. Lockheed Missiles and Space Company, Sunnyvale, Calif., LMSC-667876, October 1965.

33. Tavakoli, M.: An Integral Method for Analysis of the Aerothermochemical Behavior of Refractory-Fiber Reinforced Char-Forming Materials. American Institute of Aeronautics and Astronautics, 4th Aerospace Sciences Meeting, Los Angeles, Calif., June 27-29, 1966, AIAA Paper No. 66-435.

34. Brogan, J. J.: A Numerical Method of Solution for Heat Conduction in Composite Slabs with a Receding Surface. Lockheed Missiles and Space Division, Lockheed Aircraft Corp., Sunnyvale, Calif., LMSD 288204, January 1960.

35. Kendall, R. M., and Bartlett, E. P.: Nonsimilar Solution of the Multicomponent Laminar Boundary Layer by an Integral Matrix Method. American Institute of Aeronautics and Astronautics, Fifth Aerospace Sciences Meeting, New York, New York, January 23-26, 1967, AIAA Paper No. 67-218.

36. Spalding, D. B.: A Standard Formulation of the Steady Convective Mass-Transfer Problem. International Journal of Heat and Mass Transfer, Vol. 1, No. 2/3, August 1960, pp. 192-207.

37. Spalding, D. B.: Convective Mass Transfer. McGraw-Hill Publishing Co., New York, 1963.

38. Kendall, R. M., and Rindal, R. A.: Analytical Evaluation of Rocket Nozzle Ablation. American Institute of Aeronautics and Astronautics, Solid Propellant Rocket Conference, Palo Alto, Calif., January 29-31, 1964, AIAA Paper No. 64-101.

39. Rosner, D. E.: Similitude Treatment of Hypersonic Stagnation Heat Transfer. ARS Journal, Vol. 29, No. 3, March 1959, pp. 215-216.

40. Spalding, D. B.: Heat Transfer from Chemically Reacting Gases. Modern Developments in Heat Transfer. W. Ibele, ed., Academic Press, New York, 1963, pp. 19-64.

41. Lees, L.: Convective Heat Transfer with Mass Addition and Chemical Reactions. Combustion and Propulsion, Third AGARD Colloquium (Palermo, Sicily, March 17-21, 1958), Thring, M. W., et al., eds., Pergamon Press, New York, 1958, pp. 451-498.

42. Fay, J. A., and Riddell, F. R.: Theory of Stagnation Point Heat Transfer in Dissociated Air. Journal of the Aeronautical Sciences, Vol. 25, No. 2, February 1958, pp. 73-85.

43. Aerotherm Corporation, Palo Alto, Calif.: User's Manual, Aerotherm Equilibrium Surface Thermochemistry Program, Version 2. June 1966.

44. Kendall, R. M.: Final Report: An Analysis of the Coupled Chemically Reacting Boundary Layer and Charring Ablator - Part V - A General Approach to the Thermochemical Solution of Mixed Equilibrium-Non-Equilibrium, Homogeneous or Heterogeneous Systems. Aerotherm Corporation, Palo Alto, California, March 14, 1967 (prepared for National Aeronautics and Space Administration, Manned Spacecraft Center, Houston, Texas, under Contract NAS9-4599; Part V of the series of reports of which the present report is Part II).

45. Green, L., Jr: Heat, Mass, and Momentum Transfer in Flow Through Porous Media. ASME-AIChE Heat-Transfer Conference, August 11-15, 1957.

46. Aerotherm Corporation, Palo Alto, Calif.: User's Manual, Aerotherm Charring Material Ablation Program, Version 2. January 1966.

47. Aerotherm Corporation, Palo Alto, Calif.: Fortran Variable Names, Aerotherm Charring Material Ablation Program, Version 2. February 1966.

48. Aerotherm Corporation, Palo Alto, Calif.: Flow Charts, Aerotherm Charring Material Ablation Program, Version 2. April 1966.

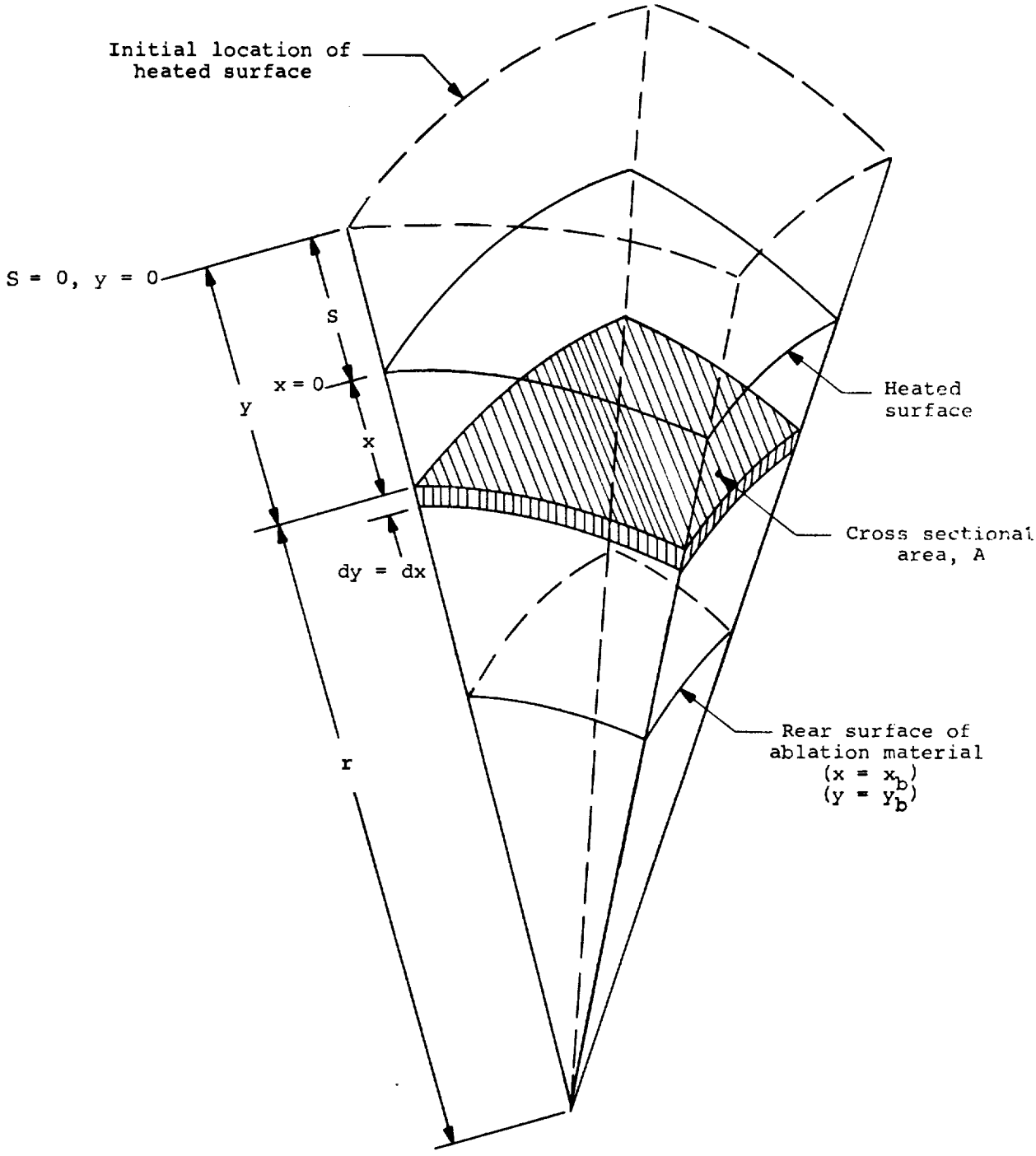

Figure 1. Geometrical configuration and coordinate system illustration.

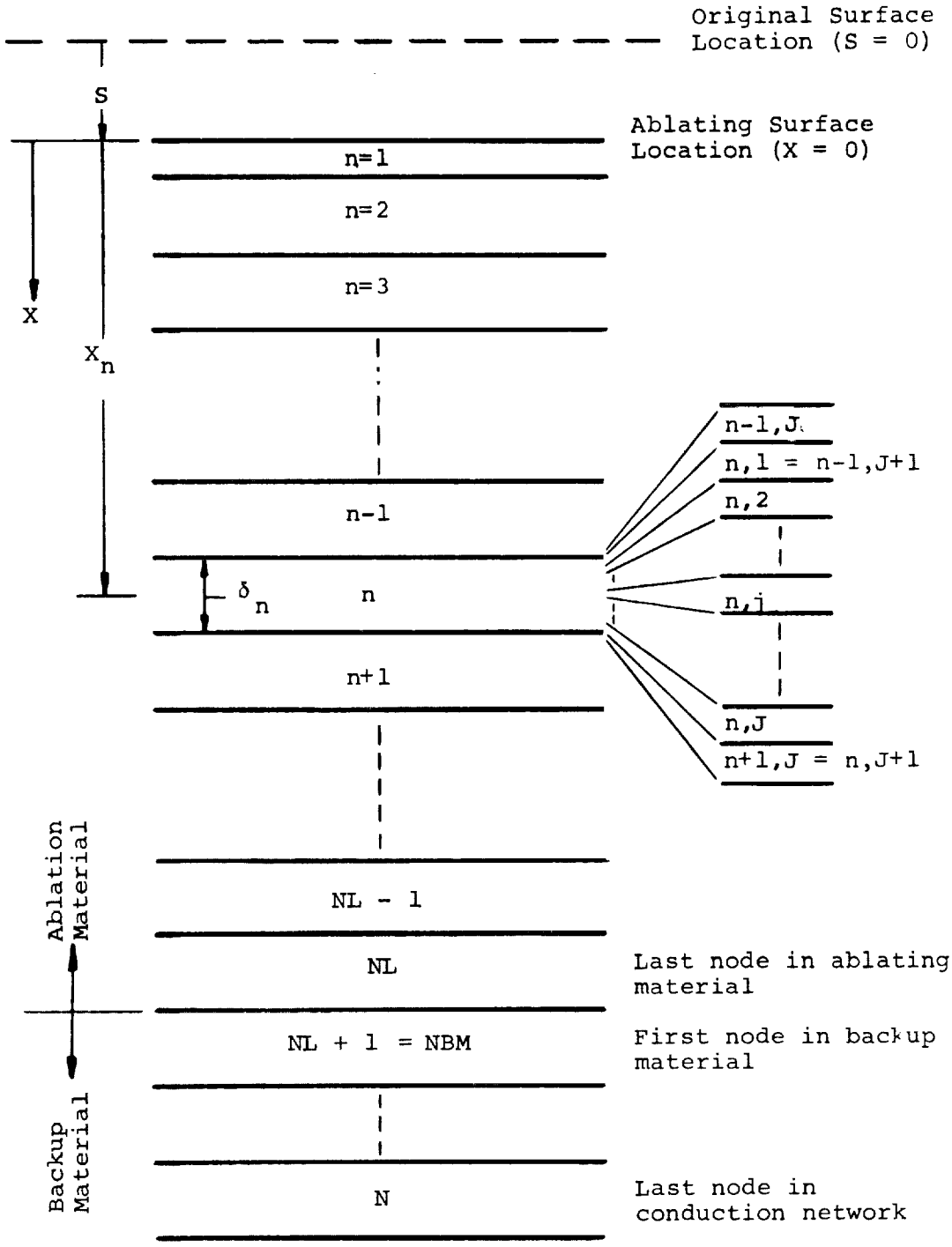

Figure 2. Finite difference representation.

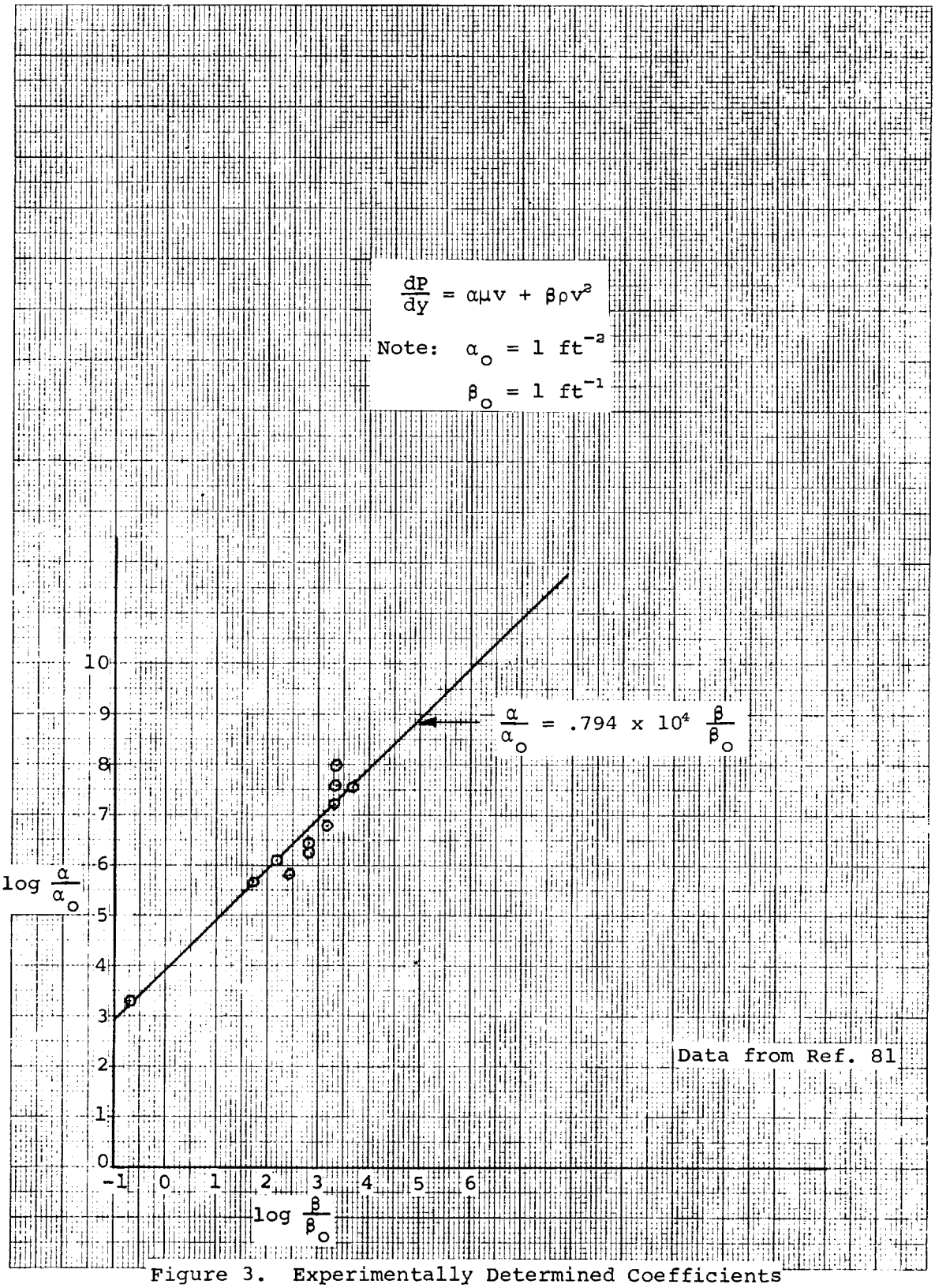

Figure 3. Experimentally Determined Coefficients for Flow Through Porous Media

- - - - - - - - - - - - - - - - 24.0000 SECONDS - - - - - - - - - - - - - - - -

TIME STEP	SURF NODE	SURFACE RECESSION (IN)	H WALL (BTU/LB)	H EDGE (BTU/LB)	HEAT COEFF (LB/SQ FT-SEC)	CH/CHO
100	1	2	.2389	0	0	2.00000

---ABLATION RATES---

H EDGE (BTU/LB)	H WALL (BTU/LB)	M DOT CHAR (LB/SQ FT-SEC)	M DOT GAS	M CHAR (LB/ORIG SQ FT)	M GAS
********	********	.022673	.020445	.713226	.837494

---RECESSIONS/RECESSION RATES---
(IN) / (IN/SEC)

SURFACE	CHAR (.50)	PYROLYSIS (.98)
.[illegible]/ .003710	.2834292/ .0076713	.3669941/ .0091897

---SURFACE ENERGY FLUX TERMS---
CURRENT RATES (BTU/SQ FT SURFACE-SEC)
AND INTEGRATED VALUES (BTU/ORIG SQ FT)

	CONVECTED IN	RADIATED IN	RADIATED OUT	CHEMICAL GENERATION	CONDUCTION AWAY
RATE	0	0	0	0	2.065E 02
TOTAL	0	0	0	0	8.461E 03

---INTERIOR ENERGY TERMS---
CURRENT RATES (BTU/SQ FT SURFACE-SEC)
AND INTEGRATED VALUES (BTU/ORIG SQ FT)

	PYROL GAS FLOW UP	DECOMP ABSORPTION	CONVECTION WITH SOLIDS	STORAGE IN SOLID	LOSS AT REAR FACE
RATE	7.303E 01	1.178E 01	6.061E 01	5.544E 01	8.936E-04
TOTAL	2.[illegible]E 03	5.139E 02	1.865E 03	4.234E 03	5.584E-03

NODE	MAT	TEMP (DEG R)	DENSITY (LB/CU FT)	ENTHALPY (BTU/LB)	NODE	MAT	TEMP (DEG R)	DENSITY (LB/CU FT)	ENTHALPY (BTU/LB)
1	0	3456.00	73.445	1516.65	12	1	912.97	91.300	-247.09
2	0	3549.38	73.338	1369.26	13	1	805.42	91.300	-285.81
3	0	3285.13	73.446	1226.86	14	1	701.81	91.300	-315.74
4	0	2992.71	73.543	1089.31	15	1	624.99	91.300	-337.64
5	0	2742.15	73.722	957.29	16	1	581.54	91.300	-350.02
6	0	2473.39	74.104	820.76	17	1	557.46	91.300	-356.89
7	0	2208.49	75.125	664.85	18	1	541.00	91.300	-361.58
8	0	1955.12	79.410	390.45	19	1	533.55	91.300	-363.70
9	0	1704.91	87.258	58.97	20	1	531.10	91.300	-364.40
10	0	1247.57	90.344	-105.43	21	1	530.20	91.300	-364.65
11	0	1057.62	91.211	-193.56	22	1	530.05	91.300	-364.70

Figure 4. Typical Output Page

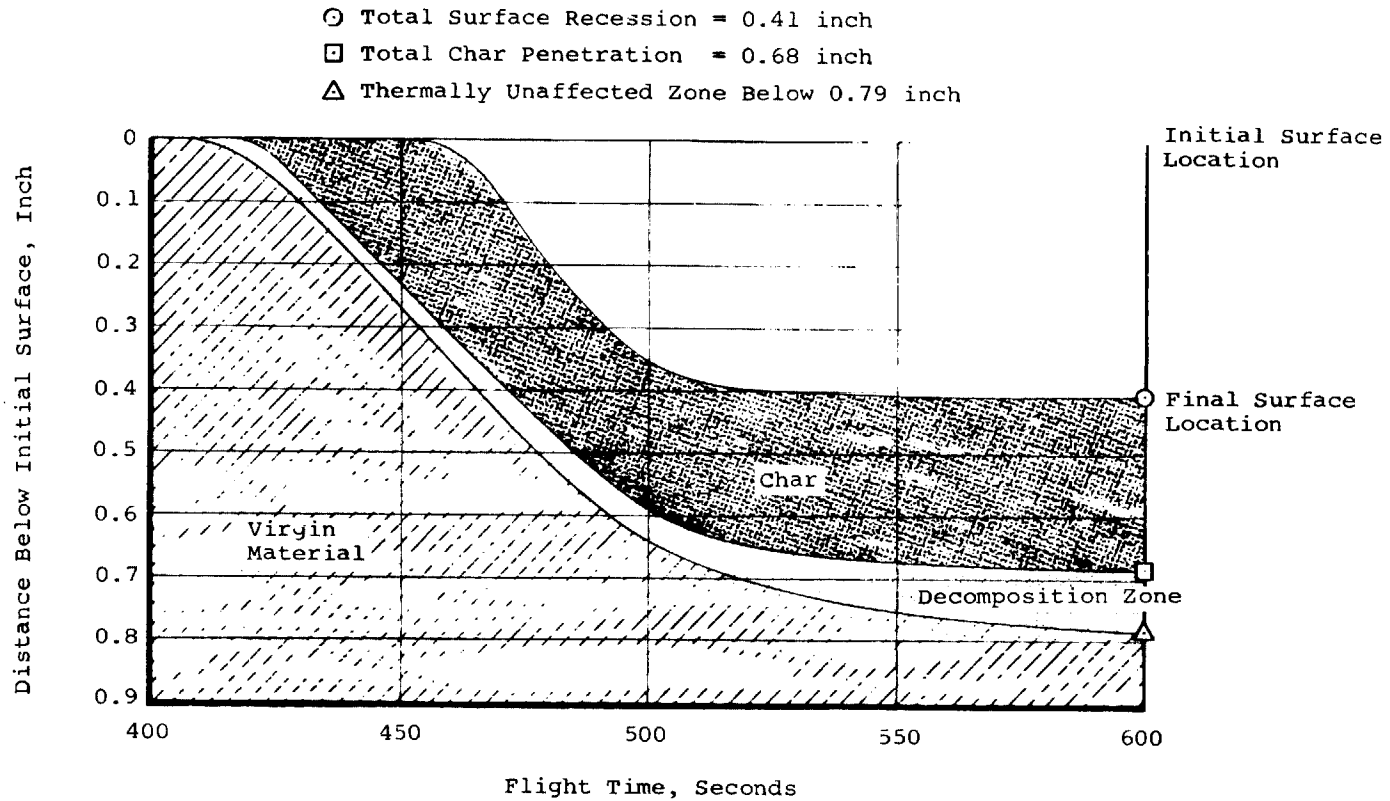

Figure 5. Predicted Degradation Depth Histories, Nylon Phenolic Re-entry Problem.

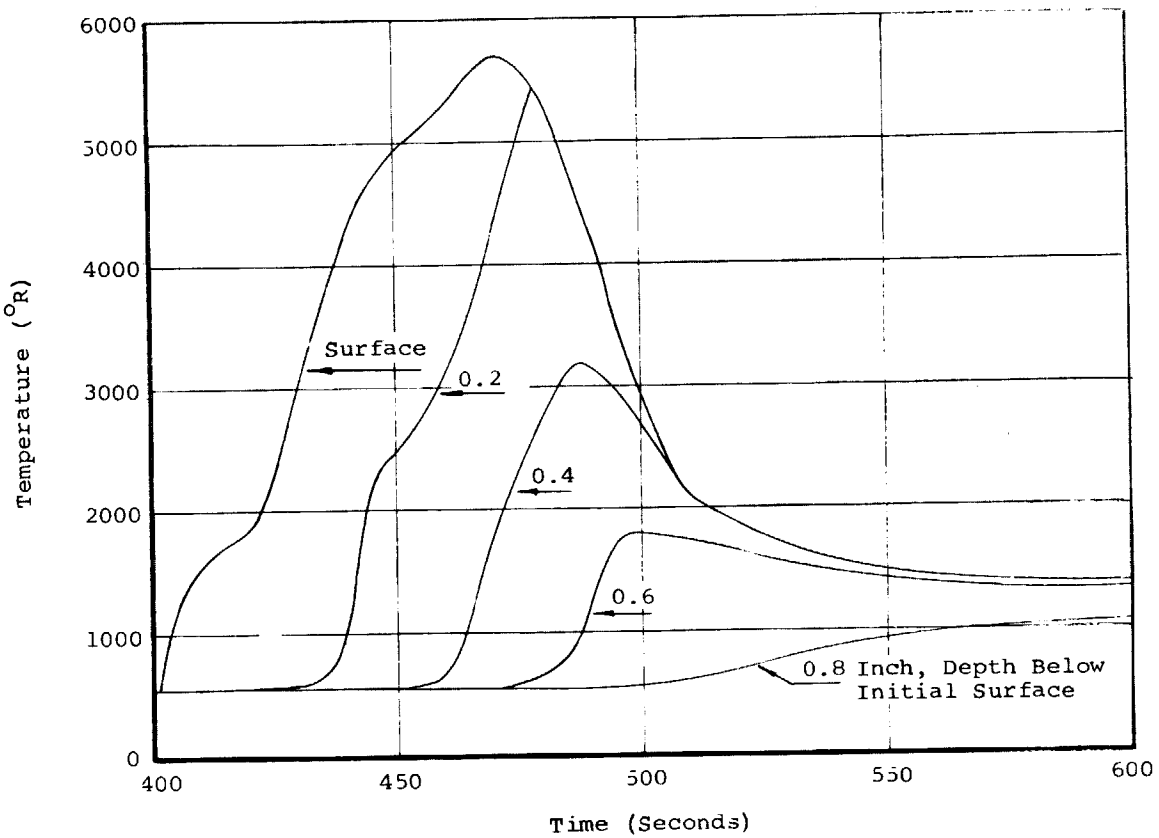

Figure 6. Predicted Temperature Histories at Surface and Selected Thermocouple Locations, Nylon Phenolic Re-entry Problem.

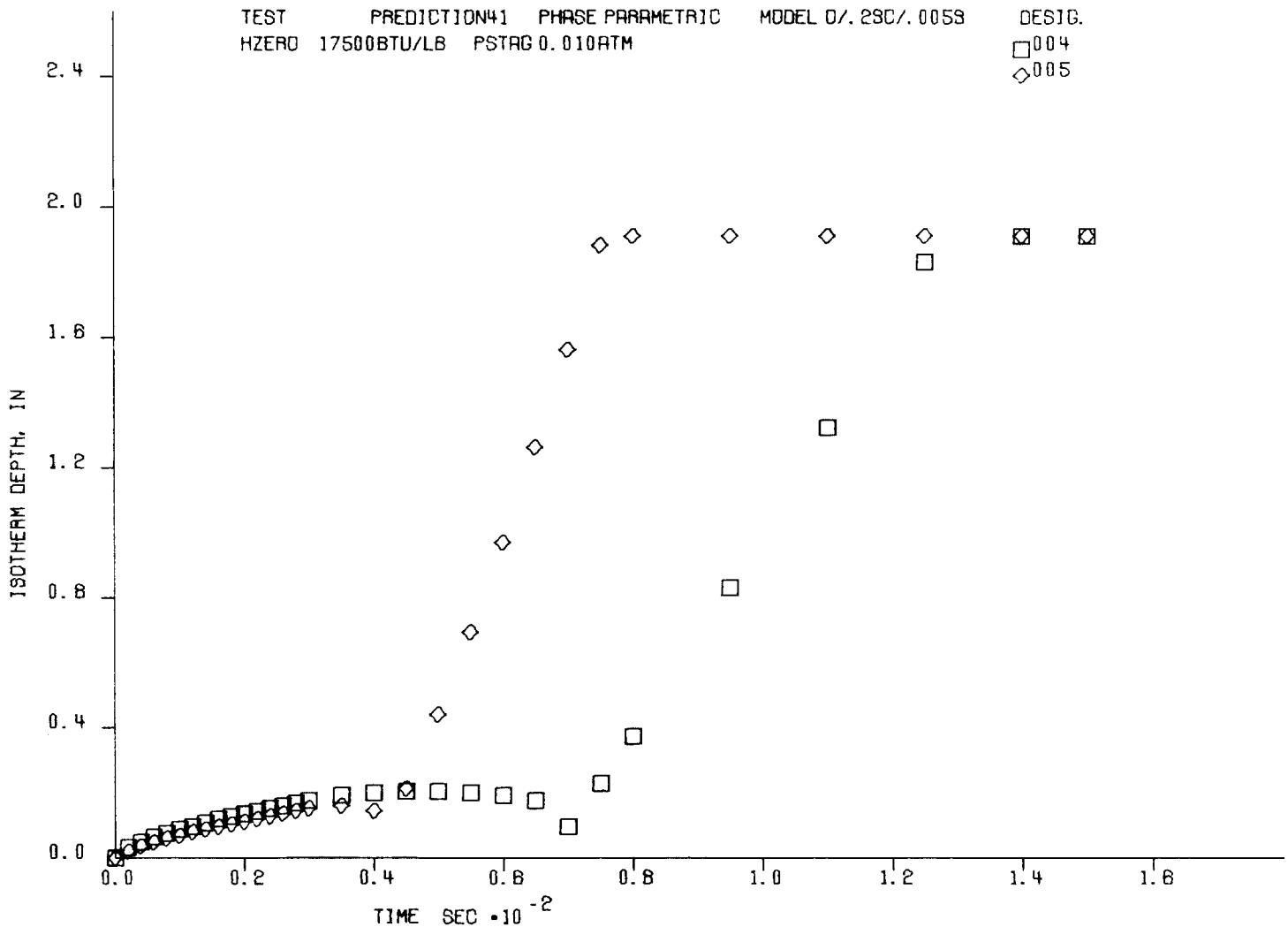

Figure 7. Typical Machine Plotted Isotherm Depths

APPENDIX A

EQUATIONS FOR COEFFICIENTS A_n, B_n, C_n, AND D_n IN IN-DEPTH ENERGY EQUATION ARRAY

APPENDIX A

EQUATIONS FOR COEFFICIENTS A_n, B_n, C_n, and D_n IN IN-DEPTH ENERGY EQUATION ARRAY

The coefficients A_n, B_n, C_n, and D_n in the array of Equation (58) are determined by Equations (54), (56), and (57).

For nodes in the ablating material except the first and last, from Equation (54),

$$A_n = -\frac{\Delta\theta}{\delta_n A_n} \frac{1}{\left[\frac{\delta_{n-1}/2}{k_{n-1}A'_{n-1}} + \frac{\delta_n/2}{k_n A'_n}\right]} \tag{A-1}$$

$$B_n = (\rho'\overline{C}_p) - A_n + \frac{\Delta\theta}{\delta_n A'_n} \frac{1}{\left[\frac{\delta_n/2}{k_n A'_n} + \frac{\delta_{n+1}/2}{k_{n+1} A'_{n+1}}\right]} - \left(\frac{\partial h_g}{\partial T}\right)_n \left(\frac{\partial \rho_n}{\partial \theta}\right)_y \Delta\theta$$

$$+ \frac{\dot{m}_{g_n}}{A'_n \delta_n}\left(\frac{\partial h_g}{\partial T}\right)_n \Delta\theta + \frac{\dot{S}\Delta\theta}{\delta_n}(\rho C_p)_{n,1} \tag{A-2}$$

$$C_n = \frac{-\Delta\theta}{\delta_n A_n} \frac{1}{\left[\frac{\delta_n/2}{k_n A'_n} + \frac{\delta_{n+1}/2}{k_{n+1} A'_{n+1}}\right]} - \frac{\dot{m}_{g_n}}{A'_n \delta_n}\left(\frac{\partial h_g}{\partial T}\right)_{n+1} \Delta\theta - \frac{\dot{S}\Delta\theta}{\delta_n}(\rho C_p)_{n+1,1} \tag{A-3}$$

$$D_n = T_n\left[(\rho'\overline{C}_p)_n - \left(\frac{\partial h_g}{\partial T}\right)_n \left(\frac{\partial \rho_n}{\partial \theta}\right)_y \Delta\theta + \frac{\dot{m}_{g_n}}{A'_n \delta_n}\left(\frac{\partial h_g}{\partial T}\right)_n \Delta\theta + \frac{\dot{S}\Delta\theta}{\delta_n}(\rho C_p)_{n,1}\right]$$

$$+ T_{n+1}\left[-\frac{\dot{m}_{g_n}}{A'_n \delta_n}\left(\frac{\partial h_g}{\partial T}\right)_{n+1} \Delta\theta - \frac{\dot{S}\Delta\theta}{\delta_n}(\rho C_p)_{n+1,1}\right]$$

$$+ \Delta\theta\left[h_{g_n}\left(\frac{\partial \rho_n}{\partial \theta}\right)_y - \overline{h}_n\left(\frac{\Delta\rho}{\Delta\theta}\right)_n + \frac{\dot{m}_{g_n}}{A'_n \delta_n}(h_{g_{n+1}} - h_{g_n})\right.$$

$$\left. + \frac{\dot{S}}{\delta_n}\left((\rho h)_{n+1,1} - (\rho h)_{n,1}\right)\right] \tag{A-4}$$

For the surface node of the ablating material, to which Equation (54) applies, $A_1 = 0$, B_1 and C_1 retain the forms of Equations (A-2) and (A-3) above, while D_1 has the form of Equation (A-4) <u>plus</u> the term $q_{cond}^{\Delta} / \delta_1$.

For the last node of ablating material, to which Equation (57) applies,

$$A_{NL} = - \frac{\Delta\theta}{\delta_{NL} A'_{NL}} \frac{1}{\left[\frac{\delta_{NL-1}/2}{k_{NL-1} A'_{NL-1}} + \frac{\delta_{NL}/2}{k_{NL} A'_{NL}} \right]} \tag{A-5}$$

$$B_{NL} = (\rho' \overline{C}_p)_{NL} - A_{NL} - C_{NL} - (C_{p_g})_{NL} \left(\frac{\partial \rho_{NL}}{\partial \theta} \right)_y - \frac{\dot{S} \Delta\theta}{\delta_{NL}} \left[(\rho C_p)_{NL} - (\rho C_p)_{NL,1} \right] \tag{A-6}$$

$$C_{NL} = - \frac{\Delta\theta}{\delta_{NL} A'_{NL}} \frac{1}{\left[\frac{\delta_{NBM}/2}{k_{NBM} A_{NBM}} + \frac{\delta_{NL}/2}{k_{NL} A'_{NL}} \right]} \tag{A-7}$$

$$D_{NL} = T_{NL} \left[(\rho' \overline{C}_p)_{NL} - C_{p_{g_{NL}}} \left(\frac{\partial \rho_{NL}}{\partial \theta} \right)_y \Delta\theta + \frac{\dot{S} \Delta\theta}{\delta_{NL}} \left(-(\rho C_p)_{NL} + (\rho C_p)_{n,1} \right) \right]$$

$$+ \Delta\theta \left[h_{g_{NL}} \left(\frac{\partial \rho_{NL}}{\partial \theta} \right)_y - \overline{h}_{NL} \frac{\Delta \rho_{NL}}{\Delta \theta} + \frac{\dot{S}}{\delta_{NL}} \left((\rho h)_{NL} - (\rho h)_{NL,1} \right) \right] \tag{A-8}$$

Here NBM refers to the first node of the back-up material. If there is no back-up material, the resistance $\delta_{NBM}/k_{NBM}A_{NBM}$ is replaced by the back wall resistance $1/h_{total}A'_{NL}$ where h_{total} is an effective heat transfer coefficient for convection and radiation. Since T'_{NBM} will then refer to a known "reservoir" temperature, the term $C_{NL}T'_{NBM}$ may be added to D_{NL}, leaving only two unknown temperatures.

For back-up materials the coefficients are simply

$$A_n = - \frac{\Delta\theta}{\delta_n A_n} \frac{1}{\left[\frac{\delta_n/2}{k_n A_n} + \frac{\delta_{n-1}/2}{k_{n-1} A_{n-1}} \right]} \tag{A-9}$$

$$B_n = (\rho \overline{C}_p)_n - A_n - C_n \tag{A-10}$$

$$C_n = -\frac{\Delta\theta}{\delta_n A_n} \frac{1}{\left[\frac{\delta_{n+1}/2}{k_{n+1}A_{n+1}} + \frac{\delta_n/2}{k_n A_n}\right]} \qquad \text{(A-11)}$$

$$D_n = T_n (\rho\bar{C}_p)_n \qquad \text{(A-12)}$$

For the first back-up node, n = NBM and n-1 - NL. For the last back-up node (n = N), n+1 refers to the back-wall condition, described above. The term $\delta_{n+1}/k_{n+1}A_{n+1}$ becomes $1/h_{total}A_N$ and D_N is modified as described above for the case where the last node of ablating material is the last node.

APPENDIX B

CONDUCTION SOLUTION CHECK-OUT OF THE CHARRING MATERIAL ABLATION PROGRAM

TABLE OF CONTENTS

Appendix B

LIST OF SYMBOLS

Appendix B

GENERAL

A	area
A	dimensionless constant employed in equations (4) and (5)
B	constant defined in equation (A-18)
c_p	specific heat
d	nodal thickness
E_1, E_2	defined by equations (A-7), (A-8) respectively
erf( )	error function
erfc( )	$\triangleq$ 1 - erf ( )
h	enthalpy
i	index
k	thermal conductivity
n	dimensionless constant employed in equations (4) and (5)
q_e	heat flux per unit area at surface
r	radius coordinate (origin at center)
r_1 r_e	external radius
$\dot{s}$	surface recession rate
T	solution to difference equation for temperature
t	solution to differential equation for temperature
t*	$(t - t_o)/(t_e - t_o)$
x	distance coordinate with origin tied to receding surface
x*	similarity variable $x/2\sqrt{\alpha\theta}$

SUBSCRIPTS

c	value at center
e	value at edge or surface
min	minimum value in region of interest
n	node index
0	initial value, value as x ∞

GREEK

α	thermal diffusivity $k/\rho c_p$
β	arithmetic error
$\Delta\theta$	time increment
δ	slab thickness
ϵ	error $T^* - t^*$
θ	time

SPECIAL

$\triangleq$	equal to by definition
$\cong$, $\approx$	approximately equal to

CONDUCTION SOLUTION CHECK-OUT OF THE CHARRING MATERIAL ABLATION PROGRAM

B.1 INTRODUCTION

This report presents the results of a series of check-out computations testing the heat conduction aspects of the Aerotherm Charring Material Ablation (CMA) Program, Version 2. Calculations included transient conduction cases for slabs, semi-infinite solids, spheres, cylinders, and receding semi-infinite solids.

B.2 ASPECTS OF PROGRAM

The program treats the heat conduction and solid convection in a fully implicit manner. Thus the difference equation at each finite-difference "node" is, for a constant density material,

$$\rho c_p(T'_n - T_n) = \frac{\Delta\theta}{A_n d_n}\left[\frac{T'_{n-1} - T'_n}{\frac{d_{n+1}/2}{k_{n-1}A_{n-1}} + \frac{d_n/2}{k_n A_n}} - \frac{T'_n - T'_{n+1}}{\frac{d_n/2}{k_n A_n} + \frac{d_{n+1}/2}{k_{n+1}A_{n+1}}}\right]$$

$$+ \frac{\dot{s}\Delta\theta}{d_n}\left[(\rho h)_{n+1} + (\rho c_p)_{n+1}(T'_{n+1} - T_{n+1}) - (\rho h)_n - (\rho c_p)_n(T'_n - T_n)\right] \quad \text{(B-1)}$$

Here primes denote "new" temperatures at the end of the time step $\Delta\theta$.

B.3 CONSTANT PROPERTIES SLAB

A single problem was computed for a 10-inch slab with insulated back face, uniform initial temperature, and a step change in front surface temperature. Property values were constant at

$$k = 1 \text{ Btu/sec ft } {}^{o}F$$

$$c_p = 1 \text{ Btu/lb } {}^{o}F$$

$$\rho = 1 \text{ lb/ft}^3 .$$

The nodal distribution was, from the surface,

1 node of 0.10 inches thickness,
2 nodes of 0.20 inches thickness,
2 nodes of 0.25 inches thickness,
4 nodes of 0.50 inches thickness,
5 nodes of 1.00 inches thickness,
1 node of 2.00 inches thickness.

The maximum time step permitted was 0.002 seconds.

Figure B-1 shows the computed results compared to exact curve presented by Schneider (Reference B-1) which have been computed according to the solution

$$\frac{t - t_o}{t_e - t_o} = 1 - \frac{4}{\pi} \sum_{i=1}^{\infty} \frac{1}{i} e^{-(i\pi/2)^2(\alpha\theta/\delta^2)} \sin \frac{i\pi}{2\delta} x \quad i = 1,3,5.... \qquad (B-2)$$

The agreement between the exact curves and the points produced by the program is very satisfactory.

B.4 CONSTANT PROPERTIES CYLINDER

A computation exactly similar to the slab computation described above was done for a cylinder with an external radius of 10 inches. Property values, nodal sizes, and time step limit were as in Section 3.

Figure 2 displays the results with computed points shown as open symbols. In contrast to the slab case, agreement between computed points and the exact solution is not good for the deepest nodes, which respond faster in the cylinder problem than in the slab problem due to their smaller mass.

The problem was recomputed with the maximum time step halved to 0.001 seconds and with the following nodal size distribution.

1 node of 0.10 inches thickness,
2 nodes of 0.20 inches thickness,
2 nodes of 0.25 inches thickness,
18 nodes of 0.12 inches thickness.

The results for this calculation are shown in Figure 2 in the solid figures. The exact solution curves are given by Schneider (Reference B-1) computed from the relation (Reference B-2).

$$\frac{t - t_o}{t_e - t_o} = 1 - 2 \sum_{i=1}^{\infty} \frac{1}{M_i} e^{-\frac{M_i^2 \alpha\theta}{r_1^2}} \frac{J_o\left(M_i \frac{r}{r_1}\right)}{J_1(M_i)} \qquad (B-3)$$

where the M_i are the roots of the zero order Bessel function J_o. (For checking solutions at r/r_1 ratios different from those presented by Reference B-1 and for greater accuracy in checking, a small program for computing

Equation (B-3) was generated. For this purpose, Reference B-3 gives convenient Bessel Function expansions as

(1.) $(x) \leq 3$

$$J_o(x) = 1 - 2.2499997\left(\frac{x}{3}\right)^2 + 1.2656208\left(\frac{x}{3}\right)^4 - 0.3163866\left(\frac{x}{3}\right)^6 + 0.0444479\left(\frac{x}{3}\right)^8 - 0.0039444\left(\frac{x}{3}\right)^{10} + 0.0003100\left(\frac{x}{3}\right)^{12} + \beta \qquad \text{(B-4)}$$

The quoted error β is $< 5 \times 10^{-8}$, but Aerotherm experience shows that machine computations introduce errors of about 10^{-7}.

(2.) $x \geq 3$

$$J_o(x) = x^{-1/2} f_o \cos \theta_o \qquad \text{(B-5)}$$

where

$$f_o = 0.79788456 - 0.00000077\left(\frac{3}{x}\right) - 0.00552740\left(\frac{3}{x}\right)^2 - 0.00009512\left(\frac{3}{x}\right)^3 + 0.00137237\left(\frac{3}{x}\right)^4 - 0.00072895\left(\frac{3}{x}\right)^5 + 0.00014476\left(\frac{3}{x}\right)^6 + \beta \qquad \text{(B-6)}$$

with

$$\beta < 1.6 \times 10^{-8} \qquad \text{(B-7)}$$

and

$$\theta_o = x - 0.78539816 - 0.4166397\left(\frac{3}{x}\right) - 0.00003954\left(\frac{3}{x}\right)^2 + 0.00262573\left(\frac{3}{x}\right)^3 - 0.00054125\left(\frac{3}{x}\right)^4 - 0.00029333\left(\frac{3}{x}\right)^5 + 0.00013558\left(\frac{3}{x}\right)^6 + \beta \qquad \text{(B-8)}$$

with

$$\beta < 7 \times 10^{-8}. \qquad \text{(B-9)}$$

Reference B-3 also gives a useful tabulation of the values $J_1(M_i)$ for use in Equation (B-3).

The agreement between the exact solution and the computed points is excellent.

B.5 CONSTANT PROPERTIES SPHERE

Two computations were made for a 10-inch sphere, the property values, time step limits, and nodal sizing corresponding to both cylinder calculations described in Section 4 above.

Figure B-3 shows some computed results (as plotting symbols) compared to an exact solution. The exact solution is given by Reference B-2 as

$$\frac{t - t_o}{t_e - t_o} = 1 - \frac{2}{\pi} \frac{r_1}{r} \sum_{n=1}^{\infty} \frac{(-1)^{n+1}}{n} e^{-(n+1)^2 \frac{\alpha\theta}{r_1^2}} \sin\left(n\pi \frac{r}{r_1}\right) \qquad \text{(B-10)}$$

$$\frac{t_c - t_o}{t_e - t_o} = 2 \sum_{n=1}^{\infty} (-1)^{n+1} e^{-(n\pi)^2 \frac{\alpha\theta}{r_1^2}} \qquad \text{(B-11)}$$

These solutions are conveniently plotted in Reference B-1. A small program for producing results of greater accuracy and at general r/r_1 points was generated to facilitate comparisons.

Figure B-3 indicates that for a "proper" choice of nodal sizes, the computed results match exact solutions.

B.6 SEMI-INFINITE SOLID WITH CONSTANT PROPERTIES

A semi-infinite slab was simulated with a number of nodes large enough to insure that the final node showed no temperature response during the computation. Property values were taken as

$$k = 1 \text{ Btu/sec ft } {}^{\circ}R$$

$$c_p = 1 \text{ Btu/lb } {}^{\circ}R$$

$$\rho = 1 \text{ lb/ft}^2$$

The nodal distribution was, from the surface,

1 node of 5 inches thickness,
4 nodes of 10 inches thickness,
1 node of 12 inches thickness,
1 node of 15 inches thickness,
7 nodes of 24 inches thickness,
5 nodes of 48 inches thickness,
5 nodes of 96 inches thickness,
6 nodes of 192 inches thickness.

The maximum time step was limited to 5.0 seconds.

The exact solution to the semi-infinite solid problem with uniform initial temperature t_o and step surface temperature t_e at time $\theta = 0$ is a similarity solution

$$\frac{t - t_o}{t_e - t_o} = 1 - \text{erf}(x^*) \qquad \text{(B-12)}$$

where

$$x^* \triangleq \frac{x}{2\sqrt{\alpha\theta}} \qquad \text{(B-13)}$$

Figure B-4 shows the exact similarity profile compared to two of the many computed profiles. The circled points are for the computed response at 1 second, after only 8 computational steps. Even at this early time the computed profile is very close to the exact profile. The points in triangles are for time $\theta = 64$ seconds, after 64 computational steps.* By this time the computed points correspond to the exact solution to three significant figures.

As a further check for this problem, exact solutions are available for surface heat flux rate. Figure 5 shows the surface heat flux rate and integrated heat flux plotted versus dimensionless time. (The arbitrary length r_1 has been introduced in order to non-dimensionalize.) Agreement between the exact solutions of Schneider (Reference B-1) and the computed results is excellent.

B.7 SEMI-INFINITE SOLID WITH VARIABLE THERMAL CONDUCTIVITY

Halle (Reference B-4) has presented exact solutions for certain variable property problems useful for checking the computer programs. Of these solutions, the one for the step wall temperature problem with conductivity varying with temperature is

$$\frac{t - t_o}{t_e - t_o} = A\ \text{erfc}(x^*) + (1\text{-}A)\ \text{erfc}(nx^*) \qquad \text{(B-14)}$$

where

$$x^* \triangleq \frac{x}{2\sqrt{\alpha_o\theta'}} \quad \text{and} \quad \alpha_o \triangleq \frac{k_o}{\rho c_p} \quad \text{and} \quad k_o \triangleq k(t_o),$$

provided that k varies as

$$\frac{k}{k_o} = \frac{Ae^{-x^{*2}} + (1 - A)\,\frac{1}{n}\,e^{-n^2x^{*2}}}{Ae^{-x^{*2}} + (1 - A)\,n\,e^{-n^2x^{*2}}} \qquad \text{(B-15)}$$

*Although the maximum time step allowed is five seconds, the program applies various limiting criteria during rapid transients so that the average time step is less than five seconds.

The constants A and n may be chosen to give a useful k(t) function, which is obtained by cross-solving or cross-plotting between Equations (B-14) and (B-15).

Two cases were computed for check-out, one with A = 0.5 and n = 2.0 (corresponding to Case 4 on Figure 2 of Reference B-4) and the second with A = 1.85 and n = 2.0. Nodal sizes, maximum time step, specific heat, and density were all identical to those in the constant properties computation described in Section 6 above. The conductivity k_o was taken as 1.0 Btu/ft sec ^oF. Figure B-6 shows the thermal conductivity variations for the two cases, with k/k_o plotted against $(t - t_o)/(t_e - t_o)$. Tabular values used in the program are circled. The tabular values used are as follows:

Case 1
A = 0.5, n = 2.0
$t_o = 0^oR$, $t_e = 1000^oR$

$t(^oR)$	k/k_o
0	1.0
100	0.91
200	0.76
300	0.66
400	0.60
500	0.56
600	0.53
700	0.52
800	0.51
900	0.50
1000	0.50

Case 2
A = 1.85, n = 2.0
$t_o = 0^oR$, $t_e = 1000^oR$

$t(^oR)$	k/k_o
0	1.000
88.2	1.000
165.3	1.009
287.0	1.036
366.5	1.066
457.0	1.109
555.5	1.201
656.6	1.340
753.4	1.575
838.3	1.989
905.3	2.762
952.1	4.306
968.5	5.566
981.2	7.174
991.3	8.783
1000.0	9.500

During the computation the program obtains thermal conductivity values by linear interpolation between these points.

The first case corresponds to a material whose thermal conductivity decreases rapidly but nearly linearly with temperature, as for example, a pure metal, while the second case models a material whose conductivity increases very rapidly at high temperatures. This case resembles the charring ablator, for which the char layer has a much higher conductivity than the virgin material.

Figure B-7 shows the exact and the computed results for the two cases, along with the constant properties exact solution to illustrate the degree of departure of the two cases from the constant properties case. Agreement between the computed and the exact solutions is excellent.

B.8 SEMI-INFINITE RECEDING SOLID

Check-out of the convection aspects of the computation requires a problem with surface recession. An analytical solution is available for the transient response of a semi-infinite solid initially at uniform temperature exposed to a step in surface temperature and to a step in surface recession rate $\dot{S}$.

For the constant properties problem it can readily be shown that the temperature profile approaches a quasi-steady form

$$\frac{t - t_o}{t_e - t_o} = e^{-\frac{\dot{S}x}{\alpha}} \qquad \text{(B-16)}$$

where the x coordinate origin is tied to the receding surface. The work of Reference B-5 shows that a useful measure of the approach to steady state is provided by the variable

$$\frac{\rho c_p \dot{S}(t_e - t_o)}{q_e}$$

comparing the amount of solid convection pick-up to the amount of energy conducted into the solid. This term is initially zero and approaches unity in the steady state.

Figure B-8 shows the exact transient response, calculated from results of Reference B-5, compared to computed results for a problem with the same nodal size distribution as the infinite slab problem described in Section 6 above. The property values were

$$k = 1 \text{ Btu/ft sec } ^{o}F$$
$$c_p = 0.1 \text{ Btu/lb } ^{o}F$$
$$\rho = 1 \text{ lb/ft}^3$$

The specified surface recession rate $\dot{S}$ was 0.5 ft/sec., which limited the time step to a maximum value of 1/6 second. (The program will not allow more than 20 percent of the thickness of the smallest node to be ablated away in a single computational step.)

The agreement between computed results and the exact solution is excellent.

Three separate problems were calculated in order to judge the accuracy of the computation of the steady state temperature profile. Parameter assignments for these calculations were as follows:

	Case 1	Case 2	Case 3
k (Btu/ft sec ^{o}F)	1.0	1.0	1.0
c_p (Btu/lb ^{o}F)	1.0	0.1	0.1
ρ (lb/ft^3)	1.0	1.0	1.0
α (ft^2/sec)	1.0	10.0	10.0
$\dot{S}$ (ft/sec)	0.5	0.5	0.5
$\Delta\theta_{max}$(sec)	0.167	1.6	1.6
"Steady State" time (sec)	100.0	300.0	300.0
Dimensionless "Steady State" time $\dot{S}^2\theta/\alpha$	5.0	2.739	2.739
Parameter $\dot{S}d_{min}/\alpha$	0.5	0.2	0.1

	Case 1	Case 2	Case 3
Nodes	1 at 5"	9 at 48"	25 at 24"
	4 at 10"	5 at 96"	9 at 48"
	1 at 12"	6 at 192"	5 at 96"
	1 at 15"	5 at 500"	6 at 192"
	7 at 24"		5 at 500"
	5 at 48"		
	5 at 96"		
	6 at 192"		

Figure B-9 shows the results of these three calculations and indicates that Case 1 gives a poor steady state profile while Case 2 is improved but still not good, and Case 3 gives a good result. The key difference between the three cases lies in the relative sizes of a single heat conduction term and a single solid convection term in the finite difference energy balance, Equation (B-1).

$$\text{conduction term} \approx \frac{k}{d}\,(T_{n+1} - T_n) \qquad \text{(B-17)}$$

$$\text{convection term} \approx \rho c_p \dot{s}\,(T_{n+1} - T_n) \qquad \text{(B-18)}$$

$$\frac{\text{convection term}}{\text{conduction term}} = \frac{\rho c_p \dot{s} d}{k} = \frac{\dot{s} d}{\alpha} \qquad \text{(B-19)}$$

The value of this parameter for d_{min} is given in the table above.

Thus Figure B-9 suggests that an accurate calculation requires

$$\frac{\dot{s} d_{min}}{\alpha} < 0.1\ . \qquad \text{(B-20)}$$

It can be shown through an analysis of truncation errors (see Sub-Appendix B-1) that this conclusion is <u>not</u> generally valid. It holds only if

1. The nodes are small enough that truncation errors in the conduction terms are "small,"
2. The temperature profile is "close" to $e^{-\dot{s}x/\alpha}$.

Even though the criterion (B-20) is not generally valid, it is still a useful one since many ablation problems approximately satisfy the two conditions.

B.9 SUMMARY AND CONCLUSIONS

The purpose of the test calculations was to show that the Aerotherm Charring Material Ablation (CMA) Program, Version 2 (Implicit) performs heat conduction calculations properly. Checks included computations for slab, cylinder, spherical, and semi-infinite solid geometries exposed to step surface temperature increases and several calculations of semi-infinite solid geometries exposed to simultaneous steps in surface temperatures and surface recession rate.

Results indicated that when nodes were sized properly, the results generated by the program matched exact solutions and that, therefore, the program is judged to operate properly in its heat conduction and solid convection aspects.

Poor choices of node sizes can of course lead to unsatisfactory results, but a complete analysis of this subject is outside the intended scope of this appendix.

REFERENCES

B-1 Schneider, P. J.: Temperature Response Charts. John Wiley and Sons, Inc., New York, 1963.

B-2 Schneider, P. J.: Conduction Heat Transfer. Addison-Wesley Publishing Company, Inc., Cambridge, Massachusetts, 1955, pp. 238-239.

B-3 Abramowitz, M., and Stegun, I. A., eds.: Handbook of Mathematical Functions. National Bureau of Standards, Applied Mathematics Series No. 55, United States Government Printing Office, Washington, D. C., 1964, pp. 369-370.

B-4 Halle, H.: Exact Solution of Elementary Transient Heat Conduction Problem Involving Temperature Dependent Properties. Transactions of the American Society of Mechanical Engineers, Series C, Journal of Heat Transfer, Vol. 87, No. 3, August 1965, pp. 420-421.

B-5 Baer, D., and Ambrosio, A., Heat Conduction in a Semi-Infinite Slab With Sublimation at the Surface. Space Technology Laboratories, Inc., Pasadena, California, TR-59-0000-00610, February 24, 1959.

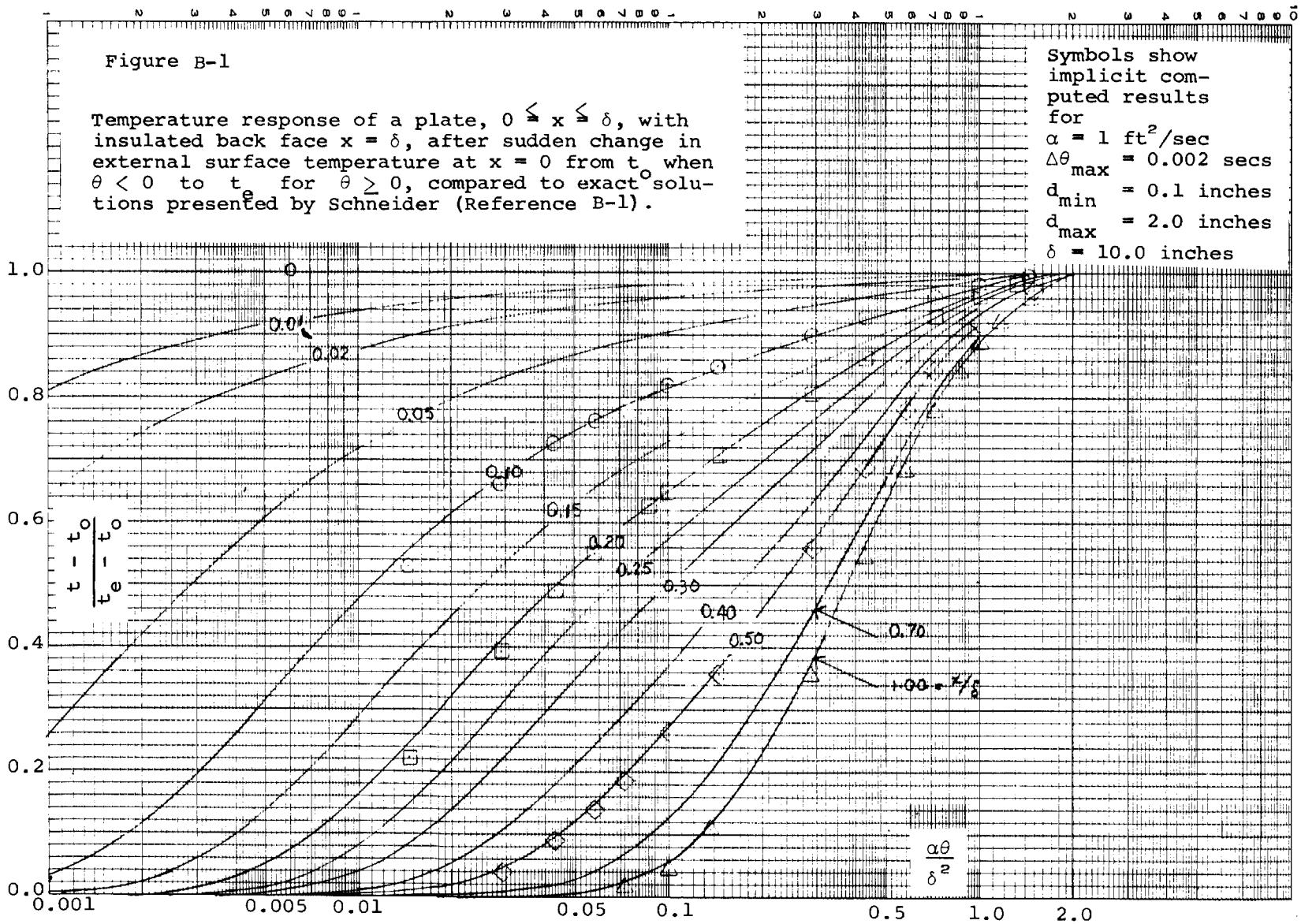
Figure B-1
Temperature response of a plate, $0 \leq x \leq \delta$, with insulated back face $x = \delta$, after sudden change in external surface temperature at $x = 0$ from t_o when $\theta < 0$ to t_e for $\theta \geq 0$, compared to exact solutions presented by Schneider (Reference B-1).
Symbols show implicit computed results for
$\alpha = 1$ ft^2/sec
$\Delta\theta_{max} = 0.002$ secs
$d_{min} = 0.1$ inches
$d_{max} = 2.0$ inches
$\delta = 10.0$ inches
$\frac{t - t_o}{t_e - t_o}$
0
0.01
0.02
0.05
0.10
0.15
0.20
0.25
0.30
0.40
0.50
0.70
1.00 = F/S
$\frac{\alpha\theta}{\delta^2}$
1.0
0.8
0.6
0.4
0.2
0.0
0.001
0.005
0.01
0.05
0.1
0.5
1.0
2.0

Figure B-2

Temperature Response of a Cylinder, $\theta \leq r \leq r_e$, after a sudden change in external surface temperature from t_o when $\theta < 0$ to t_c for $\theta \geq 0$, compared to exact solutions presented by Schneider (Reference B-1).

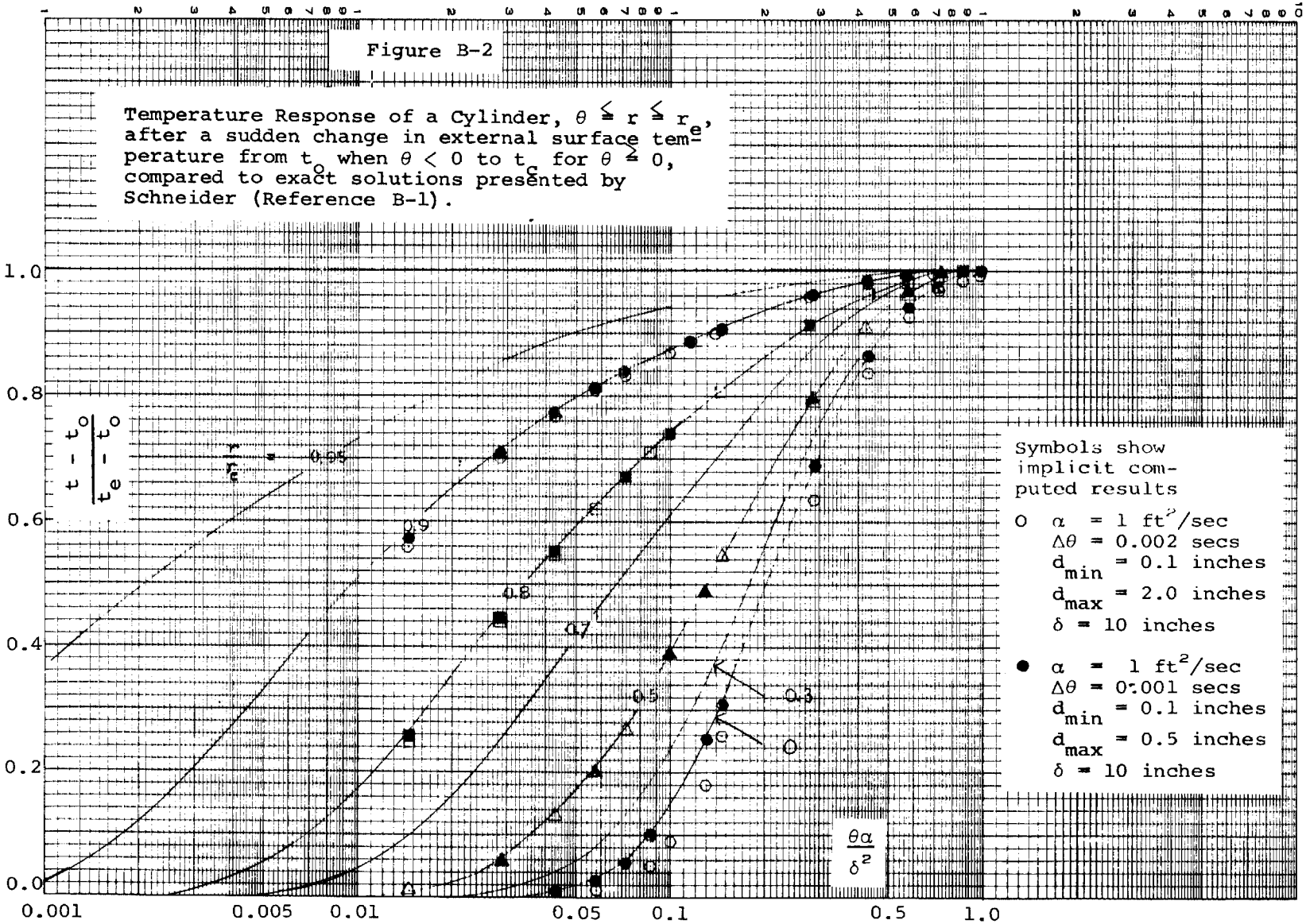

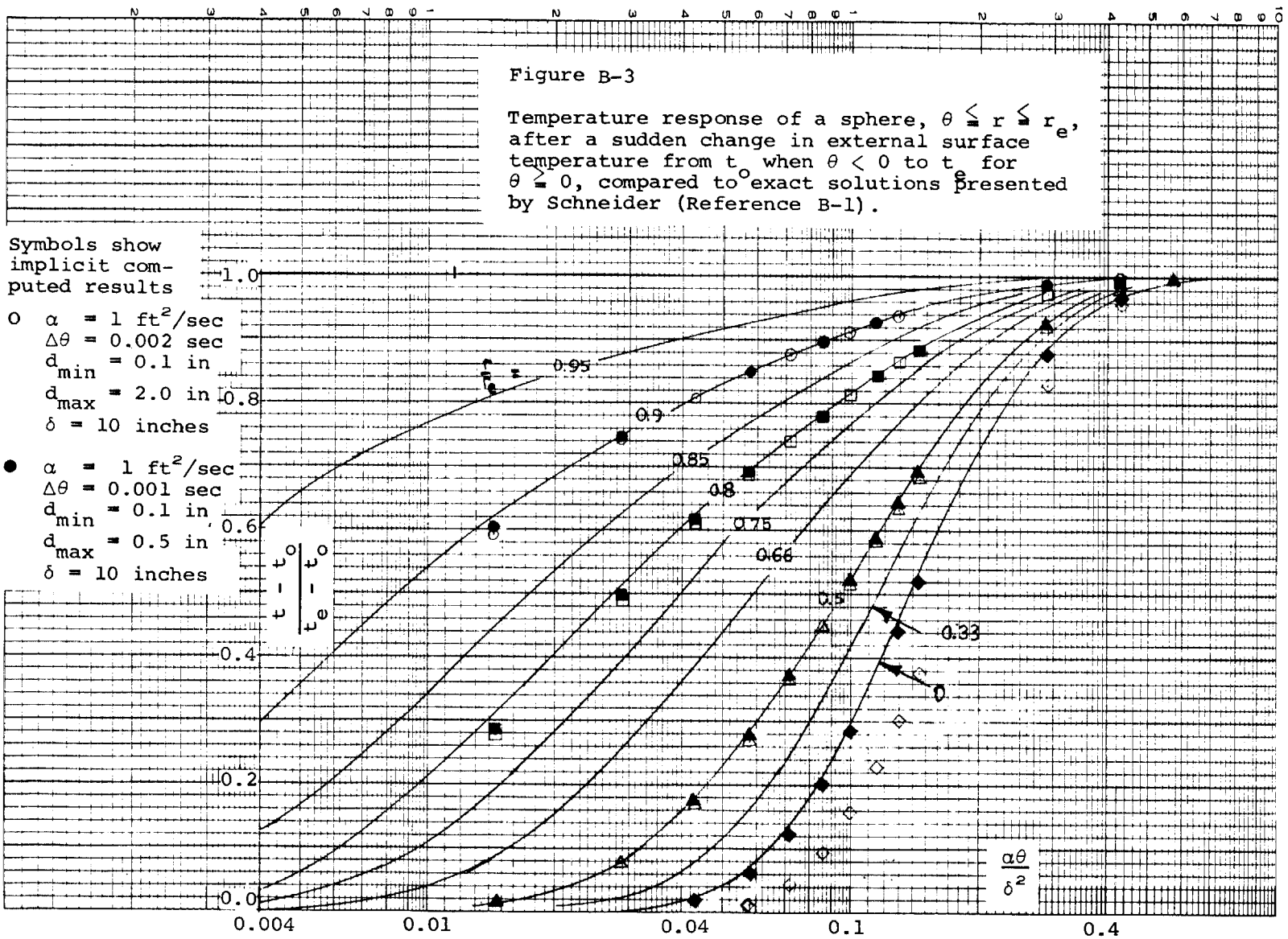

Figure B-3

Temperature response of a sphere, $\theta \leq r \leq r_e$, after a sudden change in external surface temperature from t_o when $\theta < 0$ to t_e for $\theta \geq 0$, compared to exact solutions presented by Schneider (Reference B-1).

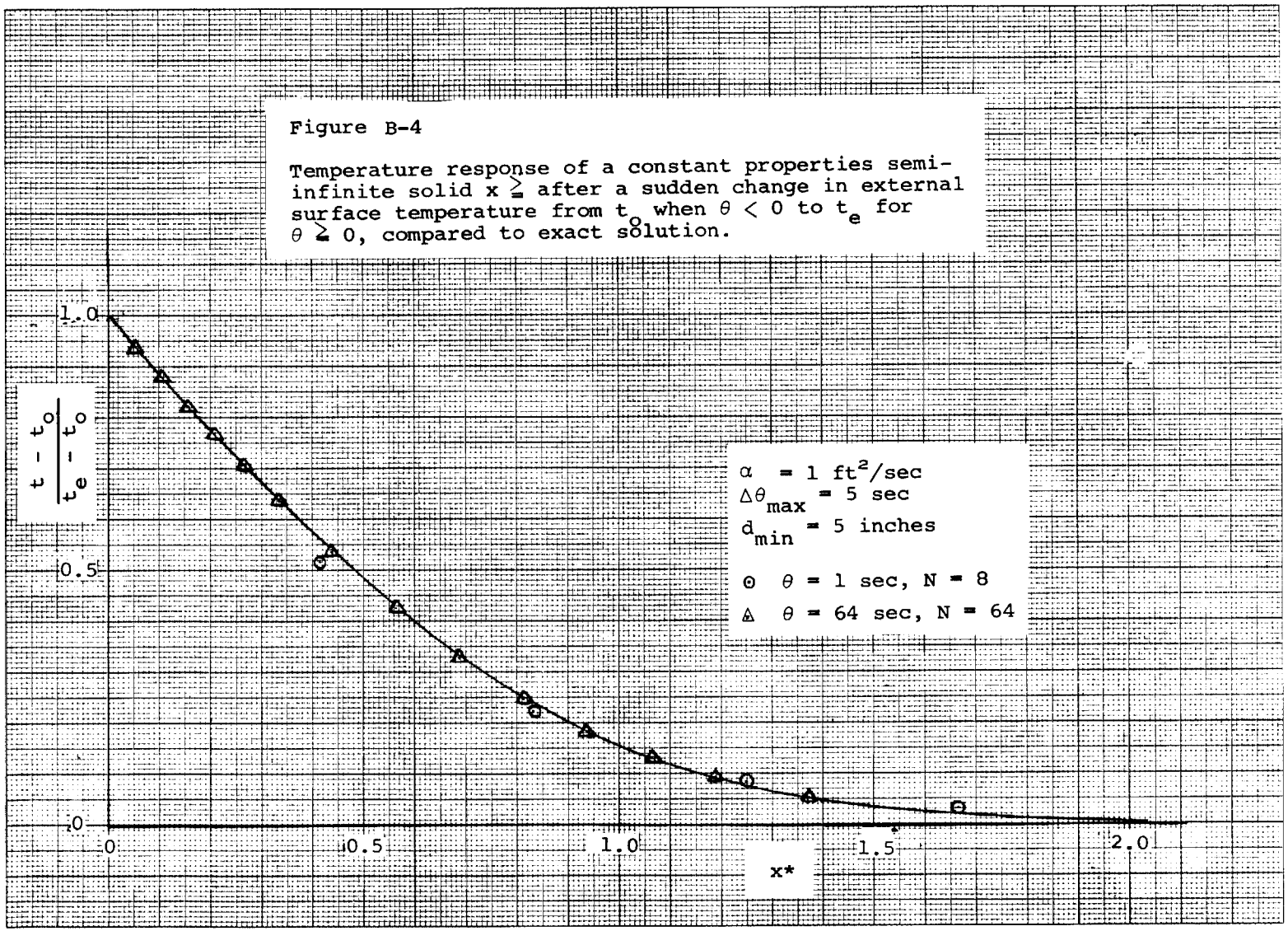
Figure B-4
Temperature response of a constant properties semi-infinite solid x ≥ after a sudden change in external surface temperature from t_o when θ < 0 to t_e for θ ≥ 0, compared to exact solution.
$\frac{t - t_o}{t_e - t_o}$
1.0
0.5
0
0
0.5
1.0
1.5
2.0
x*
α = 1 ft²/sec
$\Delta\theta_{max}$ = 5 sec
d_{min} = 5 inches
⊙ θ = 1 sec, N = 8
△ θ = 64 sec, N = 64

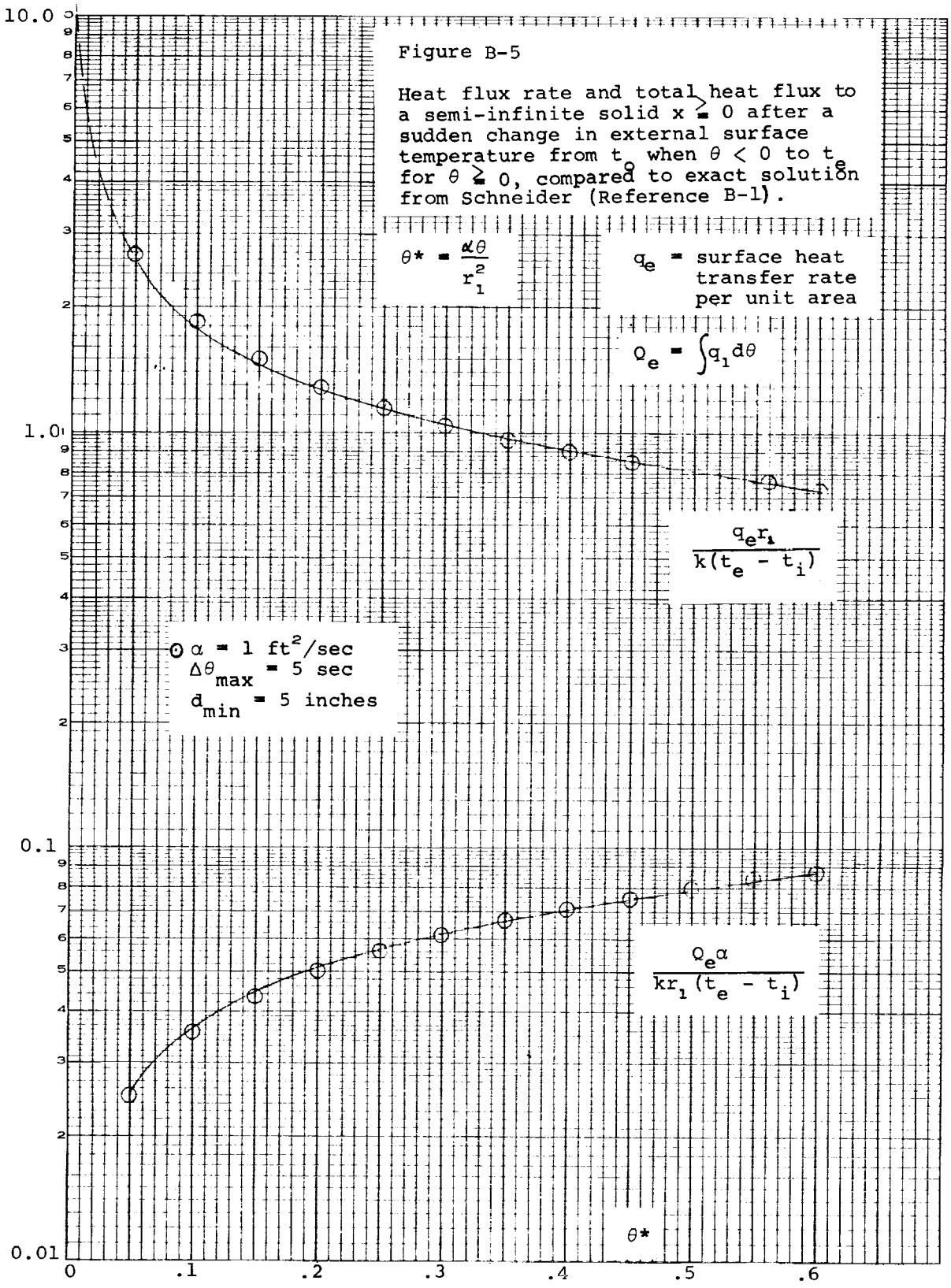
Figure B-5
Heat flux rate and total heat flux to a semi-infinite solid x ≥ 0 after a sudden change in external surface temperature from t_o when θ < 0 to t_e for θ ≥ 0, compared to exact solution from Schneider (Reference B-1).
θ* = αθ / r_1^2
q_e = surface heat transfer rate per unit area
Q_e = ∫ q_1 dθ
q_e r_1 / k(t_e - t_i)
⊙ α = 1 ft^2/sec
Δθ_max = 5 sec
d_min = 5 inches
Q_e α / k r_1 (t_e - t_i)
θ*
10.0
1.0
0.1
0.01
0
.1
.2
.3
.4
.5
.6

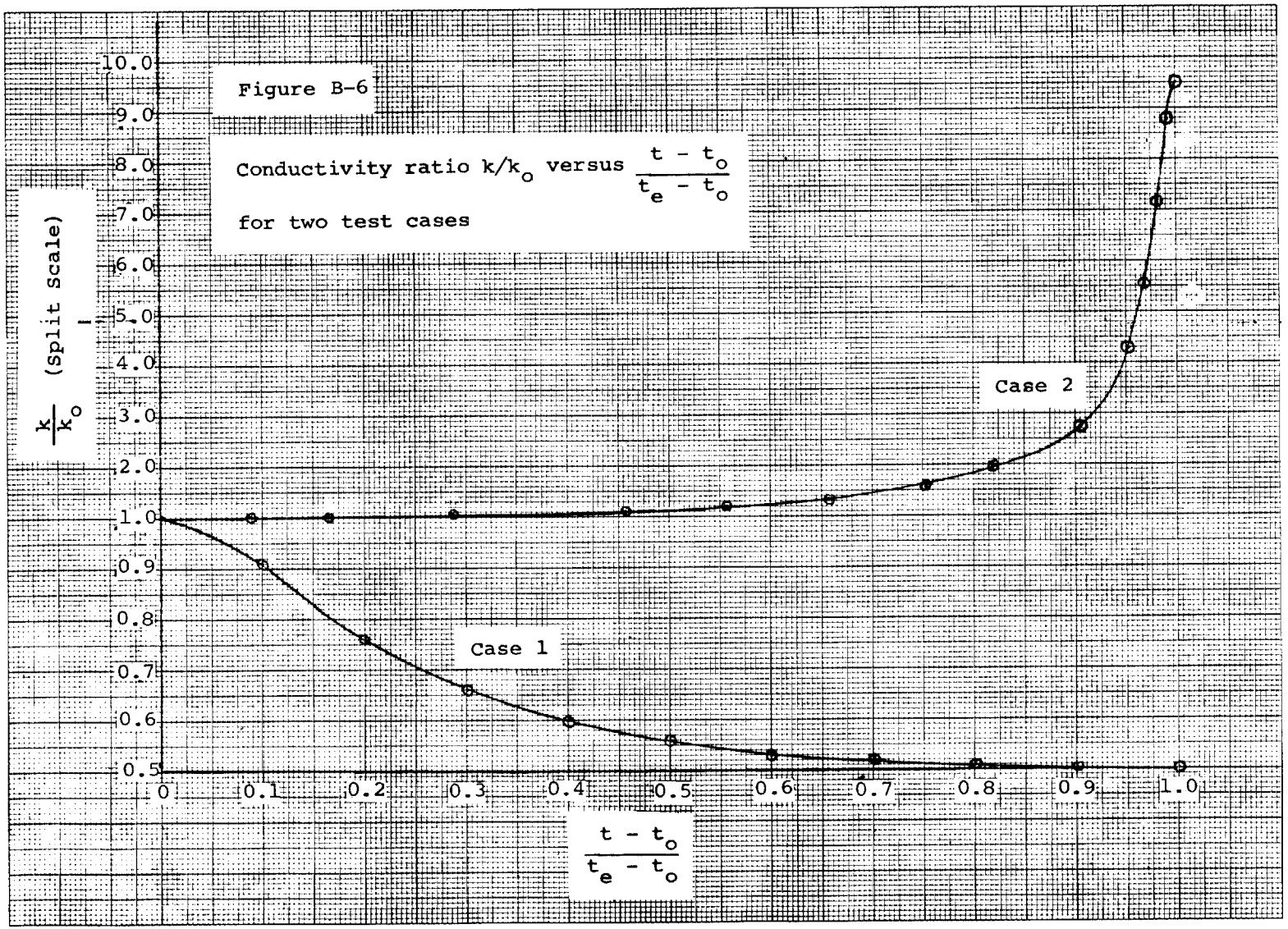
Figure B-6
Conductivity ratio k/k_o versus $\frac{t - t_o}{t_e - t_o}$
for two test cases
$\frac{k}{k_o}$ (Split scale)
10.0
9.0
8.0
7.0
6.0
5.0
4.0
3.0
2.0
1.0
0.9
0.8
0.7
0.6
0.5
0
0.1
0.2
0.3
0.4
0.5
0.6
0.7
0.8
0.9
1.0
Case 1
Case 2
$\frac{t - t_o}{t_e - t_o}$

Figure B-7

Temperature response of a semi-infinite solid $x \geq 0$ after a sudden change in exterial surface temperature from t_o when $\theta < 0$ to t_e for $\theta \geq 0$, compared to exact solution for two varying thermal conductivity cases.

$$\frac{k}{k_o} = \frac{Ae^{-x^{*2}} + (1 - A)\frac{1}{n}e^{-n^2x^{*2}}}{Ae^{-x^{*2}} + (1 - A)\, n\, e^{-n^2x^{*2}}} \quad \text{where } k_o = k(t_o)$$

$$\frac{t - t_o}{t_e - t_o} = A\,\text{erfc}(x^*) = (1 - A)\,\text{erfc}(nx^*)$$

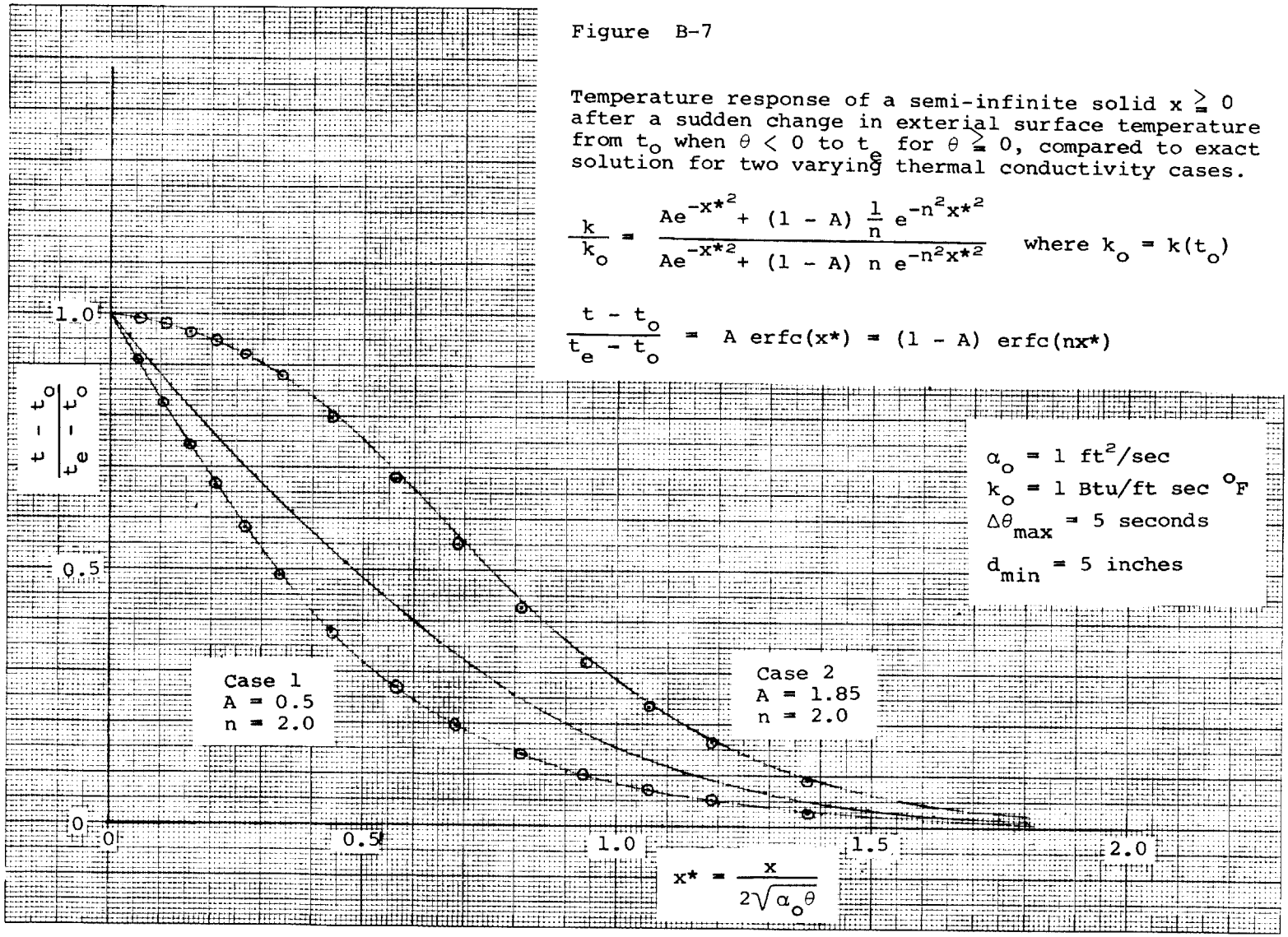

Figure B-8

Transient response of a semi-infinite solid $x \geq 0$ after a sudden change in external surface temperature from t_o when $\theta < 0$ to t_e for $\theta \geq 0$ and a sudden increment in surface recession rate from 0 when $\theta < 0$ to $\dot{s}$ for $\theta \geq 0$ compared to exact solution of Reference B-5).

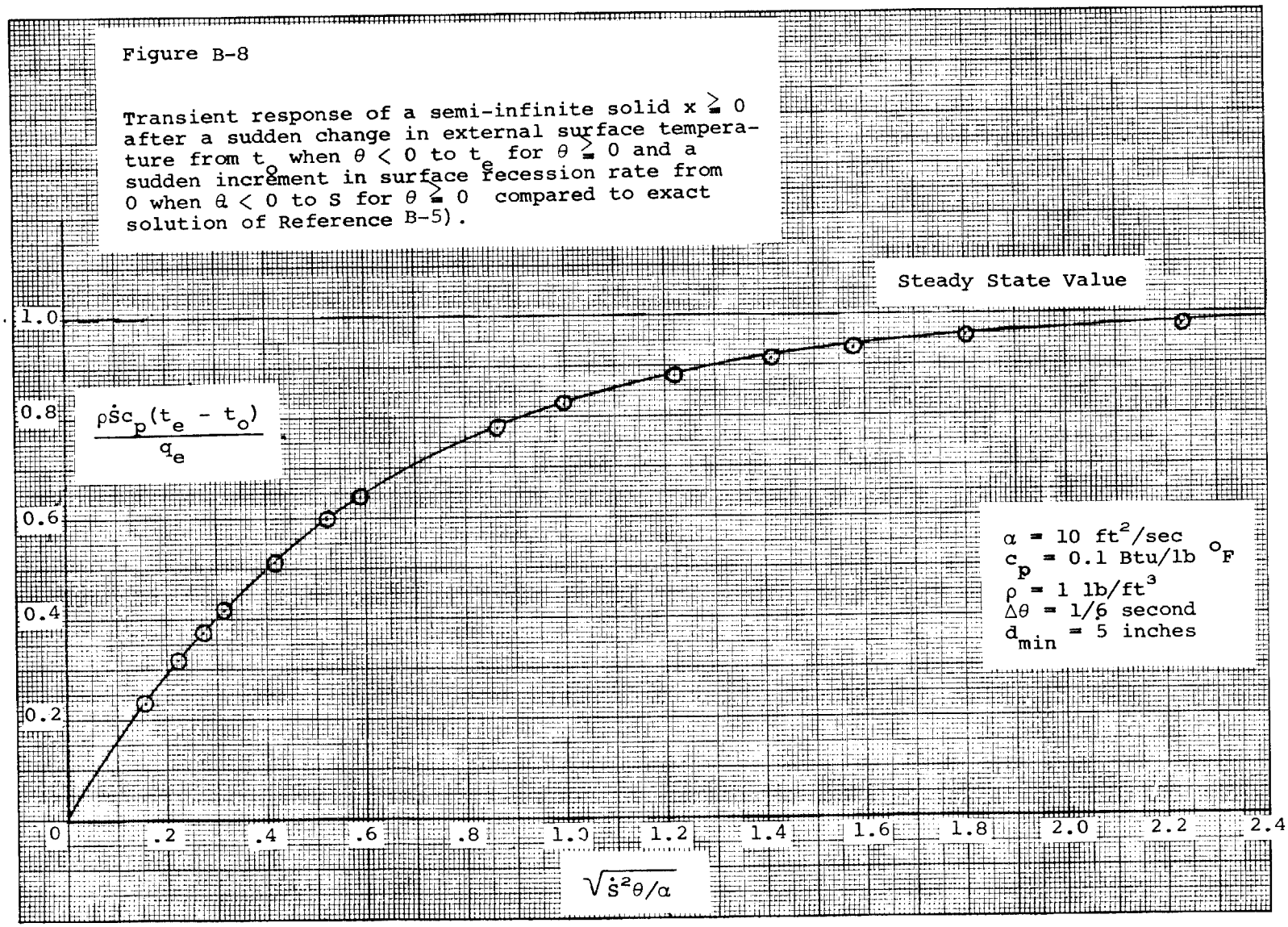

Figure B-9

Steady state temperature profile for a semi-infinite solid $x \geq 0$ for a constant surface temperature t_o, a constant surface recession rate S, and a temperature t_e for $x \longrightarrow \infty$.

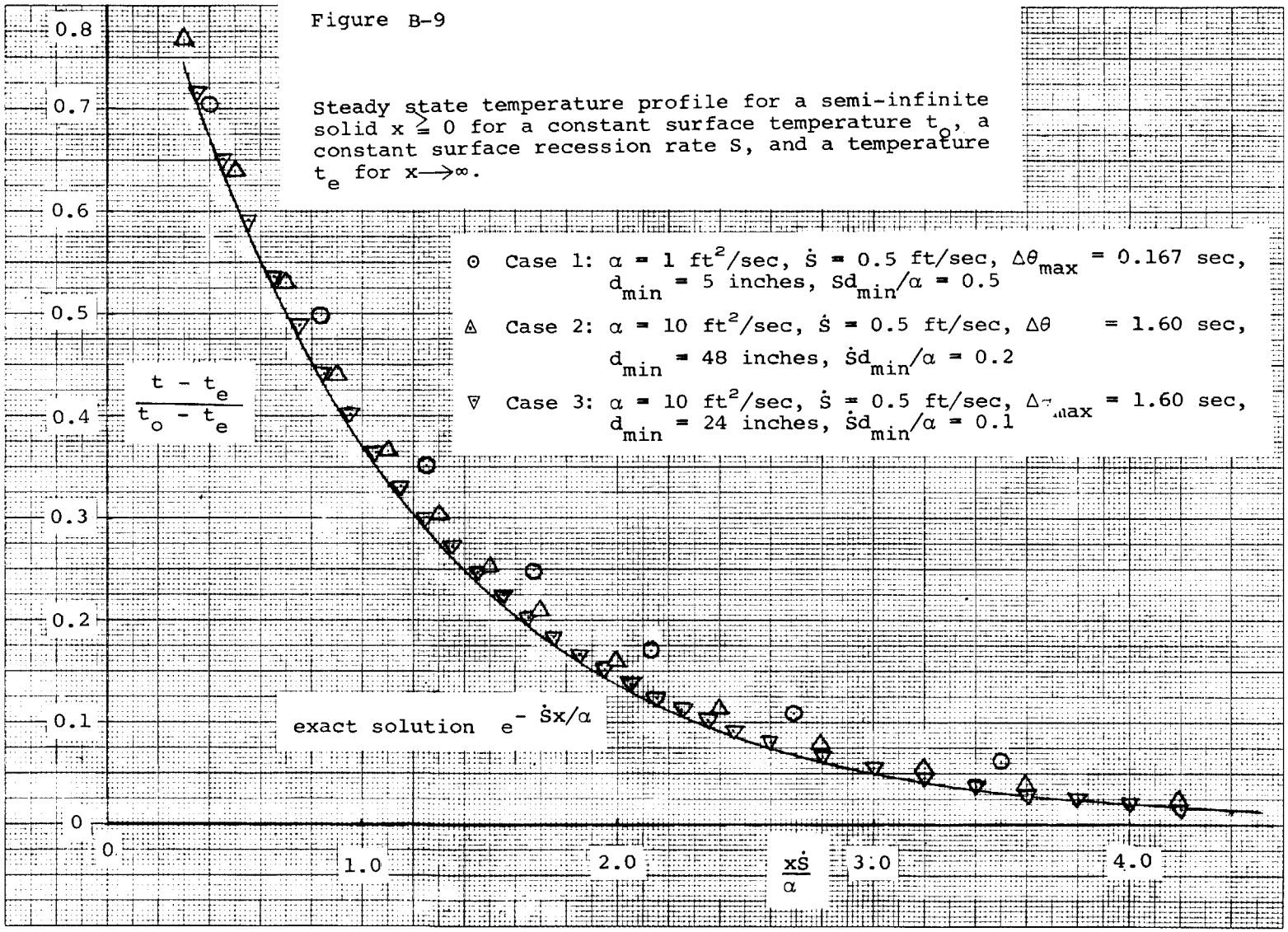

SUB-APPENDIX B-1

ERROR ANALYSIS OF STEADY STATE SOLUTION FOR A CONSTANT PROPERTIES SEMI-INFINITE RECEDING SOLID WITH CONSTANT SURFACE TEMPERATURE AND CONSTANT SURFACE RECESSION RATE

B-1.1 INTRODUCTION

The differential equation for this problem is

$$\rho c_p \frac{\partial t(x,\theta)}{\partial \theta} = k \frac{\partial^2 t(x,\theta)}{\partial x^2} + \rho c_p \dot{s} \frac{\partial t(x,\theta)}{\partial x} \qquad \text{(B-1-1)}$$

Here the origin of the x-coordinate is fixed to the receding surface. Thus the left-hand side represents rate of energy storage (at constant x); the first term on the right-hand side represents net heat conduction, and the final term represents net energy convection with the solid material.

The associated boundary conditions are

$$t(0,\theta) = t_e \qquad \text{(B-1-2)}$$

$$t(x,\theta)_{x\to\infty} = t_o \qquad \text{(B-1-3)}$$

It can readily be shown that a steady state solution of the system (B-1-1), (B-1-2), and B-1-3) is

$$\frac{t - t_o}{t_e - t_o} = e^{-\dot{s}x/\alpha} \qquad \text{(B-1-4)}$$

B-1.2 FINITE DIFFERENCE FORM

The Version 2 program uses Equation (B-1) as the finite difference form of the energy equation. In the steady state this relation becomes (considering for convenience constant areas, constant properties, and constant nodal thicknesses)

$$\frac{k\Delta\theta}{d^2}\left[T'_{n-1} - 2T'_n + T'_{n+1}\right] + \rho c_p \dot{s} \frac{\Delta\theta}{d}\left(T'_{n+1} - T'_n\right) = 0 \qquad \text{(B-1-5)}$$

The difference forms in this equation have the following associated Taylor expansions:

$$\frac{T(x+d) - 2T(x) + T(x-d)}{d^2} = \frac{\partial^2 T(x)}{dx^2} + \frac{d^2}{12}\frac{\partial^4 T(x)}{\partial x^4} + O(d^4) = E_1 \quad \text{(B-1-6)}$$

$$\frac{T(x+d) - T(x)}{d} = \frac{\partial T(x)}{\partial x} + \frac{d}{2}\frac{\partial^2 T(x)}{\partial x^2} + O(d^2) = E_2 \quad \text{(B-1-7)}$$

Truncating the Taylor series expansions after the second term in both cases gives, for the two expansions,

$$E_1 = \frac{d^2 T}{dx^2}(x) + \frac{d^2}{12}\frac{d^4 T(x_1)}{dx^4} \quad \text{(B-1-8)}$$

$$E_2 = \frac{dT(x)}{dx} + \frac{d}{2}\frac{d^2 T(x_2)}{dx^2} \quad \text{(B-1-9)}$$

where

$$x - d \leq x_1 \leq x + d \quad \text{(B-1-10)}$$

and

$$x \leq x_2 \leq x + d \quad \text{(B-1-11)}$$

Now the original differential equation for the steady state profile is

$$\frac{kd^2 t}{dx^2} + \rho c_p \dot{s}\frac{dt}{dx} = 0 \quad \text{(B-1-12)}$$

or

$$\frac{d^2 t}{dx^2} + \left(\frac{\dot{s}}{\alpha}\right)\frac{dt}{dx} = 0 \quad \text{(B-1-13)}$$

From Equation (B-1-13) may be derived the useful relation

$$\frac{d^4 t}{dx^4} = -\left(\frac{\dot{s}}{\alpha}\right)^3 \frac{dt}{dx} \quad \text{(B-1-14)}$$

Now if $T \approx t$, these relations may be employed to simplify the expansions. Substitution of (B-1-14) into (B-1-8) and (B-1-13) into (B-1-9) gives

$$E_1 \cong \frac{d^2 T(x)}{dx^2} - \frac{d^2}{12}\left(\frac{\dot{s}}{\alpha}\right)^3 \frac{dT(x_1)}{dx} \quad \text{(B-1-15)}$$

$$E_2 \cong \frac{dT(x)}{dx} - \frac{d}{2}\left(\frac{\dot{s}}{\alpha}\right)\frac{dT(x_2)}{dx} \quad \text{(B-1-16)}$$

B-1.3 ESTIMATION OF ERROR

Equations (B-1-5), (B-1-7), (B-1-7), (B-1-15), and (B-1-16) imply that the solution to the difference equation corresponds to a solution of the differential relation

$$\frac{kd^2T}{dx^2} + \rho c_p \dot{S} \frac{dT}{dx} - \left[\frac{kd^2}{12} \left(\frac{\dot{S}}{\alpha}\right)^3 \frac{dT(x_1)}{dx} + \rho c_p \dot{S} \frac{d}{2} \left(\frac{\dot{S}}{\alpha}\right) \frac{dT(x_2)}{dx} \right] = 0 \quad \text{(B-1-17)}$$

If d is small, then $x_1 \approx x_2 \approx x$, and so an approximate solution to this equation and its associated boundary conditions is

$$T = \frac{T - T_o}{T_e - T_o} \cong e^{-\frac{\dot{S}x}{\alpha} + \frac{Bx}{\alpha}} \quad \text{(B-1-18)}$$

where

$$B \triangleq \frac{kd^2}{12} \left(\frac{\dot{S}}{\alpha}\right)^3 + \rho c_\beta \dot{S} \frac{d}{2} \left(\frac{\dot{S}}{\alpha}\right). \quad \text{(B-1-19)}$$

Since

$$\frac{Bx}{k} = \frac{Sx}{\alpha} \left[\frac{1}{12} \left(\frac{\dot{S}d}{\alpha}\right)^2 + \frac{1}{2} \left(\frac{\dot{S}d}{\alpha}\right) \right], \quad \text{(B-1-20)}$$

then generally

$$\frac{Bk}{k} << 1 \quad \text{if} \quad \frac{\dot{S}x}{\alpha} \approx 1 \quad \text{and} \quad \frac{\dot{S}d}{\alpha} << 1 \quad \text{(B-1-21)}$$

so that the approximate solution is nearly

$$T^* = e^{-\frac{\dot{S}x}{\alpha}} \left[1 + \left(\frac{Bx}{K}\right) \right]. \quad \text{(B-1-22)}$$

Since $e^{-\dot{S}x/\alpha}$ is the true solution, the relative error of the approximate solution is Bx/k, or

$$\frac{T^* - t^*}{t^*} = \frac{\epsilon}{t^*} \cong \frac{Bx}{k} \cong \frac{\dot{S}x}{\alpha} \left[\frac{1}{12} \left(\frac{\dot{S}d}{\alpha}\right)^2 + \frac{1}{2} \left(\frac{\dot{S}d}{\alpha}\right) \right] \quad \text{(B-1-23)}$$

For the relative error to be small, the parameter $\dot{S}d/\alpha$ must be small. In this case, the relative error is given by

$$\frac{\epsilon}{t^*} \simeq \frac{1}{2}\left(\frac{\dot{s}x}{\alpha}\right)\left(\frac{\dot{s}d}{\alpha}\right) \quad . \qquad \text{(B-1-24)}$$

It is interesting to note that this expression very closely predicts the error magnitudes for the three cases shown in Figure B-8.*

B-1.4 CONCLUSION

The discussion has shown that errors in the steady state profile of the constant properties semi-infinite receding solid with constant surface temperature and constant recession rate are given by Equation (B-1-24), provided that total errors, including those due to a poor choice of node sizes (conduction errors), are small.

The criterion for errors to be small is $\dot{s}d/\alpha \ll 1$. This criterion pertains only to this problem, since it is a function of the exact solution. Since many ablation problems model this sample problem closely, the criterion should be of more general utility.

In effect, Equation (B-1-24) gives an estimate of the size of errors due to the relatively crude convection term (errors $O(d)$), provided that errors due to the more accurate conduction term (errors $O(d^2)$) are small. If conduction errors are not small, errors due to the convection term are not readily estimated. Problems of estimating conduction term errors lie outside the scope of this appendix.

*Only in cases 2 and 3 was the nodal spacing sufficiently uniform to permit a true comparison.

APPENDIX C

STUDY OF ALTERNATIVE TREATMENTS OF THE DECOMPOSITION KINETICS EQUATION IN THE CHARRING MATERIAL ABLATION PROGRAM

TABLE OF CONTENTS

Appendix C

LIST OF SYMBOLS

Appendix C

A	cross sectional area	(ft^2)
C_p	specific heat	(Btu/lb°F)
Ea/R	activation energy	(°R)
F	fraction, nodes actively decomposing/total number of nodes	(---)
$\bar{h}$	defined as $(\rho_p h_p - \rho_c h_c)/(\rho_p - \rho_c)$	(Btu/lb)
h_g	pyrolysis gas enthalpy	(Btu/lb)
I	number of decomposing components in the material	(---)
J	number of nodelets per node	(---)
k	thermal conductivity	(Btu/ft sec °F)
k_i	pre-exponential factor	(sec^{-1})
K	number of surface energy balance iterations per time step	(---)
$\dot{m}_g$	pyrolysis gas flow rate past a point	(lb/ft^2 sec)
m_i	density reaction order for component i in decomposition	(---)
N	total number of nodes	(---)
S	total surface recession	(ft)
$\dot{S}$	surface recession rate	(ft/sec)
T	temperature	(°R)
T	total execution time	(μsec/step)
x	distance coordinate normal to receding heated surface, with origin fixed in that surface	(ft)

y	distance coordinate normal to receding heated surface with origin fixed in space at the initial location of the heated surface	(ft)
Greek		
δ	nodal thickness	(ft)
Δ	denotes differences over a time step	(---)
Γ	volume fraction of resin (components A and B)	(---)
ϵ	relative (fractional) error	(---)
θ	time	(seconds)
μ	10^{-6}	(---)
ρ	density	(lb/ft^3)
ρ_o	component initial density	(lb/ft^3)
ρ_r	component residual density	(lb/ft^3)
Subscripts		
A, B, C	enumerate decomposing components	
c	denotes pure char	
g	denotes pyrolysis gas	
i	denotes component	
n	denotes node	
p	denotes pure virgin plastic	

STUDY OF ALTERNATIVE TREATMENTS OF THE DECOMPOSITION KINETICS EQUATION IN THE CHARRING MATERIAL ABLATION PROGRAM

C.1 INTRODUCTION

This appendix reports the results of a number of computational experiments aimed at defining and eliminating causes of irregular or uneven internal response solutions occasionally produced by the Aerotherm Charring Material Ablation Program (CMA). For economy reasons, the calculations described here were limited to one material and a small number of transient conditions. Hence, it has not been possible to extract many general conclusions. However, the key problems have been fairly clearly identified, and in the process of doing so some significant improvements were made in the program operation.

The appendix includes a number of graphs which illustrate the effect of various computational techniques. To present all the interesting aspects of the results would require an enormous mass of detail and many pages of computer output. Obviously a short memorandum can only touch upon a limited number of aspects, and hence the report necessarily omits many details and takes on a descriptive nature.

C.2 SUMMARY OF CONCLUSIONS

The history of the instantaneous pyrolysis gas rate provides the most sensitive index to the smoothness of the internal response solution. Plots of this gas rate for slowly decomposing materials such as the phenolics are smooth and regular regardless of the transient. The solutions to certain rather rare problems have irregular gas rates. These do not affect the important overall aspects of the solution and so generally even these rare irregular solutions can be accepted. The boundary layer program (BLIMP) cannot accept irregular solutions, however. Efforts to eliminate oscillations for this application showed that:

1. Replacement of the explicit treatment of density in the decomposition kinetic equation by exact integrated relations smoothed most solutions and shortened computation time
2. Remaining unsmooth solutions could be smoothed by reductions in node size
3. The number of nodelets per node has no importance for such problems. Nodelets may be eliminated, or greatly reduced in number, with great savings in computation time.

C.3 GENERAL BACKGROUND

Determination of the internal thermal response of an ablating, charring material requires the solution of a differential energy transport equation in depth. One form of this equation is

$$\rho\, C_p \left.\frac{\partial T}{\partial \theta}\right)_x = \frac{1}{A}\frac{\partial}{\partial x}\left(k\, A \left.\frac{\partial T}{\partial x}\right)_o + \left(h_g - \bar{h}\right)\left.\frac{\partial \rho}{\partial \theta}\right)_y + \dot{S}\,\rho\, C_p \left.\frac{\partial T}{\partial x}\right)_\theta + \frac{\dot{m}_g}{A}\left(\frac{\partial h_g}{\partial x}\right)_\theta \qquad \text{(C-1)}$$

Here the origin of the x-coordinate is tied to the moving heated surface, whereas the origin of the y-coordinate is fixed in space (at the original location of the heated surface).

This energy equation is coupled to some decomposition kinetic equation for $(\partial\rho/\partial\theta)_y$. In the CMA program this decomposition equation is

$$\left.\frac{\partial \rho}{\partial \theta}\right)_y = \Gamma\left(\frac{\partial \rho_A}{\partial \theta} + \frac{\partial \rho_B}{\partial \theta}\right)_y + (1 - \Gamma)\left(\frac{\partial \rho_C}{\rho\,\theta}\right)_y \qquad \text{(C-2a)}$$

where

$$\left.\frac{\partial \rho_i}{\partial \theta}\right)_y = -k_i e^{-E_i/RT}\,\rho_{o_i}\left(\frac{\rho_i - \rho_{r_i}}{\rho_{o_i}}\right)^{m_i} \quad \text{for } i = A,B,C \qquad \text{(C-2b)}$$

If all computations are done in terms of a nodal network tied to the receding surface, then to keep track of nodal (constant x) densities it is necessary to add to equations (C-1) and (C-2) above the convective relation

$$\left.\frac{\partial \rho}{\partial \theta}\right)_x = \left.\frac{\partial \rho}{\partial \theta}\right)_y + \left.\frac{\partial \rho}{\partial x}\right)_\theta \dot{S} \qquad \text{(C-3)}$$

Computational details for this equation will be discussed later.

These three equations, with appropriate boundary and initial conditions, usually require finite-differencing for solution. Finite differencing may be done in a variety of ways, each of which has special aspects.

The aspects of interest here pertain to the treatment of the decomposition equation (C-2). If not treated properly in relation to the treatment of the energy equation (C-1), this equation can cause great computational difficulties. These difficulties are illustrated below.

C.4 FULLY EXPLICIT TREATMENT OF ENERGY AND DECOMPOSITION EQUATIONS, NODES ONLY

"Explicit" denotes that each "new" quantity, such as a nodal temperature, is computed in terms of "old" quantities only. Thus temperatures valid at the end of a time step are computed with temperatures and other properties values valid at the beginning of the time step. Similarly, a new density is computed from Equation (C-2) and (C-3) as

$$\rho_n' = \rho_n + \left(\frac{\partial \rho}{\partial \theta}\right)_y \Delta\theta + \left(\frac{\partial \rho}{\partial x}\right)_\theta \dot{s}\Delta\theta \qquad \text{(C-4)}$$

Here n refers to a fixed "node" or zone or lump of material defined by the finite differencing process.

An important feature of explicit techniques is the instability of the finite-difference solution if the time step size exceeds some critical value. Even for time steps below this critical value, however, the solution for typical charring materials is apt to have severe oscillations due to irregularities in the decomposition calculation. This in turn is due to the extremely sensitive dependence of the decomposition rate, Equation (C-2), on both nodal density, since the reaction order m_i is usually at least unity, and in the nodal temperature, through the exponential term. For example, an increase (or an error) in temperature of 50° from one time step to the next can double or triple the decomposition rate. This results in excessive cooling of the nodes nearer the surface due to pyrolysis gas blow-by. These effects result in too low nodal temperatures and very much reduced decomposition rates. In the following time step, too much conduction occurs, resulting in too high temperatures again, and the cycle repeats.

Irregularities of this type indicate that the decomposition event must be handled carefully. One such treatment is described in the next section.

C.5 FULLY EXPLICIT TREATMENT OF ENERGY AND DECOMPOSITION EQUATIONS WITH NODES FOR THE ENERGY EQUATION AND NODELETS FOR THE DECOMPOSITION EQUATION

One computational strategem to reduce this oscillatory decomposition problem is to employ a finer difference network for computing the decomposition than for computing the energy equation, with the aim of better characterizing the local decomposition temperatures and of more sharply defining the very steep density profile in the decomposition reaction zone. (One wishes to avoid this fine network for the difference form of the energy equation since the maximum time step allowed for stability reasons varies as the square of the nodal thickness.)

This sub-network of fine nodes ("nodelets") has been used with good results. Experience shows that about ten nodelets per node adequately characterize the density profile and also damp out grossly oscillatory behavior for most materials of interest.

Computation time with this method, although generally "acceptable", is long due to the large number of decomposition calculations required by the fine nodelet network. Nevertheless, an Aerotherm program based upon this procedure has proved to be of great utility in a wide variety of rocket nozzle and heat shielding calculations (Reference C-1). The computation time of the program depends, of course, on the problem considered, but a typical problem requires three times real time (IBM 7094). The next section describes a technique for shortening this time.

C.6 FULLY IMPLICIT TREATMENT OF ENERGY EQUATION WITH NODES, FULLY EXPLICIT TREATMENT OF DECOMPOSITION AND MASS CONVECTION WITH NODELETS

It has long been known that certain "implicit" treatments of the heat conduction equation, in which "new" temperatures are computed in terms of "new" temperatures, always give stable solutions regardless of the length of time step employed. For example, in simple transient conduction for constant material properties, a nodal equation would be

$$\rho\, C_p \frac{(T'_n - T_n)}{\Delta\theta} = \frac{k}{\delta^2}\,(T'_{n-1} - 2T'_n + T'_{n+1}) \qquad \text{(C-5)}$$

This formulation allows much longer time steps than the corresponding explicit expression.

The more complex energy equation for a charring, ablating material, Equation (C-1), can be written in analogous fashion. The decomposition term $\partial\rho/\partial\theta)_y$ and the pyrolysis gas flow $\dot{m}_g$, however, depend upon the nonlinear decomposition Equation (C-2), and render solution of the resulting series of equation very complex. The most straightforward solution method would be some iteration procedure, but it is not clear whether or not much time can be saved over the explicit procedure in this manner, since the number of iterations required may be large and various convergence testing techniques might have to be added.

An alternative procedure is to leave both the temperature and density dependence decomposition events in explicit form, so that these nonlinear equations can be solved explicitly. These results, in terms of $\partial\rho/\partial\theta)_y$ and $\dot{m}_g$, can then be used in an implicit form of the iteration procedure; the suggested computational step implies that this one step gives adecuate accuracy.

An earlier version of the present program incorporated this general scheme. This experience has shown that after the program worked "well" in the sense that the solutions usually displayed a regular and smooth behavior in contrast to the irregular or oscillatory behavior which one might expect for long time steps. For these successful problems, the time steps were much longer than those required in the analogous explicit solution and typical computation time was cut by a factor of three from that for the explicit program. Thus these problems ran in roughly real time (IBM 7094). (Improvements to be described below will reduce this time still further.)

Figure C-1 shows a typical transient rocket nozzle solution. Although the example of Figure C-1 indicates that this computational technique works well for most problems, experience has shown that the implicit treatment of the energy equation combined with a fully explicit treatment of the decomposition equation does not always produce smooth solutions, particularly for rapid decomposers, such as nylon phenolic, exposed to large scale slow transients (a term to be defined later), such as occur in reentry problems.

Figure C-2 shows a sample calculation of such a problem in terms of the pyrolysis gas flow rate out the surface as a function of time. (This is the most sensitive indicator of the smoothness of the solution.) The material is a low density nylon phenolic. Decomposition reaction kinetics are computed with a three component model. Boundary conditions are a specified surface temperature beginning at $540^{\circ}R$ and rising linearly in time to $5000^{\circ}R$ at 10 seconds (and remaining at $5000^{\circ}R$ thereafter), combined with a specified surface recession of 30 mils/sec beginning at 10 seconds. Appendix A gives further problem specification details.

Figure C-2 shows that during the ramp temperature input, before surface recession begins (at 10 seconds), the computation has great difficulties in producing a smooth gas rate and displays both small irregularities and a large scale waviness. After surface recession begins the gas rate displays sharper oscillations of a smaller magnitude.

To examine the effect of surface recession, the problem was rerun with the surface recession turn on at 5 seconds rather than 10 seconds. Figure C-4 shows the pyrolysis gas rate results.

The results display a number of very irregular appearing peaks and valleys. The rough appearance of the solution is accentuated in the plot by the straight lines drawn between output points; since computation has in fact produced a number of intermediate points not shown, the actual course of the calculation may have been much smoother than Figure C-3 indicates. In any case, however, the gas rate is changing value in a rapid and presumably unrealistic manner.

Fortunately, the uneven behavior shown in Figures C-2 and C-3 is not usually important. Abundant computational evidence, not to be reported here, indicates that the overall aspects of the solution (total surface recession, total pyrolysis gas generation, surface temperature behavior, thermocouple temperature behavior, char thickness, and isotherm penetration) are affected in only a very minor degree by the irregularities.

There is at least one important case, however, for which unevenness in the gas rate would be unacceptable, and that is for the coupled boundary layer solution (CABLE). Convergence of the boundary layer computation will be adversely affected by too large jumps in the pyrolysis gas injection rate.

Therefore although uneven gas rate results are rare (being confined to a limited number of materials exposed to a special kind of transient) and not usually of importance, their influence on the boundary layer solution dictates a closer study attempting to eliminate uneven behavior. Such a study has been made and has resulted in significant improvements in computation procedures, as described below.

C.7 TIME STEP LIMITATION BASED ON DENSITY CHANGE RATE

An early device employed to smooth out irregularities limited the time step size according to an empirically determined limit on the density change per time step of the fastest decomposing component in the material. This device worked well in many problems, but for difficult cases it caused a sizable increase in computation time. Thus there was a strong economic incentive to remove this "decomposition clamp".

C.8 CHANGE IN TREATMENT OF DENSITY POTENTIAL IN DECOMPOSITION EQUATION FROM FULLY EXPLICIT FINITE DIFFERENCE FORM TO EXACT INTEGRATED FORM

C.8.1 Introduction

Up to this point the decomposition relation, Equation (C-2), and the convection relation, Equation (C-3), have been treated in the following explicit manner:

1. Given "old" temperatures and "old" nodelet desnities for each component i, "temporary" nodelet densities are computed with the finite difference convection relation (C-5).
2. These "temporary" densities are inserted into the decomposition kinetic relation (C-4) and "new" nodelet densities computed.

3. Pyrolysis gas evolution rates are computed from accumulated density change rates and are then used in the energy equation solution for "new" temperatures.

This general procedure is a common idea and has been used previously (Reference (C-3).

Reference C-4 has pointed out, however, that the variables in the decomposition relation (C-2), if temperature T is treated explicitly as is done here (T fixed during the integration), may be separated and the integration on density performed exactly. The equation

$$\left.\frac{\partial \rho_i}{\partial \theta}\right)_y \rightarrow \frac{d\rho_i}{d\theta} = -k_i \exp(-Ea_i/RT)\, \rho_{o_i}\left(\frac{\rho_i - \rho_{r_i}}{\rho_{o_i}}\right)^{m_i} \tag{C-6}$$

can be written as

$$\frac{d(\rho_i - \rho_{r_i})}{(\rho_i - \rho_{r_i})^{m_i}} = -k_i \rho_o^{(1-m_i)} \exp(-Ea_i/RT)\, d\theta \tag{C-7}$$

which for $m_i \neq 1$ integrates to

$$\frac{\Delta(\rho_i - \rho_{r_i})^{1-m_i}}{(1-m_i)} = -k_i \rho_o^{(1-m_i)} \exp(-Ea_i/RT)\, \Delta\theta \tag{C-8}$$

giving the density change rate

$$\frac{\rho_{i_2} - \rho_{i_1}}{\Delta\theta} = \frac{-(\rho_{i_1} - \rho_{r_i}) + \left[(\rho_{i_1} - \rho_{r_i})^{1-m_i} - k_i(1-m_i)\rho_{o_i}^{(1-m_i)} \exp(-Ea_i/RT)\Delta\theta\right]^{\frac{1}{1-m_i}}}{\Delta\theta} \tag{C-9}$$

If $m_i = 1$, integration gives

$$\Delta \ell n\, (\rho_i - \rho_{r_i}) = -k_i \exp(-Ea_i/RT)\Delta\theta \tag{C-10}$$

which yields the density change rate

$$\frac{\rho_{i_2} - \rho_{i_1}}{\Delta\theta} = \frac{(\rho_{i_1} - \rho_{r_i})}{\Delta\theta} \left\{ \exp \left[- k_i \, \Delta\theta \, \exp \left(- Ea_i / RT \right) \right] - 1 \right\} \qquad \text{(C-11)}$$

This technique will obviously be "better" than the previous explicit treatment of the density, since a study of the computer results for the problem shown in Figure C-3 indicates that much of the oscillatory behavior of the solution is due to the coupling between the decomposition and the energy equations, which causes temperatures to be depressed after excessive decomposition, shutting off decomposition in the next step and allowing too great a temperature rise again the the following step. This problem is now presumably eliminated and longer time steps should be allowable. In particular, the "decomposition clamp" should no longer be necessary.

In fact, the improvement offer by the density integration procedure is very great, as will be seen in the examples cited below.

C.8.2 Favorable Examples

Figure C-3 provides graphic evidence of the powerful damping effect provided by the exact integration forms of the decomposition kinetic equations. The figure displays the same problem as treated in Figure C-2. Almost all the "high frequency" irregularities have been removed, and the computation steps much reduced (144 time steps at 11.9 seconds instead of 224 time steps in the older technique). This saving is primarily due to the removal of the decomposition clamp.

Figure C-5 shows the same problem as Figure C-4 but with the new exact decomposition relations. Here the smoothing effect is even more dramatic, especially in the region after the start of surface recession (5 seconds). Computation has been cut from 645 time steps to 171 time steps at 12 seconds.

C.8.3 Less Favorable Examples

Figures C-3 and C-5, when compared to Figures C-2 and C-4, indicate that a significant improvement has been made in computing technique. However, these same figures suggest that all is not yet well, and that the new decomposition relations are not a cure-all. In particular, in Figure C-3, the time between 3 and 5 seconds (before surface recession starts) still shows a fairly unsmooth gas rate. Furthermore, there is a provocative change in solution character after 10 seconds, when the surface temperature rise flattens out at a fixed value of $5000^{\circ}R$. Both these aspects seem associated with the same general phenomenon: the

approach to steady state. Before 5 seconds there is no surface recession and the imposed linear surface temperature rise makes the problem everywhere "transient". Between 5 and 10 seconds the imposed high surface recession rate greatly steepens the temperature profile and causes the problem to be more like a steady state problem. After 10 seconds the constant surface temperature allows the internal response to approach a steady condition very rapidly.

Therefore, it appears that the computational technique is tending to have difficulties when the transient nature of the problem is dominating, that is, when the temperature profile and the pyrolysis zone (region of density change) are progressing through the nodal network; unless the decomposition is slow and the pyrolysis zone smeared out over many nodes (as in the case with the rocket nozzle problem shown in Figure C-1).

A slower and less artificial transient than that of Figures C-2 through C-5 provides a good test of these suspicions. The problem represents the same nylon phenolic 3-component material, this time exposed to a ballistic entry. The material is exposed to air with a recovery enthalpy of about 15,000 Btu/lb; the heat transfer coefficient peaks at about 80 seconds. The first node is 0.020 inches thick, 15 following nodes are 0.040 inches thick. Additional thicker nodes follow. (Complete specification of the problem conditions would, of course, be very lengthy. Since the problem serves only illustrative purposes here, further description is omitted (except for the property data in Appendix 3-1).) Figure C-6 shows the pyrolysis gas rate as a function of time.

The figure confirms the idea that a continuing transient condition can cause computational difficulties even for the improved decomposition procedure. An examination of the detailed nodal output reveals that in the period 0 to 70 seconds the pyrolysis zone moves steadily through the nodal network from the surface node to approximately node 10. After 70 seconds the pyrolysis zone location stabilizes in the neighborhood of node 10. Figure C-6 shows that during the transient portion the surface pyrolysis gas rate is uneven (again it is pertinent that the output plot does not show every point computed so that the actual succession of gas rate points would presumably have a smoother appearance) whereas after 70 seconds the output is much more smooth.

A careful examination of other output information for this problem reveals that the unevennesses in the gas rate stem from a problem different from the coupled, on-off "oscillatory" problem observed before the introduction of the exact integrated decomposition relations. For example, Figure C-7 shows the density histories of a number of nodes. This plot reveals two undesirable features of the computation:

1. There is a tendency for one node to finish decomposing a little before the next node enters the rapid decomposition part of its history, so that for most of the time the surface gas rate is mainly determined by the events at a single node

2. The progress of decomposition of each node, although apparently smooth, attains a maximum value when the nodal density is about midway between the virgin material density and the char density.

Clearly these two aspects define the uneven appearance of Figure C-6, where the number of peaks corresponds closely to the number of nodes through which the pyrolysis zone has moved (this will later turn out not to be a general phenomenon, however).

Thus the unevenness problem seems associated with the nodal structure. This aspect is somewhat surprising, since the assignment of 10 nodelets per node was previously thought ample to define the pyrolysis zone and to provide, by linear interpolation between nodes, sufficiently accurate temperatures for decomposition. Indeed, a study of the node to node density variation (not to be presented here) indicates that the density profile is well defined by such a nodelet spacing for the node size used here.

Additional computational tests were made to confirm the identification of the unevenness problem with the nodal structure. Figure C-8 shows a short calculation on essentially the same problem with the time step limited to 0.05 seconds between 18 and 22 seconds and output called for every time step in the interval. (To save computation time the kinetic data has been changed to a single component model and the problem definition has been changed to one of specified surface temperature and recession rate. These changes cause no important differences in the internal response.) The first plot on Figure C-8 shows the gas rate plotted, as previously, every second. The second shows the gas rate between 18 and 22 seconds on an expanded scale, with every time step indicated. Study of the nodal density data (not presented here) shows that this expanded plot displays chiefly the decomposition of the second node. Figure C-8 thus seems to confirm that the decomposition computation is smooth enough but tends to occur in waves associated primarily with the nodal size.

This preliminary conclusion suggests a number of further diagnostic calculations aimed at understanding the exact nature of the unevenness in the gas rate and illuminating the role of nodal size. The sections below describe some of these calculations.

C.9 CHANGE FROM LINEAR INTERPOLATION BETWEEN NODAL TEMPERATURES TO CUBIC CURVE FIT

To ascertain whether or not the linear interpolation between nodal temperatures to determine nodelet decomposition temperatures was perhaps imposing a nodal-scale inaccuracy on the total gas rates, the program was temporarily modified to employ a cubic curve fit between each pair of nodal temperatures to obtain more accurate temperatures for decomposition. The Aerotherm curve fit routines SLØPQ and ØGLE (Reference C-2) were used to generate the necessary parameters. Only minor improvements in gas rate smoothness resulted.

C.10 EXPERIMENTS ON NODAL SIZE

C.10.1 Introduction

The failure of a better interpolation scheme to produce smoother results points directly to nodal size as the dominant aspect, which in turn suggests that the uneven gas rate problem is directly connected to the accuracy of the energy equation solution. Additionally, this failure calls into question the utility of the nodelet concept in the present computation technique. Originally, nodelets were introduced to better define dcomposition events without having to accept any penalties in computation time in the old explicit solution. This computational technique proved to be extremely useful for "mild decomposers" such as the phenolics, which decompose slowly over a range of temperatures. Little experience was gained with the explicit program on such materials as nylon, which decompose very rapidly in a very narrow, sharply defined temperature range, but even the brief experience indicated that computational performmance, in terms of a smooth gas evolution rate, was going to be poor. Now the more extensive experience described here with the implicit program confirms the difficulty of the "rapid decomposer" problem and suggests that the nodelet concept is less useful for this kind of problem.

In all the calculations reported up to this point, there have been 10 nodelets per node and the nodal sizes have been chosen with only one criterion in mind: to provide "enough" nodal points to define the temperature profile accurately. With a material like carbon phenolic and a typical transient, this procedure leads to temperature and density profiles roughly like:

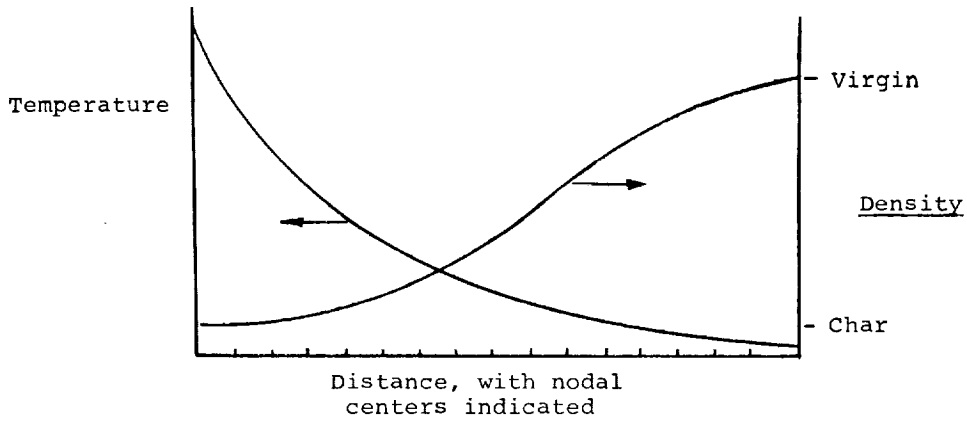

With nylon phenolics, for example, such a nodal sizing procedure is likely to yield temperatures and density profiles like:

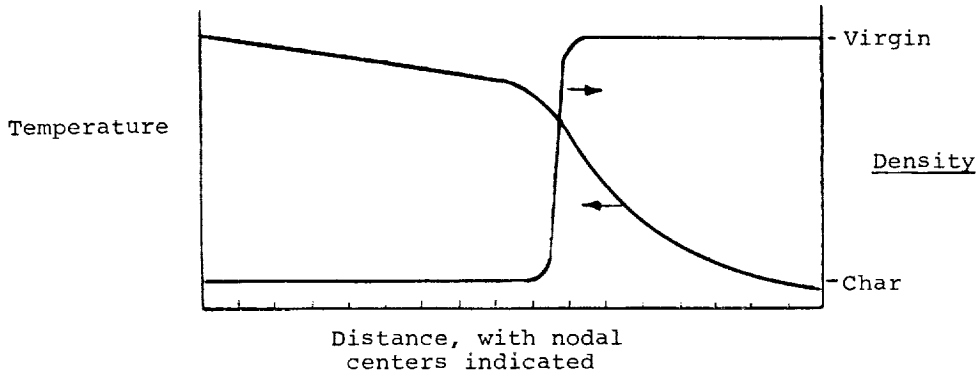

The use of nodelets in this problem thus serves to help define the sharp density profile, but the overall temperature accuracy is not likely to be sufficiently accurate to give meaningful instantaneous gas rates.

This in fact appears to be the root of the problem of the uneven gas rate predictions in the examples considered earlier. The decomposition rate of nylon depends sensitively on the temperature and even small errors in nodal temperatures will cause wide excursions in the gas rate. For example, in the single component model for nylon phenolic, the decomposition equation is

$$\left(\frac{\partial \rho}{\partial \theta}\right)_y = - k_i e^{-Ea/RT} \rho_o \left(\frac{\rho_i - \rho_r}{\rho_o}\right)^m$$

where experimentally determined values of the constants are (References C-5 and C-6)

$$k_i = 7.89 \times 10^{12} \ \text{sec}^{-1}$$

$$Ea/R = 45{,}000^{\circ}R$$

$$m = 2.0$$

Temperatures for which the reaction rate is high will be located near the temperature for which

$$k_i e^{-Ea/RT} = 1$$

which in this case gives

$$T \approx 1515^{\circ}R$$

Therefore, when the decomposition rate is of importance it will be roughly proportional to

$$\left(\frac{\partial \rho}{\partial \theta}\right)_d \propto e^{\frac{45000}{1500(1+\varepsilon)}} = e^{-30/(1+\varepsilon)} \approx e^{-30(1-\varepsilon)} = e^{-30} e^{30\varepsilon}$$

Thus a relative error in temperature of ε causes a relative error in decomposition rate of $e^{30\varepsilon}$. For $T = 1500^\circ R$, errors of $5^\circ R$, $10^\circ R$, $20^\circ R$, and $30^\circ R$ give the following errors in decomposition rate

$\Delta T(^\circ R)$	ε	$e^{30\varepsilon}$
5	1/300	1.105
10	1/150	1.221
20	2/150	1.492
30	3/150	1.822

Hence even a 5° error in a nodal temperature will cause a 10% error in the gas rate, when the temperature is high enough for the decomposition to be important. A 5° error represents about 1/2% of the total nodal temperature rise in typical problems.

The main drift of these observations then is that the accuracy of the temperature solution seems directly involved with the uneven gas rate problem. The following section adduces further evidence to this effect.

C.10.2 Experiments with Smaller Node Sizes

If accuracy of the temperature solution underlies the gas rate problem, the only solution to the trouble consists of smaller node sizes. Figure C-9 shows the same problem as illustrated earlier in Figure C-6 (aside from the minor changes to a single component decomposition and a specified surface temperature and recession rate problem rather than a surface thermochemistry problem), but with 0.02 inch nodes instead of the former 0.04 inch nodes. The improvement is striking, the amplitude of the gas rate "waves" being reduced by about half.

Thus it seems that nodal size is the dominant parameter, and that perhaps the number of nodelets per node is more or less irrelevant for this particular problem. To check this aspect, the problem of Figure C-9 was recomputed once again with 0.008 inch nodes, but with only two nodelets per node. This yields the same nodelet size as for the problem of Figure C-6. The results, shown in Figure C-10, may be compared to the earlier results for the same problem shown in Figures C-6 and C-9. Again the "wave amplitude" has been much reduced.

Figure C-10 has a conspicuous dip in the gas rate at 25 seconds. It happens that the specified surface temperature boundary condition for this problem has a marked decrease in slope at 25 seconds; to check if perhaps this caused the gas rate dip the problem was rerun with a ramp input for surface temperature and recession rate. Figure C-11 shows the results and proves that irregular behavior is characteristic of the computational system rather than the specific boundary condition.

As a final test of the effect of smaller nodes on the smoothness of the solution, the ramp input problem of Figure C-11 was rerun with a new nodal size distribution. The first node was 0.008 inch, and the next seven nodes were 0.016 inches thick. These nodes were followed by a number of nodes of 0.004 inches thickness, half as large as the nodes of the problems illustrated in Figures C-10 and C-11. Figure C-12 shows the results of this last computation. As expected, during the time the pyrolysis zone is progressing through the thick nodes (in this problem 0 to 30 seconds) the gas rate is very irregular. As soon as the pyrolysis zone passes into the thin nodes, the gas rate smooths out almost completely, except for one small wave at 38 seconds.

The computations illustrated in Figures C-6, C-9, C-10, C-11, and C-12 thus indicate that the choice of nodal size and number of nodelets per node determines the smoothness of the pyrolysis gas rate. It would, of course, be desirable to have quantitative criteria for selecting these quantities, but the overall complexity of this problem seems to dictate a trial and error procedure. To facilitate the selection of these quantities, Appendix C-2 provides some useful estimates of program execution time as a function of the number of nodes and nodelets.

C.11 CONCLUSIONS

The early versions of the Aerotherm Charring Material Ablation Program, which treated the decomposition kinetic equations explicitly in both density and temperature and which used an implicit formula for the energy equation in depth, produce excellent results for slow decomposers such as phenolics regardless of the type of transient involved. Fast decomposers such as nylon cause irregularities in the solution values of quantities of interest, especially in the rate of pyrolysis gas generation, for those particular transient problems in which the pyrolysis zone is passing rapidly through the nodal network (which is tied to the receding heated surface).

Usually these irregularities cause no problems since experience shows that they do not affect the important overall aspects of the solution, such as total surface recession and char thickness, for example. However, since it is expected that irregularities in the pyrolysis gas rate will cause convergence difficulties in the coupled boundary layer program (BLIMP), the present study included attempts to eliminate irregular or wavy gas rate predictions.

An early computational strategem lumped the rapid decomposition effect into one of the available three decomposing constituents and then applied a time step limit to the overall solution to prevent the decomposition rate (density change rate) of this component from exceeding some empirically determined amount. This semi-rational time step limit was quite effective, but turned out to be rather costly for nylon, which for many transients requires very short time steps for a smooth solution.

A better smoothing procedure abandons the explicit treatment of density in the decomposition relations in favor of exact integrated relations for the density dependence. The implicit-density nature of these relations exerts a powerful smoothing effect on the solution, and allows removal of the time step clamp on decomposition rates with a consequent saving in the number of solution steps. Although the integrated decomposition relations are about twice as slow to compute as the simpler explicit relations, the saving in time steps in difficult to handle problems was observed to be a factor of four to five in the number of time steps. Since the computation time is mainly devoted to decomposition, net computation time has been cut by about a factor of two.

Despite the strong smoothing effect of the implicit density relations, certain particularly unfavorable combinations of materials and boundary conditions can still cause markedly uneven gas rate predictions. The roots of this behavior could not be definitely identified due to the complexity of the internal response solution. Computational experiments demonstrated, however, that nodal size is the key parameter affecting the smoothness of the solution, which points to the overall accuracy of the energy solution as the key aspect. Smaller node sizes resulted in much smoother solutions and no doubt remains that entirely smooth solutions can be obtained with "sufficiently" small nodes. With small nodes the nodelet structure becomes of minor importance, and the number of nodelets can be cut down to the minimum (within the present program logic) of two without harm to the solution. Thus, the net computation time is in general not increased by the smaller node size.

It would, of course, be desirable to have a quantitative criterion for selecting nodal and nodelet sizes, but the overall complexity of the problem appears to preclude a successful analysis and to demand an empirical approach. To date, computational experience has not been sufficient to define any general rules giving good nodal sizing.

APPENDIX C

REFERENCES

C-1. McCuen, P. A., Schaefer, J. W., Lundberg, R. E., and Kendall, R. M., "A Study of Solid-Propellant Rocket Motor Exposed Materials Behavior," Final Report, Contract No. AF 04(611)-9073, AFRPL-TR-65-33 (AD-462 381), Vidya Division, Itek Corp., Palo Alto, California, Feb. 26, 1963

C-2. Aerotherm Corporation, Palo Alto, California, "Fortran Variable Names, Aerotherm Charring Material Ablation Program, Version 2," Feb. 1966.

C-3. Forsythe, G. E. and Wasow, W. R., Finite Difference Methods for Partial Differential Equations, John Wiley and Sons, Inc., New York, 1960, p. 143.

C-4. Bamford, C. H., Crank, J., and Malan, D. H., "The Combustion of Wood Part I," Proceedings of the Cambridge Philoshopical Society, Vol. 42, 1946, pp. 166-182.

C-5. Hearne, L., et al., "Study of Heat Shielding Requirements for Manned Mars Landing and Return Missions," Lockheed Missiles and Space Company, Sunnyvale, California, LMSC-4-74-64-1, December, 1964, pp. 5-32.

C-6. Kratsch, K., et al., "Study to Determine Heat Shield Requirements for an Instrumented Test Vehicle," Lockheed Missiles and Space Company, Sunnyvale, California, LMSC-4-83-64-2, September, 1964.

C-7. Kratsch, K. M., Hearne, L. F., and McChesney, H. R., "Thermal Performance of Heat Shield Composites During Planetary Entry," unnumbered paper presented at the American Institute of Aeronautics and Astronautics - National Aeronautics and Space Administration National Meeting, Palo Alto, California, September 30-October 1, 1963; (also Lockheed Missiles and Space Company, Sunnyvale, California, Report LMSC - 803099 (October, 1963), reprinted in Engineering Problems of Manned Interplanetary Exploration, American Institute of Aeronautics and Astronautics, New York, 1963).

Surface Temperature °R
Figure C-1. Carbon Phenolic Rocket Nozzle Response
Resin Mass Fraction = 0.345
Resin Residual Mass Fraction = 0.40
Surface Pyrolysis Gas Rate and
Surface Temperature Versus Time
0.050
0.040
0.030
0.020
0.010
0
$\dot{m}_g$ (lb/ft^2 sec)
0
10
20
30
40
50
60
70
80
90
100
110
Time (Seconds)

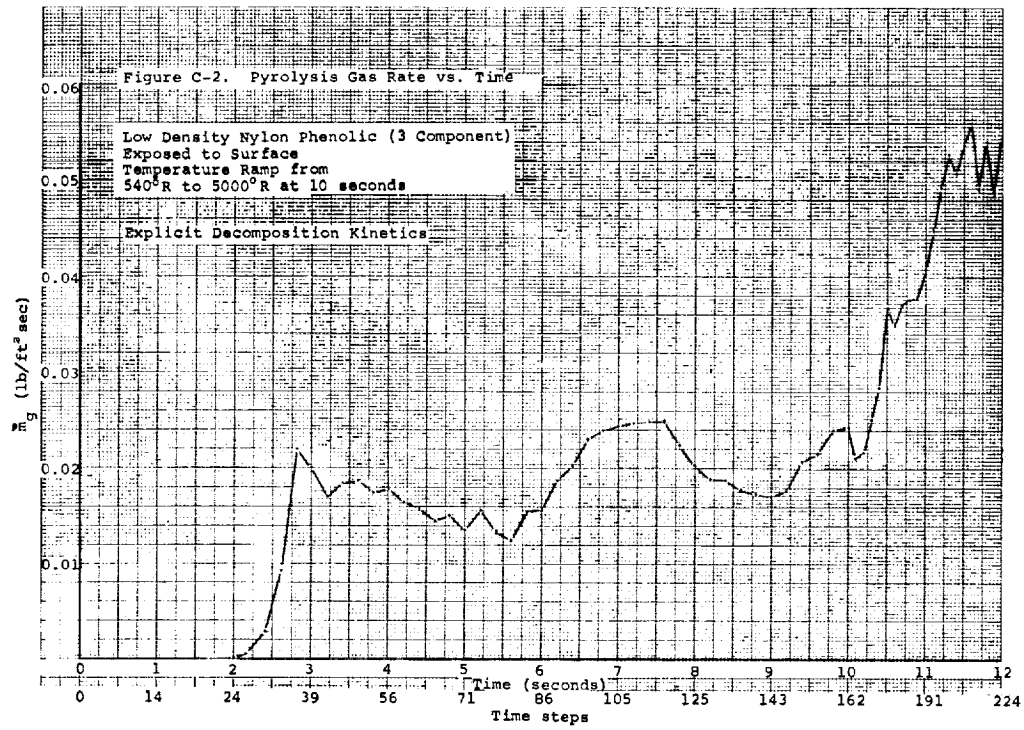
Figure C-2. Pyrolysis Gas Rate vs. Time
Low Density Nylon Phenolic (3 Component)
Exposed to Surface
Temperature Ramp from
540°R to 5000°R at 10 seconds
Explicit Decomposition Kinetics
$\rho\dot{m}_g$ (lb/ft² sec)
0.06
0.05
0.04
0.03
0.02
0.01
0 1 2 3 4 5 6 7 8 9 10 11 12
Time (seconds)
0 14 24 39 56 71 86 105 125 143 162 191 224
Time steps

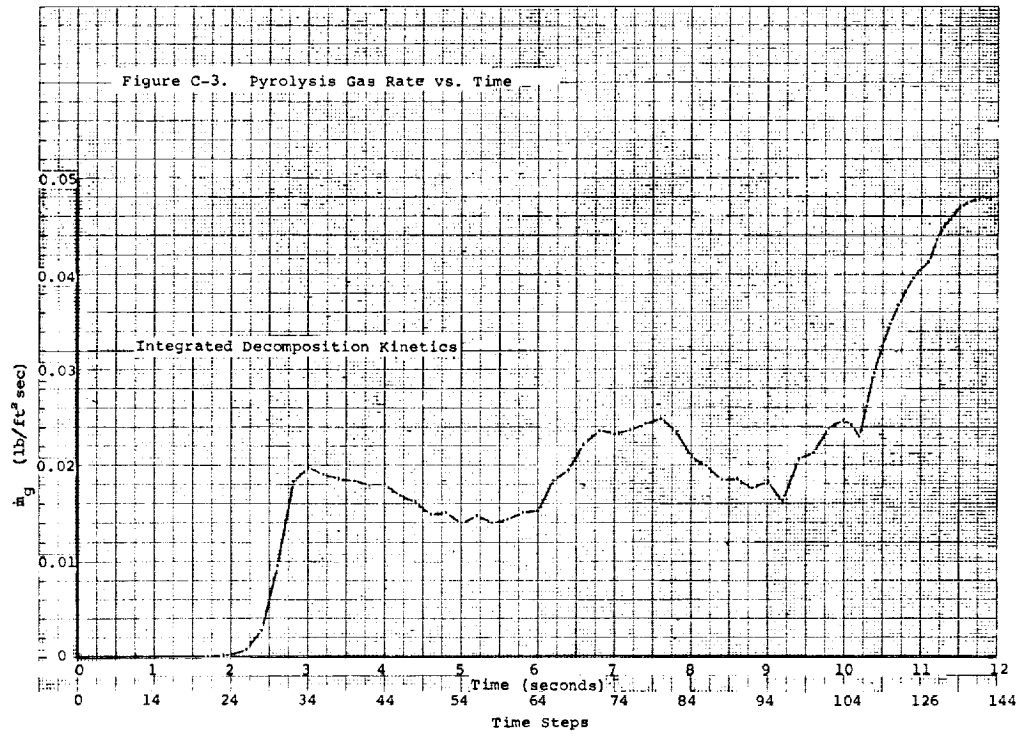
Figure C-3. Pyrolysis Gas Rate vs. Time
Integrated Decomposition Kinetics
$\dot{m}_g$ (lb/ft² sec)
0.05
0.04
0.03
0.02
0.01
0
0 1 2 3 4 5 6 7 8 9 10 11 12
Time (seconds)
0 14 24 34 44 54 64 74 84 94 104 126 144
Time Steps

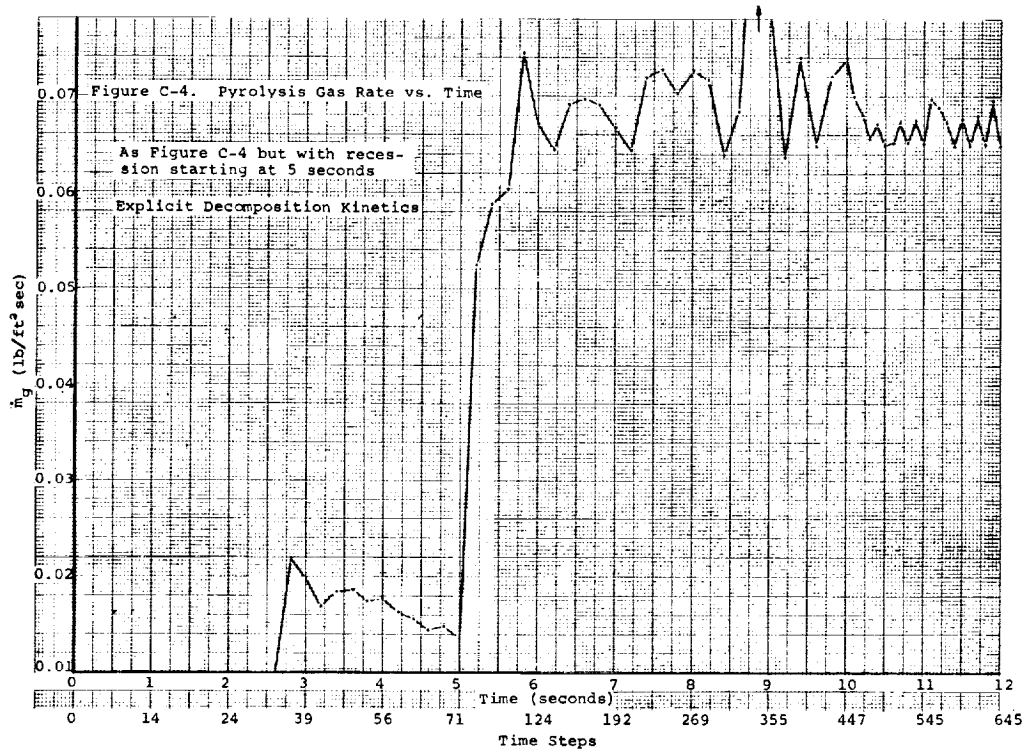
Figure C-4. Pyrolysis Gas Rate vs. Time
As Figure C-4 but with recession starting at 5 seconds
Explicit Decomposition Kinetics
$\dot{m}_g$ (lb/ft² sec)
0.07
0.06
0.05
0.04
0.03
0.02
0.01
0 1 2 3 4 5 6 7 8 9 10 11 12
Time (seconds)
0 14 24 39 56 71 124 192 269 355 447 545 645
Time Steps

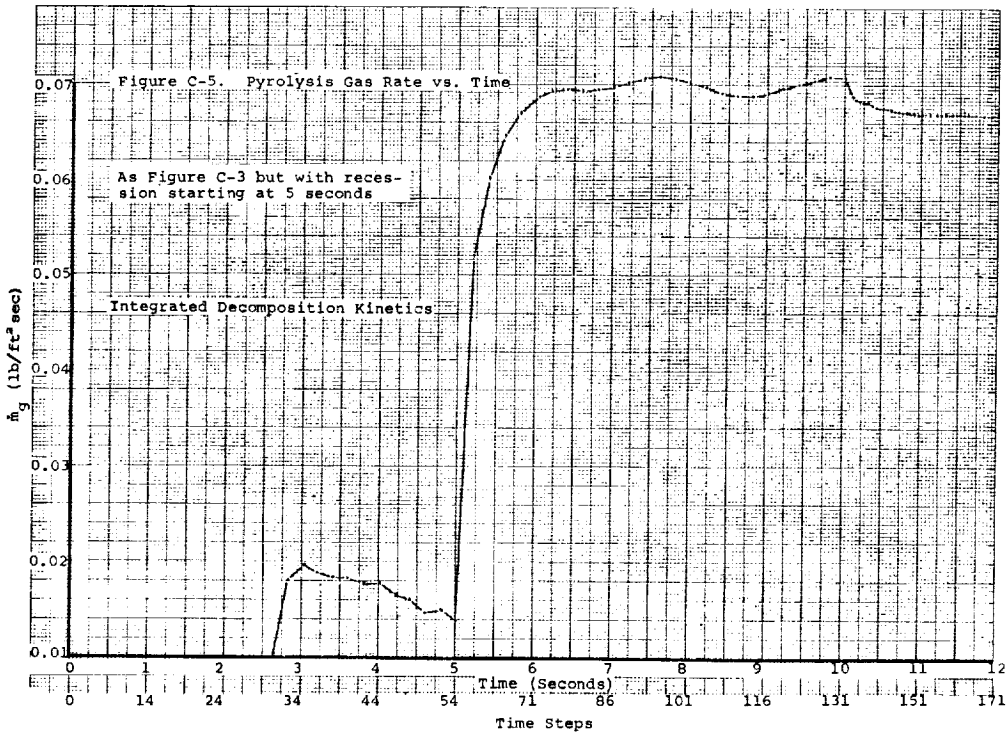
Figure C-5. Pyrolysis Gas Rate vs. Time
As Figure C-3 but with recession starting at 5 seconds
Integrated Decomposition Kinetics
$\dot{m}_g$ (lb/ft² sec)
0.07
0.06
0.05
0.04
0.03
0.02
0.01
0 1 2 3 4 5 6 7 8 9 10 11 12
Time (Seconds)
0 14 24 34 44 54 71 86 101 116 131 151 171
Time Steps

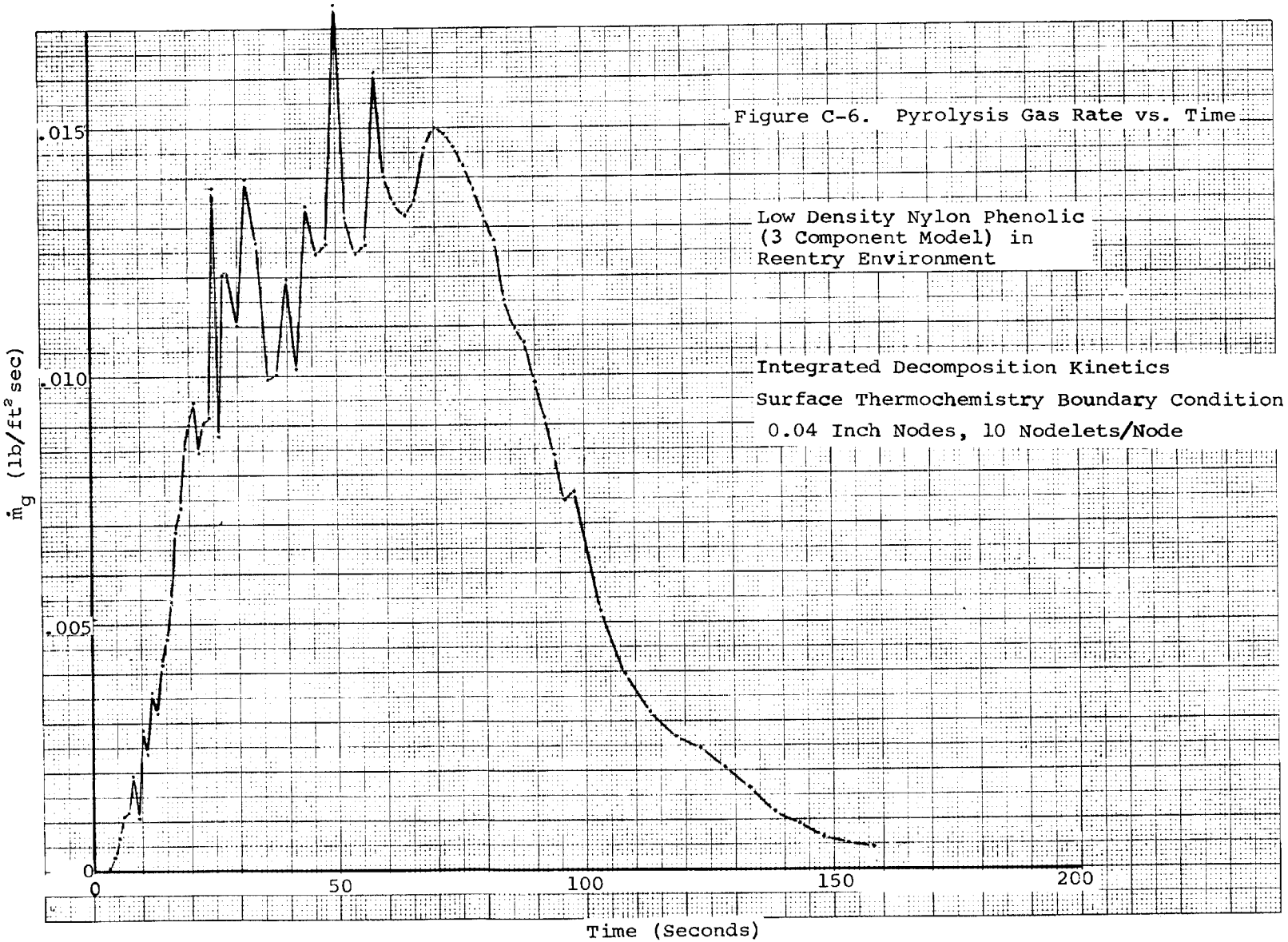
Figure C-6. Pyrolysis Gas Rate vs. Time
Low Density Nylon Phenolic
(3 Component Model) in
Reentry Environment
Integrated Decomposition Kinetics
Surface Thermochemistry Boundary Condition
0.04 Inch Nodes, 10 Nodelets/Node
$\dot{m}_g$ (lb/ft² sec)
.015
.010
.005
0
0
50
100
150
200
Time (Seconds)

Figure C-7. Nodal Density Histories for Problem of Figure 6

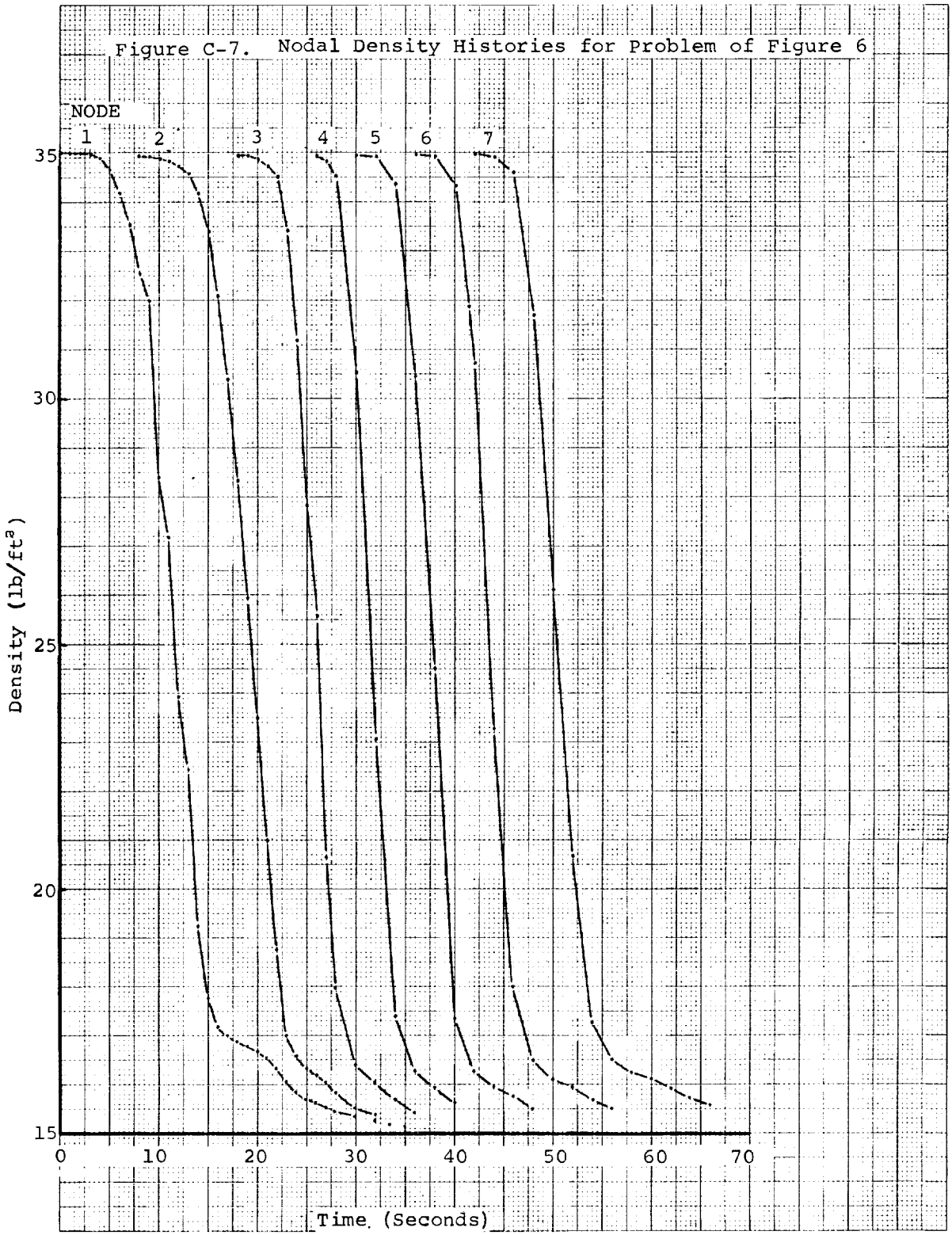

Figure C-8. Pyrolysis Gas Rate vs. Time
Problem similar to
problem of Figure 6
with time step shortened
to 0.05 seconds after
18 seconds
Single component kinetics
Boundary condition
Imposed Temperature
and Recession Rate
0.04 Inch Nodes, 10 Nodelets/Node
Expanded Plot
$\dot{m}_g$ (lb/ft^2 sec)
.015
.010
.005
0
0 10 20 30 40 50
18 19 20 21 22
Time (Seconds)

Figure C-9. Pyrolysis Gas Rate vs. Time
Low Density Nylon Phenolics
Exposed to Reentry Environment
(As Figures 6 and 8)
Nodes Reduced to 0.02 inches, 10 Nodelets/Node
Single Component Kinetics, Imposed
Surface Temperature and Recession Rate
Pyrolysis Gas Rate At Surface (lb/ft² sec)
.015
.010
.005
0
0
50
100
Time (Seconds)

Figure C-10. Pyrolysis Gas Rate vs. Time
Problem as Figure 9 but with
0.008 inch Nodes and 2 Nodelets/Nodes
$\dot{m}_g$ (lb/ft^3 sec)
.010
.005
0
0 10 20 30 40 50
Time (seconds)

Figure C-11. Pyrolysis Gas Rate vs. Time
Problem as Figure 10 but with
Ramp Boundary Condition:
Time(°R) T(°R) Ṡ(mils/sec)
0 540 0
40 4000 1.0
Nodes 0.008 inch with 2 Nodelets/Node
.015
.010
.005
0
0 10 20 30 40 50
Time(seconds)
ṁg (lb/ft³ sec)

Figure C-12. Pyrolysis Gas Rate vs. Time
Problem as Figure 11 but with Nodes as
1 at 0.008 inches
7 at 0.016 inches
Following at 0.004 inches
Pyrolysis Zone Moves into Small Nodes
$\dot{m}_g$ (lb/ft^2 sec)
.015
.01
.005
0
0 10 20 30 40 50
Time (seconds)

SUB-APPENDIX C-1

NOTES ON PROBLEM SPECIFICATION

C-1.1 PROBLEM OF FIGURES C-2 TO C-5

The material is a low density nylon phenolic with a resin mass fraction of 0.5, resin residual mass fraction of 0.5, and a nylon residual mass fraction of zero. Decomposition kinetic data, adapted from the results of Reference 9, were

Component	ρ_{o_i} (lb/ft^3)	ρ_{r_i} (lb/ft^3)	k_i (sec^{-1})	Ea_i/R ($^\circ R$)	m_i
A	6.028	0	1.4×10^4	15,400	3
B	18.084	12.056	4.48×10^9	36,400	3
C	71.0	0	1.85×10^{13}	47,700	1.5

Enthalpies of formation, reference temperature $536^\circ R$:

Virgin Plastic	0
Char	0
Pyrolysis gas	- 1311 Btu/lb

Material Properties:

	$T(^\circ R)$	Specific Heat (Btu/lb)	Thermal Conductivity (Btu/ft sec $^\circ F$)
	460	.360	1.5×10^{-6}
Virgin Plastic	550	.427	1.39
	650	.475	1.39
	760	.500	1.39
	860	.500	1.62
	910	.500	1.68
	960	.500	1.69
	1560	.500	1.69
	6460	.500	1.69
Char	460	.122	$.384 \times 10^{-4}$
	1000	.305	.650
	1500	.405	.900
	1960	.480	1.183
	2110	.500	1.275
	2260	.520	1.375

T(°R)	Specific Heat (Btu/lb)	Thermal Conductivity (Btu/ft sec °F)
3260	.600	1.891
3360	.601	1.947
3660	.605	2.109
3760	.606	2.156
3860	.608	2.212
4060	.611	2.320
4160	.612	2.416
4310	.615	2.539
4610	.619	2.966
4760	.621	3.294
5460	.630	4.931
6460	.630	4.931

Pyrolysis gas sensible enthalpy:

T(°R)	h_g(Btu/lb)
900	-1255.
1800	10.0
2700	2687.
3600	3694.
4500	6010.
5400	12006.

Nodal sizes:

1 at 0.015 inches, 9 at 0.030 inches, 2 at 0.050 inches, 1 at 0.090 inches

10 nodelets/node

Boundary conditions are described in Section 6.

C-1.2 PROBLEMS OF FIGURES C-6 TO C-12

The problems had a low density nylon phenolic slightly different from that above. For the 3-component model, the kinetic coefficients were the same as those above except that $m_c = 1$. Densities were

Component	ρ_{o_i} (lb/ft^3)	ρ_{r_i} (lb/ft^3)
A	6.55	0
B	19.60	18.68
C	71.00	0

For the single component model the kinetic data is given in Section 10.1 above. Densities for this case were

Component	ρ_{o_i} (lb/ft^3)	ρ_{r_i} (lb/ft^3)
A	35.0	15.0
B	0	0
C	35.0	35.0

Enthalpies of formation, reference temperature 536°R

Virgin Plastic	0
Char	0
Pyrolysis gas	-1117 Btu/lb

Material Properties:

	T(°R)	Specific Heat (Btu/lb)	Thermal Conductivity (Btu/ft sec °F)
	460	.29	1.26×10^{-5}
	660	.44	1.34
Virgin Plastic	760	.50	1.37
	860	.54	1.40
	960	.55	1.42
	1260	.55	1.55
	6000	.55	1.55
Char	500	.10	$.10 \times 10^{-4}$
	1460	.39	1.80
	1960	.49	2.46
	2460	.50	2.90
	3460	.50	4.00
	4460	.50	5.60
	4760	.50	6.40
	5500	.50	7.50

Plastic emissivity was 0.9; char emissivity was 0.6.

Pyrolysis gas sensible enthalpy:

$T(^{\circ}R)$	h_g(Btu/lb)
900	-2206
1800	- 854
2500	459
2700	1021
3000	1967
3600	2757
4500	3841
5400	5850

Boundary conditions:

	Time(sec)	$T_w(^{\circ}R)$	$\dot{S}$(mils/sec)
Simulation Transient			
(Figures C-8, C-9, C-10)	0	540	0
	5	1430	0
	10	1590	0.08
	17	1820	0.15
	22	2170	0.30
	25	2350	0.50
	30	2850	0.85
	35	3600	1.30
	40	4100	1.80
	45	4500	2.28
	50	4770	2.75
	55	5100	3.30
	60	5400	4.25
	65	5700	5.80
	70	5875	7.50
	75	5850	8.00
	80	5750	8.42
Ramp Transient			
(Figures C-11, C-12)	0	540	0
	40	4000	1.0

SUB-APPENDIX C-2

ESTIMATION OF EXECUTION TIME

The following table of the number of operations in each section of the charring material ablation program provides a useful estimate of execution time as a function of the number of nodes, the number of nodelets per node, and so on.

The input subroutine and all other operations, such as output, not performed each time step, have not been included. Only floating arithmetic is considered.

Table of Floating Operations
for One Time Step

	Add	Subtract	Multiply	Divide	Exp f	Log f
Miscellaneous Nodal Computations, per Node	32	36	64	25	0	0
General Decomposition, per decomposing Node	22	15	13	3	0	0
Component Decomposition, per Component for each Decomposing Nodelet*	1	3	4	3	3	2
Surface Calculations, per Iteration	25	39	50	10	1	0

*For the exact integrated relations and $m \neq 1$. For the simpler explicit decomposition relations the numbers in this row were 1, 4, 4, 2, 1, 1.

With the average operating times for the IBM 7094 (add and subtract = 14 μs, multiply = 7 μs, divide = 12 μs, exp f = 188 μs, log f = 226 μs), this table yields the following floating arithmetic time estimate per time step.

$$T = \left[(1136 \cdot I + 645)J \cdot F + 1700\right] N + K(1534) \ \mu\text{sec/step}$$

where

T = execution time for a single time step (μsec)

I = number of decomposing components in the material

J = number of nodelets per node

F = fraction of nodes decomposing

N = total number of nodes

K = number of iterations in surface energy balance

To estimate total execution time, T may be multiplied by the total number of time steps, a number approximately determined by the user in the choice of the maximum time step allowed. F should be an average value for the fraction of nodes actively decomposing during the problem (usually between 1/3 and 1/2). A study of numerous problems reveals that K averages very close to 3.

The resulting total time must be multiplied by a factor to account for "administrative" arithmetic such as DO loop indexing. Experience with this program on the 7094 suggests a factor between 1.4 and 1.5.

Additional machine time will be consumed by input and loading operations, overlay or special tape handling (if necessary), and output operations, the details of which are peculiar to individual computing facilities.

APPENDIX D

TRANSFORMATION OF THE IN-DEPTH ENERGY EQUATION

APPENDIX D

TRANSFORMATION OF THE IN-DEPTH ENERGY EQUATION

The in-depth energy equation, which is Equation (38) in the main text above, is

$$\rho C_p \left.\frac{\partial T}{\partial \theta}\right|_x = \frac{1}{A}\frac{\partial}{\partial x}\left(kA \left.\frac{\partial T}{\partial x}\right|_\theta - \bar{h} \left.\frac{\partial \rho}{\rho \theta}\right|_x + \frac{\partial}{\partial x}(\rho h)_\theta \dot{S}\right.$$

$$\left. + \frac{\dot{m}_g}{A}\left.\frac{\partial h_g}{\partial x}\right|_\theta + h_g \left.\frac{\partial \rho}{\partial \theta}\right|_y \right. \qquad \text{(D-1)}$$

where

$$\bar{h} \triangleq \frac{\rho_p h_p - \rho_c h_c}{\rho_p - \rho_c} \qquad \text{(D-2)}$$

This form of the energy equation turns out to be convenient for differencing and for machine treatment, but it lacks a certain amount of physical clarity, primarily because no single "energy of decomposition" term can be identified. Equation (D-1) can be cast into more appealing form by definitely identifying this quantity. The necessary operations involve chiefly an expansion of the $\partial/\partial x(\rho h)_\theta$ term in Equation (D-1), as follows:

Since Equation (21) of the main text gives

$$\rho h = \epsilon_p \rho_p h_p + (1 - \epsilon_p)\rho_c h_c$$

then, dropping the "constant-θ" subscript for convenience temporarily,

$$\frac{\partial(\rho h)}{\partial x} = \frac{\partial}{\partial x}(\epsilon_p \rho_p h_p) - \frac{\partial}{\partial x}(\epsilon_p \rho_c h_c) + \frac{\partial}{\partial x}(\rho_c h_c) \qquad \text{(D-3)}$$

$$= (\rho_p h_p - \rho_c h_c)\frac{\partial \epsilon_p}{\partial x} + \epsilon_p \frac{\partial}{\partial x}(\rho_p h_p - \rho_c h_c) + \frac{\partial}{\partial x}(\rho_c h_c) \qquad \text{(D-4)}$$

$$= (\rho_p h_p - \rho_c h_c)\frac{\partial \epsilon_p}{\partial x} + \epsilon_p \rho_p C_{p_p}\frac{\partial T}{\partial x} + (1 - \epsilon_p)\rho_c C_{p_c}\frac{\partial T}{\partial x} \qquad \text{(D-5)}$$

But by the defining Equation (28) of the main text

$$\rho C_p = \epsilon_p \rho_p C_{p_p} + (1 - \epsilon_p)\ \rho_c C_{p_c} \tag{D-6}$$

so that

$$\left.\frac{\partial(\rho h)}{\partial x}\right]_\theta = (\rho_p h_p - \rho_c h_c)\ \left.\frac{\partial \epsilon_p}{\partial x}\right)_\theta + \rho C_p\ \left.\frac{\partial T}{\partial x}\right)_\theta \tag{D-7}$$

Now, however, we have by Equation (20) of the main text that

$$\rho = \epsilon_p \rho_p + (1 - \epsilon_p)\rho_c \tag{D-8}$$

so that

$$\left.\frac{\partial \rho}{\partial x}\right)_\theta = \rho_p\ \left.\frac{\partial \epsilon_p}{\partial x}\right)_\theta - \rho_c\ \left.\frac{\partial \epsilon_p}{\partial x}\right)_\theta \tag{D-9}$$

or

$$\left.\frac{\partial \epsilon_p}{\partial x}\right)_\theta = \frac{\left.\frac{\partial \rho}{\partial x}\right)_\theta}{\rho_p - \rho_c} \tag{D-10}$$

Substituting this into Equation (D-7) gives finally

$$\left.\frac{\partial(\rho h)}{\partial x}\right]_\theta = \bar{h}\ \left.\frac{\partial \rho}{\partial x}\right)_\theta + \rho C_p\ \left.\frac{\partial T}{\partial x}\right)_\theta \tag{D-11}$$

where $\bar{h}$ is defined by Equation (D-2) above.

Now substitution of Equation (D-11) into the original energy Equation (D-1) gives

$$\rho C_p\ \left.\frac{\partial T}{\partial \theta}\right)_x = \frac{1}{A}\frac{\partial}{\partial x}\left(kA\ \frac{\partial T}{\partial x}\right) + \bar{h}\left[\dot{s}\ \left.\frac{\partial \rho}{\partial x}\right)_\theta - \left.\frac{\partial \rho}{\partial \theta}\right)_x\right] + \dot{s}\rho C_p\ \left.\frac{\partial T}{\partial x}\right)_\theta$$

$$+ \left.\frac{\dot{m}_g}{A}\ \frac{\partial h_g}{\partial x}\right)_\theta + h_g\ \left.\frac{\partial \rho}{\partial \theta}\right)_y \tag{D-12}$$

But the conservation of mass Equation (15) of the main text gives

$$\left.\frac{\partial \rho}{\partial \theta}\right|_x = \left.\frac{\partial \rho}{\partial \theta}\right|_y + \dot{S}\left.\frac{\partial \rho}{\partial x}\right|_\theta \qquad \text{(D-13)}$$

Putting this into the $\bar{h}$ coefficient above and collecting terms we obtain the desired final relation

$$\rho C_p \left.\frac{\partial T}{\partial \theta}\right|_x = \frac{1}{A}\frac{\partial}{\partial x}\left(kA\left.\frac{\partial T}{\partial x}\right|_\theta + (h_g - \bar{h})\left.\frac{\partial \rho}{\partial \theta}\right|_y + \dot{S}\rho C_p \left.\frac{\partial T}{\partial x}\right|_\theta + \frac{\dot{m}_g}{A}\left.\frac{\partial h_g}{\partial x}\right|_J\right) \qquad \text{(D-14)}$$

This equation may be viewed as a "conservation of sensible energy" equation at constant x, and thus has a close relation with the usual form of energy equations in applications including chemical changes. The second term on the right hand side represents the "creation of sensible energy" due to pyrolysis.